The University of Southern Mississippi

The Aquila Digital Community

Dissertations

Fall 2019

The Effect of Precursor Design and Processing on the Semi-Crystalline Morphologies of Polyacrylonitrile-Based Carbon Fiber

Katelyn Cordell
University of Southern Mississippi

Follow this and additional works at: https://aquila.usm.edu/dissertations

 Part of the Polymer Science Commons

Recommended Citation

THE EFFECT OF PRECURSOR DESIGN AND PROCESSING ON THE SEMI-
CRYSTALLINE MORPHOLOGIES OF POLYACRYLONITRILE-BASED CARBON
FIBER

by

Katelyn JoAnna Cordell

A Dissertation
Submitted to the Graduate School,
the College of Arts and Sciences
and the School of Polymer Science and Engineering
at The University of Southern Mississippi
in Partial Fulfillment of the Requirements
for the Degree of Doctor of Philosophy

Approved by:

Dr. Jeffrey S. Wiggins, Committee Chair
Dr. Sarah E. Morgan
Dr. Sergei I. Nazarenko
Dr. Derek L. Patton
Dr. Robson F. Storey

_____	_____	_____
Dr. Jeffrey S. Wiggins	Dr. Derek L. Patton	Dr. Karen S. Coats
Committee Chair	Director of School	Dean of the Graduate School

December 2019

THE UNIVERSITY OF
SOUTHERN
MISSISSIPPI.

ABSTRACT

Basic research to control the morphology of polyacrylonitrile (PAN)-based carbon fiber is crucial for next generation composites as it determines their mechanical properties and final use. Poor molecular design of PAN-based precursors and fiber processing causes morphological defects and mechanical limitations.[1,2] This research focused on utilizing the controlled polymerization technique, reversible addition-fragmentation chain transfer (RAFT), of novel acrylamide comonomers to afford well-defined precursors with precisely controlled molecular design. This controlled RAFT technique improved the overall precursor graphitic structure as evident by the increased extent of stabilization and reduced activation energy as compared to precursors prepared by traditional free radical polymerization.

The effect of increasing N-ethyl acrylamide (NEAA), N-isopropylacrylamide (NIPAM), and N-tert-butylacrylamide (NTAA) comonomer concentration on copolymer architecture and PAN ring closure was evaluated. Reactivity ratio calculations confirmed that all acrylamide comonomers would cross-propagate with acrylonitrile to yield the desired alternating PAN copolymer architecture. Increased comonomer concentration reduced the amount of cyclization sites, which resulted in an overall decrease in PAN ring closure upon heating as evident by reduced extent of stabilization and exothermic behavior. The knowledge gained on the interdependencies of precursor design on PAN copolymer architecture and ring closure was used to down-select three precursors, two RAFT-based precursors that displayed promising graphitic structure and one free radical precursor, for white fiber spinning.

Circular white fibers were spun at Deakin University through the careful selection of white fiber spinning parameters, where fiber diameters of ~ 12 µm or less were observed by scanning electron microscopy. RAFT-based white fibers exhibited more consistent break stress values than free radical-based white fibers and suggested that controlling precursor design and fiber processing afforded a more regular white fiber morphology. The amount of white fiber spun was hindered by the limited amount of RAFT precursor; therefore, attempts to synthesize several grams of high molecular weight PAN precursors were performed via a continuous reactor technique and only yielded a molecular weight of ~ 45,000 g/mol. Ultimately, this research provided new knowledge on the effect of controlling precursor molecular design and fiber processing on fiber morphology.

ACKNOWLEDGMENTS

First, I would like to express my utmost gratitude to my advisor Dr. Jeffrey Wiggins who has provided me with multiple opportunities to grow professionally via exposure to industry and academic partners, and has allowed me to accomplish personal family goals. His "hands-free" teaching style gave me the freedom to select my research and learn from my mistakes, which led to personal confidence in my research decisions. I will be forever grateful for his mentorship. I would also like to thank my research committee members Dr. Patton, Dr. Morgan, Dr. Storey, and Dr. Nazarenko for their critiques that allowed me to grow as a writer and presenter. I would like to especially thank Dr. Patton and Dr. Morgan for their additional mentorship when I was selected as a National Science Foundation Research Traineeship recipient.

Thank you to all of my industrial collaborators at The Boeing Company and Solvay including Dr. Sam Tucker, Dr. Olivia McNair, Dr. Rob Maskal, Dr. Jeremy Moskowitz, and Dr. Matthew Jackson. I am also grateful to my academic partners at Deakin University along with Carbon Nexus and the Commonwealth Scientific and Industrial Research Organization (CSIRO), Monash University, and Florida State University particularly Dr. Joselito Razal, Dr. Dylan Hegh, Dr. Claudia Creighton, Dr. Kim Quayle, Dr. Linda Hillbrick, Dr. Jasjeet Kaur, Dr. Peter Lynch, Dr. Pablo Mota Santiago, Dr. Richard Liang, and Dr. Jin Gyu Park. I am very appreciative to both my industrial and academic collaborators for challenging my ideas and encouraging me to keep pursuing answers to the "tough" questions.

I would like to acknowledge specific members from the Storey research group and the Gu research group including Dr. Corey Parada, Mr. Travis Holbrook, Mr. Logan

DEDICATION

To my husband, Jean Pierre Zapata Quintero. Without his countless sacrifices,

endless love and support, this work would not have been possible.

TABLE OF CONTENTS

LIST OF TABLES

LIST OF ILLUSTRATIONS

LIST OF SCHEMES

LIST OF ABBREVIATIONS

PAN	Polyacrylonitrile
RAFT	Reversible Addition-Fragmentation Chain-Transfer
NEAA	N-ethyl acrylamide
NIPAM	N-isopropylacrylamide
NTAA	N-tert-butylacrylamide
CFRPs	Carbon Fiber Reinforced Polymers
WRG	Wiggins Research Group
USM	The University of Southern Mississippi
TEM	Transmission Electron Microscopy
IA	Itaconic Acid
AA	Acrylic Acid
MA	Methylacrylate
MMA	Methyl Methacrylate
CLRP	Controlled Living Radical Polymerization
CTA	Chain Transfer Agent
V-70	2,2'-azobis(4-methoxy-2,4-dimethyl valernitrile)
CPDT	2-cyano-2-propyl dodecyl trithiocarbonate
DMSO	Dimethyl Sulfoxide
DMAC	Dimethyl Acetamide
T_g	Glass Transition Temperature

Đ	Dispersity
TOS	Thermo-oxidative Stabilization
TTT	Time Temperature Tension
LT	Low Temperature
HT	High Temperature
MEHQ	Mono Methyl Ether of Hydroquinone
DMF	N,N-dimethyl formamide
EC	Ethylene Carbonate
AIBN	Azobisisobutyronitrile
THF	Tetrahydrofuran
NMR	Nuclear Magnetic Resonance
dDMSO	Deuterated Dimethyl Sulfoxide
Mw	Weight Average Molecular Weight
Mn	Number Average Molecular Weight
MALLS	Multi-angle Laser Light Scattering
DSC	Differential Scanning Calorimetry
E_a	Energy of Activation
FWO	Flynn-Wall-Ozawa
A	Collision Frequency
ICA	Isoconversional Analysis
FTIR	Fourier Transform Infrared Spectroscopy
E_s	Extent of Stabilization

TGA-MS	Thermogravimetric Analysis in tandem with Mass Spectroscopy
WAXS	Wide Angle X-ray Scattering
L_c	Crystallite Thickness
FWHM	Full Width at Half Max
S_I	Stabilization Index
SAXS	Small Angle X-ray Scattering
SEM	Scanning Electron Microscopy
FSU	Florida State University
FIB	Focused Ion Beam
FR	Free Radical
BR	Batch RAFT
SB	Semi-batch RAFT
NLLS	Non-linear Least Squares
$<N_{AN}>_n$	Number Average Sequence Length of Acrylonitrile
DDR	Draw Down Ratio
GPS	Gear Pump Speed
FFT	Fast Fourier Transform

CHAPTER I - INTRODUCTION

1.1 Research Motives

Reed Hastings once said, "Stone Age. Bronze Age. Iron Age. We define entire epics of humanity by the technology they use." History has shown how the progression of mankind parallels to the development of contemporary materials that are stronger, lighter, and more durable. Now, we are in the age of plastics comprised of synthetic polymers that are versatile, diverse, and stronger than ever before.[3] Carbon fiber reinforced polymers (CFRPs) are one prime example of this age, due to their exemplary properties such as a high strength to weight ratio. Currently, CFRPs are used in high performance polymer-matrix composites in a variety of applications including: aircraft materials, space vehicles, sporting goods, energy, and general infrastructure construction materials. A leading example is the Boeing 787 *Dreamliner* that is comprised of 50 % by weight of CFRP composites.[1,4–7] However, the expansion of CFRPs into more demanding applications is limited by the lack of multi-scale scientific knowledge linking precursor molecular design with ultimate carbon fiber performance.

Although the demand for carbon fiber is high, continued advancement is necessary to improve its capabilities towards theoretical mechanical properties; currently, the tensile strength of PAN-based carbon fibers is ~7 GPa, which is almost 10 % of its theoretical tensile strength of ~100 GPa.[2,8] Even after more than 50 years of continued carbon fiber development, carbon fibers still maintain a tensile strength of ~7 GPa.[8] This difference is attributed to morphological disinclinations within the fibers whose quantity, size, and distribution ultimately define mechanical limitations of the fiber and CFRP. Factors that affect morphological defects in carbon fibers are most often associated with

precursor molecular design, comonomer composition and distribution, and precursor white-fiber processing.[1,2] It is hypothesized that research which correlates precursor design and oxidative ring closing stabilization and exotherm on white fiber morphologies will expose key findings to advance carbon fiber morphologies and properties. However, few research groups have the ability to link precursor chemistry and morphology to carbon fiber mechanical properties due to inherent complexities of linking precursor synthesis with carbon fiber preparation in a well-controlled academic environment.[9] The Wiggins Research Group (WRG) at the University of Southern Mississippi (USM) has established an international research infrastructure which provides scientific expertise in precursor synthesis, white fiber solution spinning, and carbon fiber preparation with high-quality scientific capability in all phases of research. Well-controlled polyacrylonitrile-based carbon fiber copolymers with varying semi-crystalline morphologies will be synthesized, analyzed, and screened at USM. Copolymers with promising oxidative ring closing stabilization and exotherm via precursor design will be down-selected for white fiber spinning. We will be working with WRG's collaborators at Deakin University in Geelong, Australia to spin high-quality white fibers utilizing their leading expertise in precursor spinning science. White fibers will be oxidized, stabilized, and carbonized into high-quality black fiber also at Deakin University through well-controlled stabilization and pyrolysis processes. WRG's combined scientific capabilities provide a unique academic opportunity to link precursor molecular design and morphological control with carbon fiber morphologies and mechanical properties.

1.2 Background

1.2.1 PAN-based Carbon Fiber Structure and Morphology

Carbon fiber possesses at least 92 % carbon and is produced from three main

precursors: polyacrylonitrile (PAN), mesophase pitch, and cellulose pitch.[1,2,4] Today,

over 90 % of carbon fiber is prepared from PAN as opposed to mesophase or cellulose

pitch.[1,2,10,11] PAN is favored over the use of highly oriented mesophase pitch due to

mesophase pitch having a high processing cost via coal tar purification. Cellulosic pitch

affords strong carbon fiber and low manufacturing cost; however, the carbon yield is

limited to only 20 to 30 %.[4] Therefore, PAN-based carbon fibers are primarily used for

their high performance, carbon yield, purity, and structure. It is important to note that all

PAN precursors are copolymerized with various comonomers to afford high performing

PAN-based carbon fibers.[12,13]
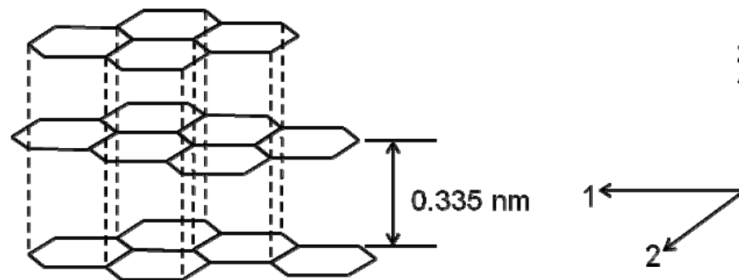
Figure 1.1 Structure of graphene sheets and directions in graphite.[4]

The atomic structure of PAN-based carbon fiber contains a hexagonal pattern of

layered carbon atoms similar to the graphene sheets in graphite, as depicted in Figure 1.1

from Huang in 2009, where the d-spacing is the distance between two graphitic sheets

and is approximately 0.335 nm. The in-plane carbon atoms are covalently bonded

through sp^2 bonding, while stacked sheets are bonded via weak Van der Waals forces.[4] In

1987, the microstructure of PAN was described as a layered turbostratic structure based

on surface analysis by transmission electron microscopy (TEM) and x-ray diffraction, which can be observed in Figure 1.2.[14] The resulting image from this analysis defined the outer sheath graphene sheets, later referred to as carbon fiber "skin" designated as ribbons with 1 to 2 nm needle shaped voids, with an inner core that is disordered with folded layer planes. This skin-core morphology was verified in 1995 through Raman spectroscopy by Huang et al. and accepted for PAN-based carbon fibers; however, there are limited scientific studies that relate PAN precursor composition to its morphology.[9,11,15,16]
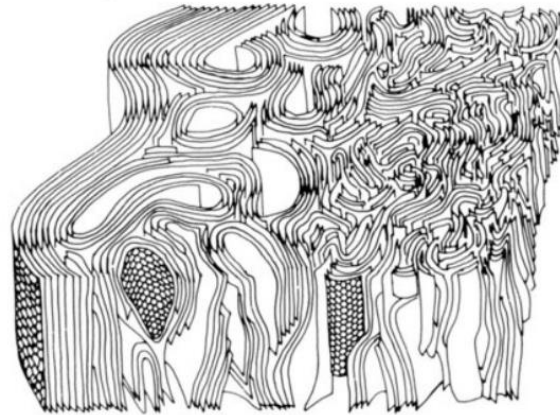
Figure 1.2 Turbostratic PAN-based carbon fiber morphology as depicted by Johnson in 1987.[14]

The crystal structure and packing directs the PAN morphology, where this morphology is highly crystalline (~ 30 %) and estimated to be ten monomer units thick.[17] This accepted morphology dictates the mechanical properties, including tensile modulus, tensile strength, and compressive strength of ultimate carbon fiber. The high modulus of carbon fiber is attributed to high crystallinity and crystal alignment in the fiber direction, while the strength of carbon fiber is limited by the morphological defects in the fiber.[4] For example, high strength carbon fiber contains fewer needle-like microvoids oriented

along the fiber, whereas high modulus carbon fiber possesses larger and longer microvoids.[18] Compressive strength is negatively affected by increased orientation, graphitic order, and crystallite size, where large crystallites are highly brittle and subject to compressive deformation.[18,19] Therefore, an in-depth understanding of the semi-crystalline PAN morphology including factors that affect the crystal structure, packing, and fiber alignment is needed to control carbon fiber mechanical properties. From this assessment, the scientific literature is comprised of analyses from various global researchers who obtained commercial carbon fiber, analyzed mechanics and morphologies, and reported results as a general case that typically lack examining all factors that impact the semi-crystalline PAN morphology including the numerous variables that control precursor design and fiber processing.

Preliminary WRG findings have demonstrated that minor variations in processing can lead to dramatic differences in carbon fiber morphology. Figure 1.3 displayed unpublished TEM images generated through the USM, University of Kentucky, and Deakin University collaboration for a poly(AN-co-NIPAM) (98:2) copolymer-based carbon fiber in the sheath, or edge region.[20] Figure 1.3 A suggested a 30-40 nm skin as evidenced through clear changes in graphitic structures and orientation leading from the carbon fiber surface into a more regular turbostratic morphological core. In contrast, Figure 1.3 B depicted much more consistent and regular turbostratic graphitic morphology from the fiber surface into the core.[20] Although the specific root-cause for this variation has not been resolved at this time, nor the influence of these changes on mechanical properties, this result highlighted the ability to govern black fiber morphology through controlled experimentation and validated the complexities of

5

processing on final structure. More importantly, researchers reporting on Fiber A or Fiber

B from Figure 1.3 would draw quite different descriptions of the same fiber without

knowledge of its chemistry or preparation. In this example, the same base chemistry and

same white fiber yielded dramatically different skin-core black fiber morphologies.
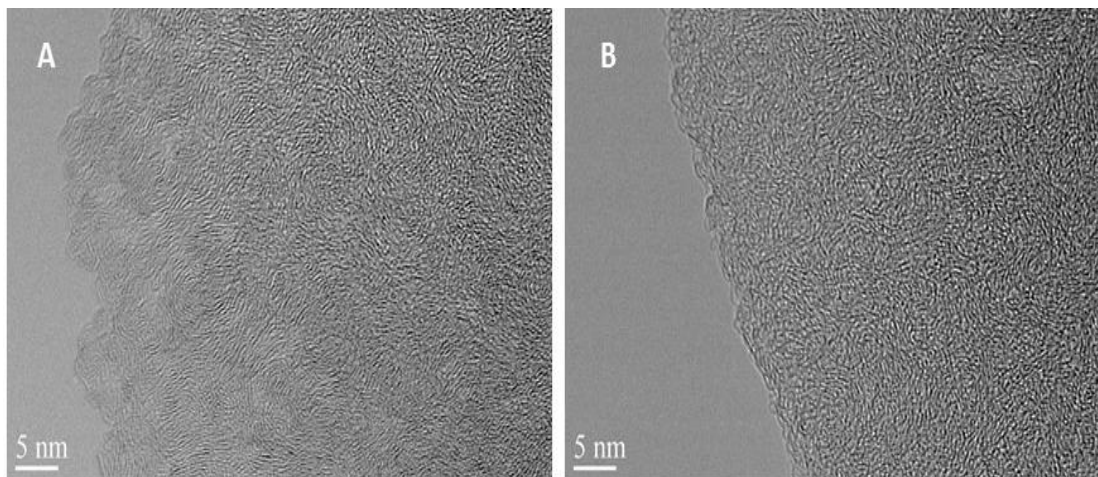
Figure 1.3 TEM of WRG poly(AN-co-NIPAM) (98:2) based carbon fiber exhibiting A) skin-core and B) regular turbostratic morphologies.[20]

In conjunction with processing parameters, the base chemistry or design of PAN

precursors also influences the final black fiber morphology as precursor synthesis is the

first step in the preparation of carbon fiber. Homopolymer PAN precursor is highly

crystalline and essentially degrades prior to stabilization and pyrolysis. As a result,

copolymerization is necessary to obtain high-performance carbon fibers. The semi-

crystalline morphology of PAN is controlled by the packing order of polymer chains,

where PAN is atactic with a mostly planar zig zag confirmation in a pseudo hexagonal

crystal lattice.[17,21] Copolymer concentration and composition affects PAN chain-packing

and therefore the relative volume of crystalline and amorphous regions. The amorphous

regions have been reported to be where oxidation and cyclization events occur due to

local mobility.[8,22,23] A high comonomer concentration in the copolymer leads to

6

disinclinations; however, a highly crystalline copolymer leads to high stress when drawing the fiber.[15,24] From a polymer science perspective, comonomer reactivity ratios, run-numbers, comonomer composition, comonomer distribution, molecular weight, and molecular weight distribution collectively create a complex series of variables for properly designing carbon fiber precursor chemistries. Therefore, it would be beneficial to systematically control these variables as foundational scientific variables for white fiber spinning and carbon fiber preparations towards the optimization of morphological and mechanical properties.

1.2.2 Precursor Design

1.2.2.1 Comonomer selection and concentration

Precursor design including comonomer selection, concentration, and distribution govern precursor morphology and, in turn, its mechanical properties. In general, PAN-based carbon fiber contains two types of comonomers, which are either acidic or neutral in nature. The total comonomer concentration within the PAN precursor is typically below 8 % to ensure high carbon yields of $\geq$ 92 % .[1,2] Homopolymer PAN is not used commercially as it is highly crystalline and exothermic, which hinders processing as previously mentioned.[8,25] Acidic comonomers, such as itaconic acid (IA) and acrylic acid (AA) are known to reduce cyclization temperature, which promotes PAN stabilization and broadens the exotherm peak in pyrolysis.[9,26] Neutral comonomers like methyl acrylate (MA) and methyl methacrylate (MMA) increase cyclization temperature but improve drawability and spinnability of white fiber PAN.[26] It would be beneficial to improve stabilization and spinnability concurrently with the use of only one comonomer; however, commercially available BlueStar fibers are terpolymers comprised of IA (1 %)

and MA (6 %), where the reactivity of the acidic IA and neutral MA comonomers are different from one another.[27,28] This variation in reactivity ratios leads to a larger incorporation of neutral comonomers in the polymer backbone (to facilitate solubility), which causes an increased cyclization temperature and lowers stabilization.[29,30] Ergo, new comonomers that possess both properties of acidic and neutral comonomers are desired to distribute the comonomer evenly throughout the PAN backbone. In recent literature, itaconic acid derivatives have been synthesized and possessed acidic and neutral comonomer qualities.[31–33] Therefore, new copolymers and comonomers that possess controlled morphology, decreased exotherm, and increased stabilization are desirable.
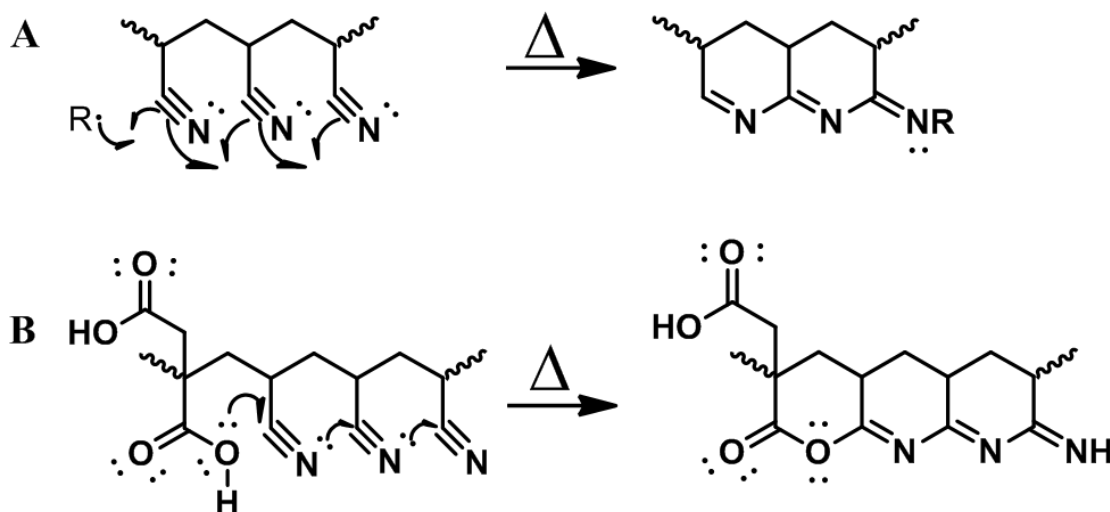
Scheme 1.1 PAN ring closing pyrolysis mechanisms A) free radical and B) ionic.[20]

Comonomers not only affect semi-crystalline morphology, exotherm, and stabilization but also the ring closing pyrolysis mechanisms. The mechanism for PAN with a neutral comonomer added proceeds through a free radical ring-closing mechanism as depicted in Scheme 1.1 A.[29] Free radical reactions occur rapidly and result in high, often uncontrollable, exotherms.[26] Large exotherms create structural defects through the

destruction of molecular chains via heat. Mechanistically, acidic comonomers progress through ionic ring-closing as described in Scheme 1.1 B.[25,34] These acidic comonomers lower the cyclization temperature, reduce the exotherm, and increase the peak breadth. Neutral comonomers with large side groups increase solubility and the amount of amorphous content and promote cyclization during oxidation. Comonomers choice influences ring closing behavior within the amorphous region, suggesting semi-crystalline morphology is a critical molecular design variable.[8,23] Unfortunately, commercially available PAN terpolymers are neutral rich as previously mentioned to aid in fiber spinning but their inherent large exotherms can also lead to polymer chain scission and degradation.[29] It would be favorable to control comonomer selection and distribution to initiate pyrolysis by an ionic cyclization to reduce exotherms, while reducing thermal molecular chain damage. It is proposed that optimizing comonomer selection will lead to improved stabilization, reduced exotherms, and desirable semi-crystalline morphologies.

As determined through prior research in WRG, N-isopropylacrylamide (NIPAM) is an effective comonomer in PAN precursors due to its ability to reduce exotherm, increase ring closing stabilization, disrupt crystallinity, and cross-propagate with acrylonitrile (AN).[35–37] Scheme 1.2 displayed the proposed incorporation of NIPAM into the stabilized ladder structure by Moskowitz et al.[35] NIPAM was selected in prior investigations to provide combined solubility and anionic ring closing pathways in stabilization, and to establish semi-batch RAFT synthetic pathways for controlling comonomer sequencing.[20] From preliminary WRG research, NIPAM offered a substantial reduction in exotherm and increased stabilization efficiencies as compared to

9

traditional itaconic acid or acrylic type comonomers.[35–37] Therefore, poly(AN-co-NIPAM) (98:2) with an absolute molecular weight of approximately 100,000 g/mol and dispersity of < 1.3 will to be used as a baseline copolymer for this research. These molecular weight and dispersity values were selected as literature highlighted that increased molecular weight and reduced dispersity values improved the performance of carbon fiber.[38–41]
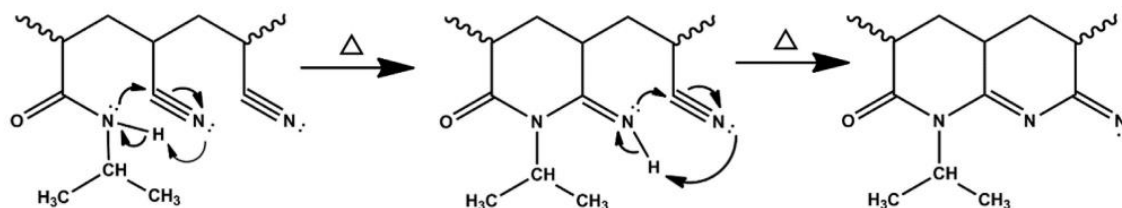
Scheme 1.2 Proposed cyclization mechanism of poly(AN-co-NIPAM).[35]

To expand upon previous WRG research by Moskowitz et al, a series of acrylamide-based comonomers including: N-ethyl acrylamide (NEAA), NIPAM, and N-tert-butylacrylamide (NTAA) will be copolymerized with acrylonitrile within this dissertation.[20] The increasing comonomer bulkiness is anticipated to systematically disrupt semi-crystalline morphologies of PAN copolymers as well as expected to maintain similar anionic ring-closing ladder forming stabilization reaction pathways as examined by Moskowitz et al.[20,37] It is hypothesized that changes in acrylamide pendant group architectures will lead to changes in precursor semi-crystalline morphologies, which will relate with exotherm and ring closing stabilization. This hypothesis will be examined in Chapters III, IV, and V.

1.2.2.2 Comonomer Distribution via Controlled Living Radical Polymerization

Controlled Living Radical Polymerization (CLRP), especially RAFT, offers as a promising method to control the polymerization and comonomer distribution of PAN. RAFT serves as a modern technique with advantages including controlling molecular weight, no metal catalyst required, and robust monomer availability.[36,42] The first RAFT polymerization of PAN was conducted in 2003 by Matyjaszewski.[43] More recently, Cai and coworkers published the first comparative study between PAN-based carbon fibers synthesized by traditional free radical and RAFT polymerization mechanisms in 2016. The latter report determined that RAFT-based carbon fibers possessed superior rheological and mechanical properties as compared to carbon fibers prepared conventionally.[41] However, it did not investigate the usage of semi-batch RAFT; as Wang et al. concluded that semi-batch CLRP and adjusted feeding profile resulted in an even distribution of comonomers along the backbone, which is desired with PAN precursors.[41,44] Semi-batch RAFT offers control of comonomer distribution and leads to predictable semi-crystalline morphologies. This favorable method uses a chain transfer agent (CTA), as illustrated in Scheme 1.3, to generate a chain transfer equilibrium which controls the growth of molecular weight. The initiator 2,2'-azobis(4-methoxy-2,4-dimethyl valernitrile) (V-70) and CTA agent 2-cyano-2-propyl dodecyl trithiocarbondate (CPDT) were selected as they have yielded well-defined PAN precursors with high molecular weights (>100,000 g/mol) in previous research.[35,36]

It is evident that precursor design including comonomer selection, concentration, and distribution plays a key role in the ring closing behavior of stabilized PAN, which influences semi-crystalline morphology of PAN. However, previous unpublished TEM

results also highlighted the significant impact of processing on black fiber morphology, where the same base chemistry was used. Therefore, an in-depth understanding of the effects of both precursor design and processing will be crucial to afford a regular turbostratic black fiber morphology with minimal defects.
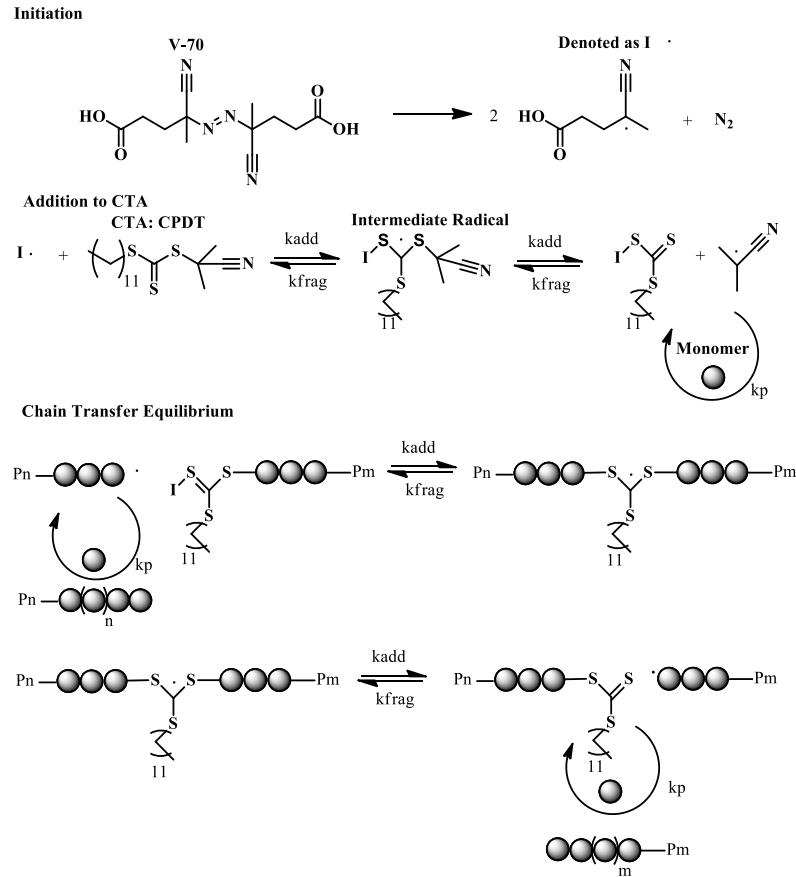
Scheme 1.3 RAFT mechanism.

1.2.3 Carbon Fiber Processing

Producing carbon fiber begins by preparing the PAN-based polymer precursor as described previously. After the PAN precursor is prepared, it is processed into white fiber typically via solution spinning which is separated into two main processes: (1) dry spinning or (2) wet spinning. Wet spinning can be further divided into either a wet-jet, air gap, or gel spinning process.[40,45] The white fibers are then converted into carbon fiber

through three general stages: thermo-oxidative stabilization, carbonization, and in some

cases, graphitization.[1,46]

1.2.3.1 White Fiber

It is reasonable to hypothesize that white fiber precursor morphology ultimately

controls the final morphologies and mechanical properties of carbon fiber, since this is

the final form of the PAN copolymers prior to pyrolysis. Wet jet spinning is the common

method for spinning PAN; however, air gap, also known as dry wet jet spinning, is

becoming more frequent.[38,40,45,47] The key difference between wet jet and air gap spinning

is the location of the spinneret, where the spinneret in wet jet spinning is located within

the coagulation bath as displayed in Figure 1.4. In the air gap process, the spinneret is

suspended above the coagulation bath and the polymer dope is passed through air

atmosphere for a short distance before entering the coagulation bath.[13,38,40,47] Herein, a

more detailed description of the wet-jet spinning process was described below as it was

utilized in Chapter V. The wet jet spinning process of PAN copolymers begins with the

spinning solution known as the polymer dope that is described as 1 in Figure 1.4.

1	Spinning Solution	4-6 Washing Baths
2	Spinneret	7 Heated Godets
3	Coagulation Bath	8 Uptake Roller
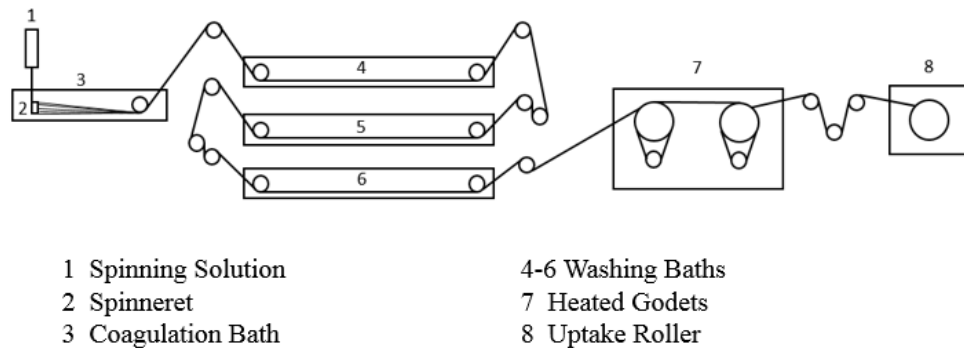
Figure 1.4 General wet-jet spinning process.

The polymer dope is typically comprised of roughly 15 to 30 wt. % PAN

copolymer dissolved in dimethyl sulfoxide (DMSO) or dimethylacetamide (DMAC).

PAN is only soluble in highly polar solvents such as DMSO due to the strong dipole-dipole interactions of the pendent nitrile groups within PAN.[40,48] The dope is then fed through a spinneret, set at a specific volumetric pump rate, within a coagulation bath that contains a mixture of PAN solvent and water at various temperatures usually ranging from 0 to 50 °C.[13,38,40,47] Within the coagulation bath the fiber is drawn, also known as jet stretch, which is affected by the diffusion of solvent (DMSO) and non-solvent (water) outflux and influx.[40,49] The diffusion of solvent and non-solvent within the white fiber is controlled by coagulation bath conditions, mainly temperature and concentration of DMSO and water. These two parameters are the most important factors for the development of circular and non-porous white fibers. For example, a non-circular fiber, also known as a bean-shaped fiber, occurs when coagulation happens too quickly due to flux of DMSO out of the fiber being less than the inward flux of water, where bath concentration drives DMSO out of the fiber and bath temperature drives the influx of water into the fiber. This fast coagulation will form as skin on the fiber and will eventually collapse, resulting in a non-circular fiber as illustrated in Figure 1.5 B.[40,50]

| A | B |

| Circular Fiber | Bean Shaped Fiber |
| Water influx rate-limited mechanism | DMSO outflux rate-limited mechanism |
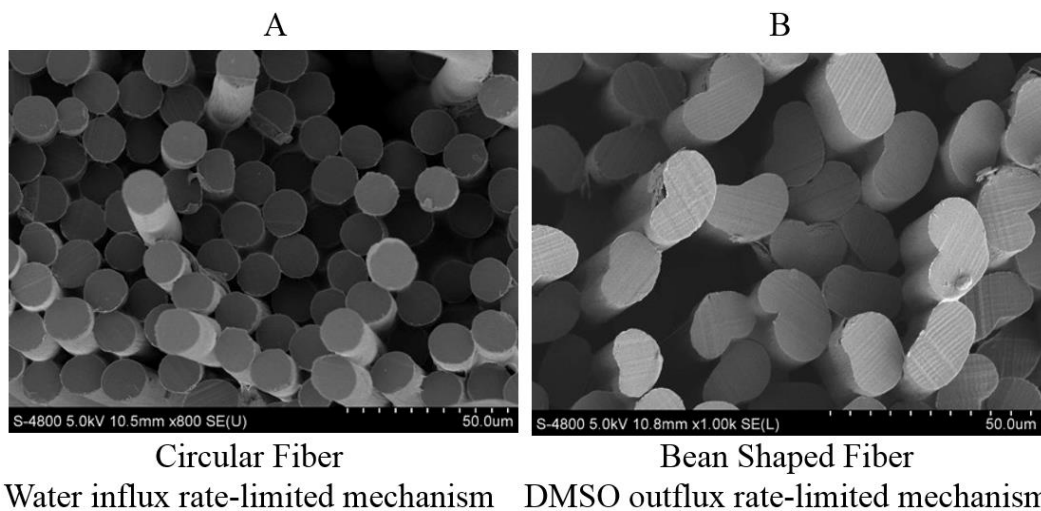
Figure 1.5 Shape of white fiber and diffusion mechanism for A) circular and B) bean.

It is difficult for this bean-shaped white fiber to survive additional processing including white fiber drawing, thermo-oxidative stabilization, and carbonization as these steps place the fiber under tension which eventually causes the white fiber to rupture due to stress concentration.[51] Additionally, when bean-shaped fibers are used in carbon fiber composites, the stress concentration around the fiber will lead to matrix microcracking, resulting in reduced CFRP strength.[1] When the proper coagulation conditions are met, a circular fiber is afforded as observed in Figure 1.5 A. To produce a circular fiber, Zeng and coworkers determined that reducing coagulation diffusion rates by optimizing dope conditions and coagulation bath conditions led to the preferred method of forming round white fibers. The volumetric pump rate, that is the rate the dope is fed through the spinneret and coagulation bath, can also affect diffusion rate. [40,49] Takahashi and coworkers determined that white fiber void content was reduced as the concentration of DMSO was increased from 0 to 70 % within the coagulation bath; therefore, a higher concentration of DMSO will be selected later in Chapter V.[50,52] Reduced bath temperatures at 40 °C has also been reported to produce the unfavorable bean-shaped fibers.[40] However, Chen and coworkers published that circular fibers were coagulated at 50 °C and that further increasing the coagulation bath temperature to 60 or 70 °C afforded ellipse or irregular-shaped cross sections.[40,51] Therefore, a higher bath temperature around 50 °C will be selected for Chapter V. The careful selection of bath concentration and temperature will be pivotal to ensure that circular fibers are will be spun with low void content.

From the coagulation bath, the white fibers are washed by a counter flow of water to remove excess solvent and post-drawn to orient the PAN copolymer chains. Additionally, spin finish can be applied to the washed white fibers to aid in reducing static and entanglement of the white fiber as they undergo thermo-oxidative stabilization and carbonization. The white fibers are then further dried and collapsed upon contact with the heated godet. Collapse occurs when water is removed from internal filament structure once heated at or above their glass transition temperature (T_g), and the fibrils move closer together. The drawing and spinning conditions during the formation of white fiber is vital for the morphological development of final carbon fiber product since this is the final form of the PAN copolymers prior to stabilization and carbonization.[11,39,40,52,53] PAN precursor chemistry including copolymer composition, molecular weight (MW) and molecular weight distribution, also known as dispersity (Đ), dictates the ability for white fibers to be spun, drawn and molecularly oriented prior to carbonization.[8] Therefore, PAN precursor design is crucial in the processing of white fibers and the mechanical properties of the ultimate carbon fiber.

1.2.3.2 Thermo-oxidative Stabilization of White Fiber

Thermo-oxidative stabilization (TOS) is a complex heat treatment starting from room temperature and steadily increasing temperature up to 350 °C in the presence of oxygen. The TOS step is critical for preparing and "stabilizing" the white fiber to ensure stability in the high temperature carbonization processes. TOS is considered a "necessary evil" in carbon fiber manufacturing since it is time and energy intensive; thermo-oxidative stabilization drives the cost in carbon fiber production, which motivates extensive research.[46] White fibers are stabilized through a series of heat treatment zones

and degrees of tensioning in multiple ovens over a period of 45 to 60 minutes under oxidative conditions as depicted in Figure 1.6 from Nunna and coworkers, where the white fiber precursor was exposed to four heat treatment zones.[28] The stabilization and carbonization expertise from Deakin University will aid in our capabilities at USM to mimic stabilization conditions when examining the thermal ring closing behavior of well-defined PAN-based precursors.
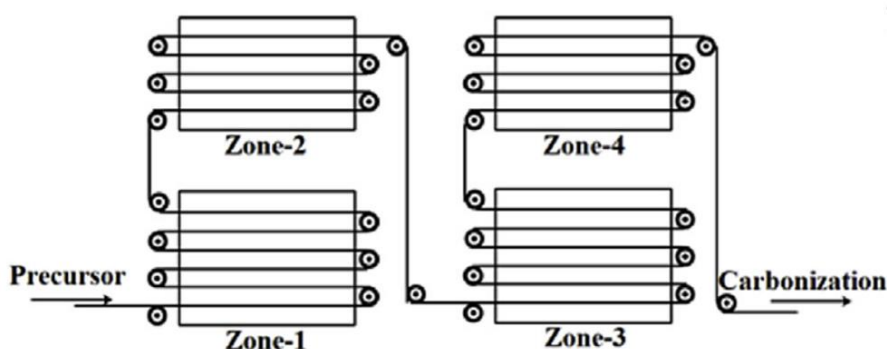
Figure 1.6 Stabilization of white fiber precursor prior to carbonization.[28]

During stabilization, PAN copolymers are converted to higher ordered and thermally stable cyclized polymer ladder structures setting the foundation for the final carbonized graphitic structure.[22,23,46] The cyclization of PAN precursor into the ladder-like structure throughout TOS and carbonization is displayed in Scheme 1.4 originally depicted by Frank and coworkers.[48] During TOS, the PAN structure undergoes dehydrogenation, cyclization, and oxidation where the order of dehydrogenation and cyclization is disputed in literature as displayed in Scheme 1.4.[46,54,55] While about fourteen factors affect the structure of the stabilized fibers, the three main processing parameters are time, temperature, and tension also referred to as TTT. Fibers that are stabilized too quickly can be damaged while long stabilization times and maximum temperatures may afford incomplete stabilization and may lead to poorly performing

carbon fibers.[28,56,57] Work from Nunna and coworkers established that increasing time and temperature while decreasing tension lead to an overall increased ring-closed structure, but radial heterogeneity or a skin-core morphology may develop.[28] Therefore, a careful balance of TTT is required to yield completely stabilized fibers without developing a skin-core morphology.
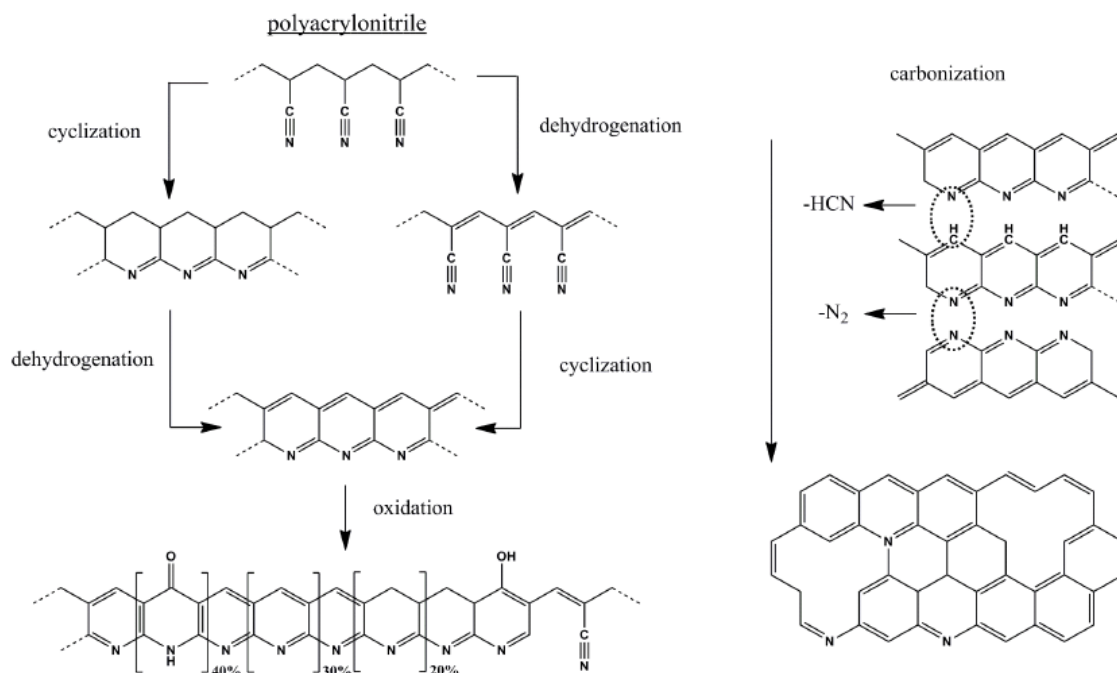
Scheme 1.4 Evolution of the graphitic structure for PAN based carbon fibers.[48]

1.2.3.3 Carbonization of Stabilized Fibers

The stabilized fibers are first carbonized in low-temperature (LT) ovens from ~350 to 800 °C, and then carbonized through high-temperature (HT) ovens from ~800 to 1800 °C. Both LT and HT ovens operate under inert atmospheres. High modulus carbon fibers are achieved through higher carbon contents and degrees of graphitization, with ultra-high modulus "graphite" fibers exceeding 2000 °C of pyrolysis.[11,46] A trade-off exists between high tensile strength and high tensile modulus carbon fibers, with ultimate properties being controlled in HT ovens. Throughout the entire stabilization and

carbonization processes, small gas molecules such as water, ammonia, carbon monoxide, carbon dioxide, hydrogen, and hydrogen cyanide are released.[11,58,59] It is known that precursor chemistry, which dictates white fiber morphology, controls ultimate carbon fiber performance.[1,2] Thus, PAN-based carbon fiber properties will be advanced through controlling precursor chemistry and fiber processing conditions.

1.2.4 Research Overview

Fundamental research which determines how PAN copolymer precursor semi-crystalline morphology ultimately controls carbon fiber morphology is necessary. It is hypothesized that systematic manipulation of precursor semi-crystalline morphology will lead to new pathways for controlling exotherm and ring-closing stabilization, and ultimately provide new knowledge for advancing key properties in PAN-based carbon fibers. The purpose of this research is to (1) synthesize PAN copolymer precursors with varying comonomer bulkiness, concentration, and distribution, (2) quantify semi-crystalline morphologies and thermal behavior of PAN copolymers, (3) analyze coagulation and drawing effects on white fiber morphologies of down-selected PAN precursors, and (4) elucidate the relationships between PAN precursor design on white and black fiber morphologies. In Chapter III, PAN precursors will be synthesized by free radical, batch RAFT, and semi-batch RAFT to investigate the effect of dispersity and acrylamide comonomer with increasing steric bulk on ring closing efficiency. In Chapter IV, comonomer content will be increased from 2 to 4 to 6 mole % to evaluate the influence of comonomer concentration on semi-crystalline morphologies, copolymer architecture, and ring closing efficiency. Reactivity ratios will be determined by multiple methods to verify the tendency for each of the comonomers proposed herein to cross-

propagate with acrylonitrile. The knowledge obtained from Chapters III and IV will be used to down-select three promising PAN copolymers for white fiber spinning and carbonization at Deakin University. In Chapter V, white fiber processing, including draw ratio and coagulation conditions, will be investigated on each of the three down-selected precursors to understand the effect of white fiber processing on white fiber morphologies. The white fiber processing conditions that afforded superior white fiber morphologies and properties were used to down-select three white fibers for thermo-oxidation stabilization and eventual carbonization. The results from this research will lead to new approaches for designing carbon fiber PAN copolymer precursors with optimized exotherm and ring-closing stabilization behaviors from a perspective of copolymer semi-crystallinity control which current scientific literature lacks.

CHAPTER II - EXPERIMENTAL

2.1 Materials

All chemicals were purchased through Sigma Aldrich unless otherwise stated.

The inhibitor mono methyl ether of hydroquinone (MEHQ) in acrylonitrile (AN, 99 %,

35-45 MEHQ ppm) and N-ethyl acrylamide (NEAA, 99 %, 150-400 ppm MEHQ) was

removed prior to use by passing through a short column of neutral aluminum oxide. N,N-

dimethyl formamide (DMF, 99 %), V-70 (Wako Pure Chemical Industries, half live of 10

h), ethylene carbonate (EC, 98 %), CPDT (97 %), azobisisobutyronitrile (AIBN, 98 %),

N-isopropyl acrylamide (NIPAM, 99 %), and N-tert-butylacrylamide (NTAA, 97%) were

used as received. Tetrahydrofuran (THF) was freshly distilled prior to use. The precursor

poly(AN-co-methacrylate) (99.5 AN: 0.5 MA) at a 50 micron particle size was purchased

from Goodfellow Corporation and stored according to the recommended guidelines for

safe storage before usage. This Goodfellow PAN copolymer was used as a control in

Chapter V. Figure 2.1 illustrates the chemical structures of all monomers used in this

dissertation along with abbreviations.
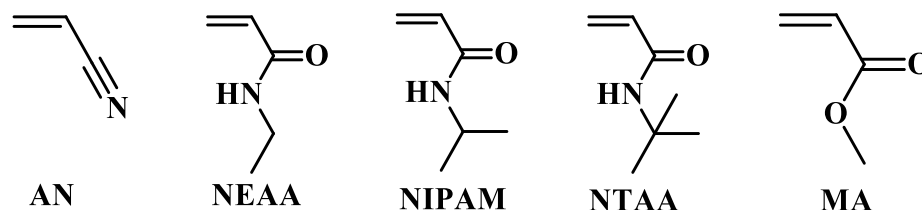
Figure 2.1 Chemical structure of monomers used with abbreviations.

2.2 Methods

2.2.1 Conventional Free Radical Polymerizations

For a typical free radical polymerization a molar ratio of [AN]: [NTAA]: [V-70] =

148: 3: 0.031 was prepared where AN (7.62 g, 20 wt. %), EC (30.47 g, 80 wt. %), NTAA

(0.37 g NTAA dissolved in 1.33 g DMF), and V-70 (0.01 g V-70 dissolved in 1 g THF) was charged to a 100 mL round bottom equipped with a stir bar. A representative free radical reaction scheme is illustrated in Scheme 2.1. Upon addition of the appropriate amounts of reagents, the reaction vessel was sparged for 1 hour with high purity nitrogen over a dewer of liquid nitrogen at 0 °C to remove air and inhibit initiation, respectively. After 1 hour, the reaction was placed into a 30 °C oil bath and stirred for 8 hours. Afterwards, the reaction was removed from the oil bath, exposed to air, and precipitated in a beaker of deionized water and methanol (80: 20 v/v), respectively. The polymer was left in the precipitation beaker for at least 4 hours to aid in EC solvent removal and then collected and dried overnight in a vacuum oven at 60 °C. Upon drying, the polymer was dissolved into DMF (20 wt. % solids) to remove residual solvent and soxhlet extracted with methanol overnight to remove excess DMF.[37]
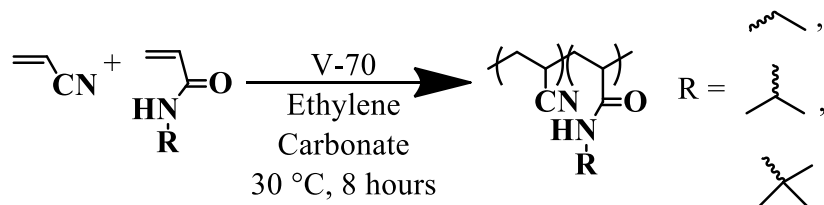
Scheme 2.1 Free radical polymerizations with NEAA, NIPAM, and NTAA comonomers.

2.2.2 RAFT Polymerizations

A common semi-batch RAFT polymerization with a molar ratio of [AN]: [NTAA]: [CPDT]: [V-70] = 9800: 200: 1: 0.67 was prepared as described below, and a typical reaction scheme is displayed in Scheme 2.2. In a 100 mL round bottom equipped with a stir bar, AN (7.62 g, 20 wt. %), EC (30.48 g, 80 wt. %), CPDT (0.005 g, prepared in a stock solution of 0.01 g CPDT in 1 g DMF), and V-70 (0.007 g, prepared in a stock solution of 0.01 g V-70 in 1 g THF) was charged into the reaction vessel. The vessel was

sealed and sparged with high purity nitrogen for 1 hour over a dewer of liquid nitrogen prior to transfer to a 30 °C oil bath. Upon transfer, a solution of NTAA (0.37 g) and DMF (0.66 g) was added to the reaction continuously over 48 hours with a programmable syringe pump; where 48 hour reaction times afforded high molecular weight polymers.[20] After 48 hours, the resulting viscous solution was precipitated and prepared in a similar manner as the aforementioned conventional free radical polymerization procedure.[37] All batch RAFT polymerizations were prepared analogously to the aforementioned semi-batch RAFT polymerization procedure without the use of the syringe pump, instead all comonomers were dissolved in the appropriate amount of DMF and charged into the reaction vessel prior to sparging the reaction solution.
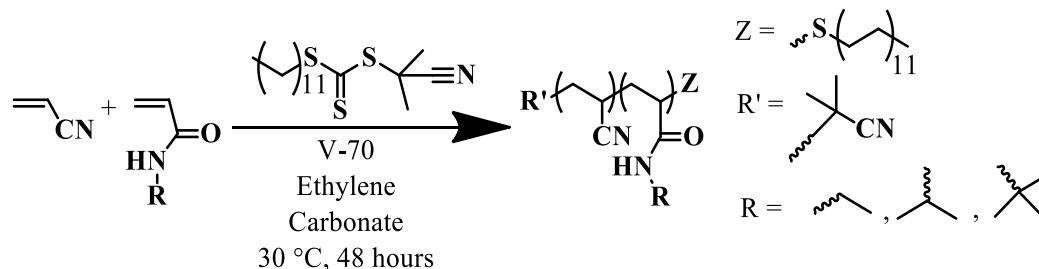
Scheme 2.2 RAFT polymerization with NEAA, NIPAM, and NTAA comonomers.

2.2.2.2 Kinetics of RAFT Polymerizations

At the time intervals of 0, 2, 4, 8, 24, and 48 hours, 1 mL of reaction solution was carefully collected by backfilling the syringe with high purity nitrogen as not to expose the reaction to air, and then analyzed by proton nuclear magnetic resonance (^{1}H NMR). The ^{1}H NMR samples were prepared by dissolving 0.1 g of reaction solution into 0.7 g of deuterated dimethyl sulfoxide (dDMSO). The consumption of AN monomer as the polymerization progressed with time was calculated by integrating the EC peak at 4.50 ppm and comparing it to the AN multiplet between 6.00-6.3 ppm as depicted in the

23

representative ^{1}H NMR in Figure 2.2 of a semi-batch RAFT polymerization containing

NTAA, where EC was used as an internal standard and the EC integration was set to 1.

With the use of a syringe pump in the semi-batch RAFT polymerizations, the comonomer

singlet between 1.2-1.3 ppm increased with time as the syringe pump dispensed more

comonomer into the reaction as displayed in Figure 2.2. As the comonomer integration

varied throughout semi-batch RAFT polymerizations, it was not used in the reaction

progression of $[M]_o$ versus $[M]$ at a given time. The comonomer integration in the [1]H

NMR spectra obtained for free radical and batch RAFT polymerizations did not gradually

increase as observed in semi-batch RAFT polymerizations, because the comonomer in

free radical and batch RAFT reactions was charged into the vessel prior to

polymerization.
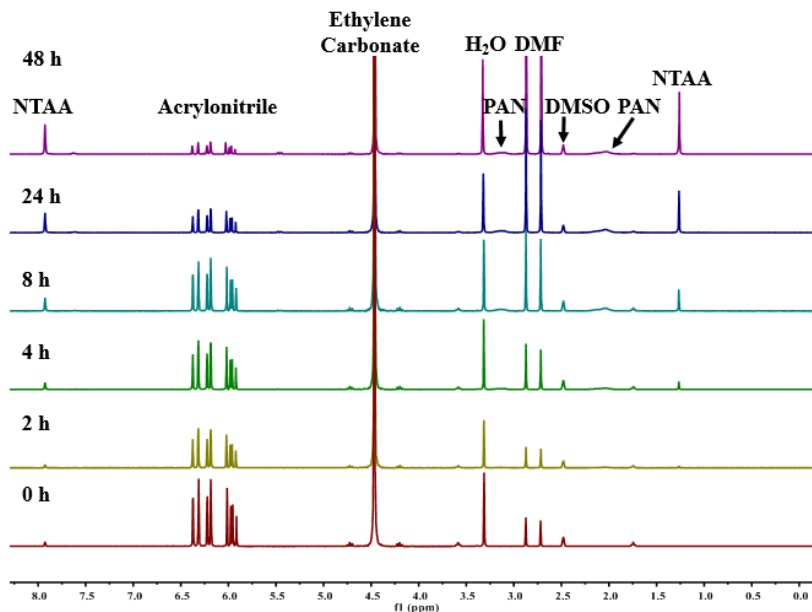
Figure 2.2 ^{1}H NMR of timed intervals with labeled peaks.

Afterwards a kinetic plot of $\ln([M]_o/[M])$ versus time was plotted in Figure 2.3 to

examine the living behavior for RAFT polymerizations, where the kinetic behavior

exhibited pseudo first order kinetics below 24 h and deviated from linearity at 48 h which

corresponded to previous findings.[20,36] Once the kinetic behavior consistently deviated from linearity below 24 h for all RAFT polymerizations, new V-70 initiator was obtained.
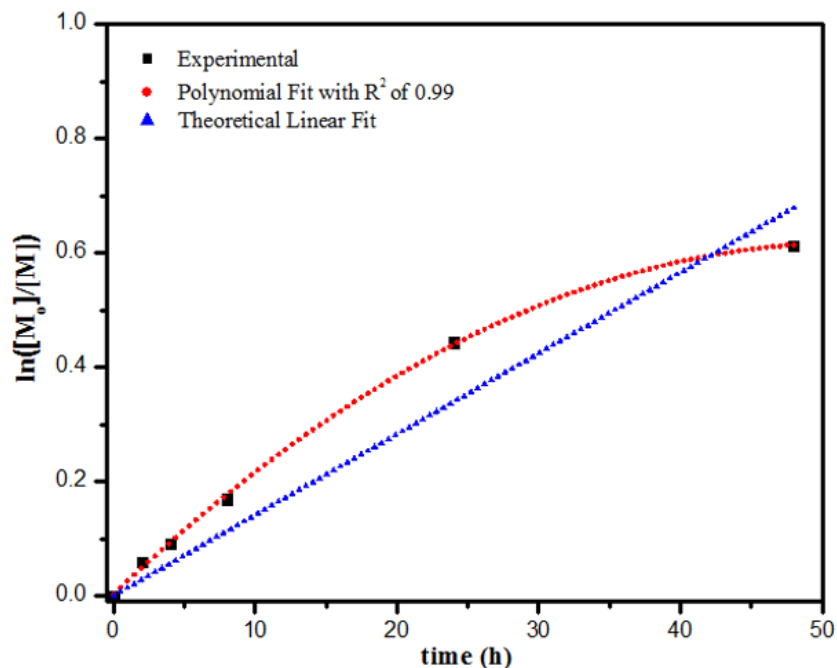
Figure 2.3 Kinetic plot of $\ln([M]_o/[M])$ versus time with polynomial and linear fit.

2.2.3 Preparation of Copolymers for Fiber Spinning

Three copolymers (poly(AN-co-NTAA) (98:2) synthesized by semi-batch RAFT, poly(AN-co-NIPAM) (98:2) synthesized by semi-batch RAFT, and poly(AN-co-NIPAM) (98:2)) were prepared in the necessary 7 to 10 g quantity for white fiber spinning by performing at least four identical polymerizations of the three respective precursors. Multiple reactions of each precursor were performed as attempts to scale up RAFT reactions to greater volumes than ~ 30 g of reaction solution were unsuccessful due to the increased amount of EC solvent that proved to be very difficult to remove. Additionally, 10 g of PAN from Goodfellow Corporation were purchased to be spun into white fiber. Prior to white fiber spinning, the multiple batches of each respective

25

precursor were dissolved into DMSO (20:80 wt. /v %) at 60 °C overnight and then homogenized in a centrifuge mixer.

2.2.4 White Fiber Spinning

White fiber spinning of the previously homogenized copolymer dopes were performed at Deakin University on their experimental fiber line as illustrated in Figure 2.4. All white fibers were spun with a 30 filament tantalum spinneret, coagulation bath temperature at 60 °C, coagulation bath contents of DMSO and H_2O (70: 30 v/v), and 3 washing baths containing 100 % water. The white fibers were dried on two heated godets and no fiber finish was used.

Figure 2.4 White fiber line located at Deakin University.

Two white fiber spinning trials were performed, where the first spinning trial contained the following spinning conditions as depicted in Figure 2.5. In trial one, the uptake roller speed varied from 20, 25, and 30 m/min. as observed in Figure 2.5 to investigate the influence of draw rate on white fiber shape and diameter. Draw ratio was calculated as the velocity of the uptake roller labeled as 8 in Figures 2.5 and 2.6 over the

velocity of the first roller which was always set to 1 m/min.[60] The second white fiber

spinning trial is displayed in Figure 2.6, where gear pump speed varied from 0.16, 0.22,

and 0.33 m/min. to determine the influence of gear pump speed on white fiber

coagulation and properties.
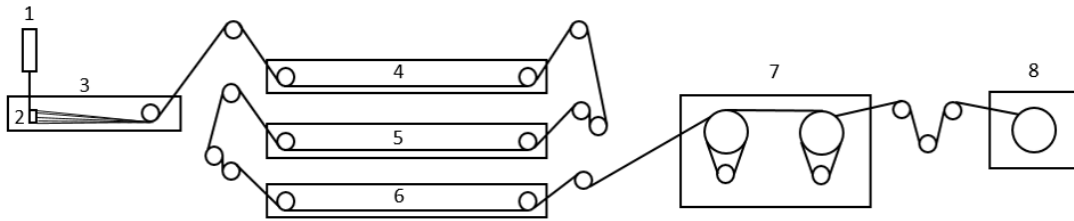
1 – Polymer Spinning Solution in
    DMSO (20 wt. /v %) set at a
    Gear Pump Speed of 0.33
    m/min.
2 – 30 hole Spinneret
3 – Coagulation Bath: 60 °C with
    DMSO and H_2O (70:30 v/v)

4-6 – Washing Baths with 100 % H_2O
7 – Heated Godet 1 at 110 °C
    Heated Godet 2 at 130 °C
8 – Uptake Roller at 20 m/min.
    Uptake Roller at 25 m/min.
    Uptake Roller at 30 m/min.

Figure 2.5 White fiber spinning conditions for the trial 1.
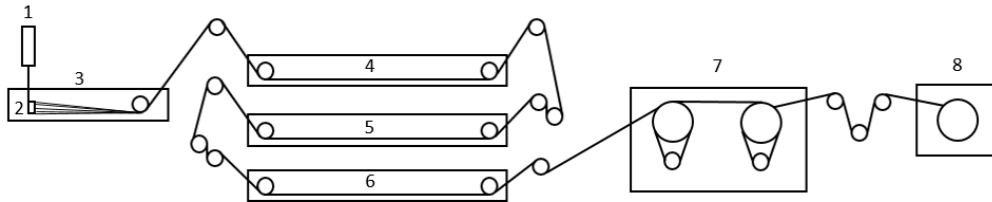
1 – Polymer Spinning Solution in
    DMSO (20 wt. /v %) set
    at a Gear Pump Speed of
      0.16 m/min.
      0.22 m/min.
      0.33 m/min.
2 – 30 hole Spinneret with
3 – Coagulation Bath: 60 °C with
    DMSO and H_2O (70:30 v/v)

4-6 – Washing Baths with 100 % H_2O
7 – Heated Godet 1 at 110 °C
    Heated Godet 2 at 130 °C
8 – Uptake Roller at 25 m/min.

Figure 2.6 White fiber spinning conditions for trial 2.

2.2.5 Oxidized and Carbonized Fiber

Oxidation of previously spun white fiber was performed on the carbon fiber simulator located at Carbon Nexus at Deakin University and is illustrated in Figure 2.7, where the oxidation and carbonization oven are labeled. Two oxidation trials were performed to examine the effect of temperature on PAN ring closing. For the first trial, eight tows of thirty white fiber filaments for a total of 240 individual white fibers from each of the white fibers spun at various spinning conditions were placed into the oxidation oven and exposed to the following heating procedure at 80 % air fan speed: ramp from room temperature to 225 °C followed by a 24 min. isothermal hold, ramp to 235 °C, 24 min. isothermal hold, ramp to 245 °C, 24 min. isothermal hold, ramp to 255 °C, and 24 min. isothermal hold. For the second oxidation trial, all conditions were kept constant except for the temperature, which was changed from 225, 235, 245, 255 °C to 260, 270, 280, 290 °C. The oxidation tension was set below the ultimate break stress of the white fiber as determined by Favimat mechanical testing prior to oxidation and carbonization. In future work, the oxidized fibers will be placed into the carbonization oven and set to the following heating protocol: 2 minute isothermal holds at 450, 650, 850, 1100, and 1400 °C. The final heating temperature of 1400 °C was selected as the maximum carbon fiber simulator temperature was 1450 °C. The carbonization tension will be carefully set under guidance from the Carbon Nexus team.

Figure 2.7 Carbon fiber simulator at Carbon Nexus with labeled oxidation and carbonization ovens.

2.3 Characterization

2.3.1 Structural Analysis

2.3.1.1 Nuclear Magnetic Resonance (NMR) Spectroscopy

^{1}H NMR was performed on a Varian Mercury Plus 300 MHz spectrometer. [1]H

NMR of the dried polymer films were prepared with 0.01 g polymer in 0.7 g of dDMSO.

The experiments were conducted using 32 scans with a 1 second relaxation time.

Copolymer composition was determined by comparing the integration of the methyl

protons on the acrylamide comonomers NTAA at δ= 1.2 ppm, NIPAM at δ= 1.1 ppm, or

NEAA at δ= 1.1 ppm to the protons on the PAN copolymer backbone between δ= 1.6-2.3

ppm. Representative ^{1}H NMR spectra of the precipitated polymers are displayed in

Figure 2.8.
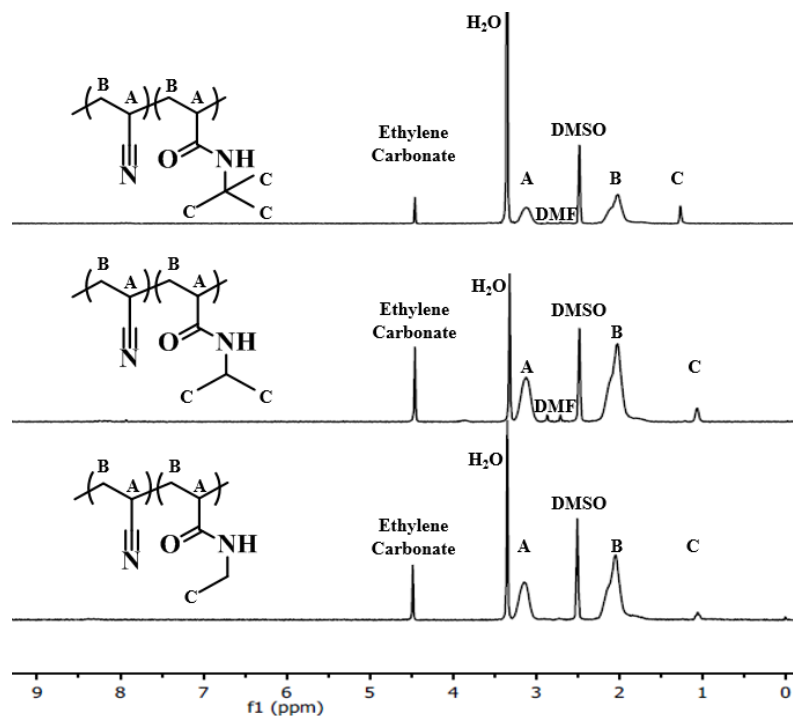
Figure 2.8 ^{1}H NMR of PAN copolymers with (top) poly(AN-co-NTAA) (middle) poly(AN-co-NIPAM) and (bottom) poly(AN-co-NEAA) precursors.
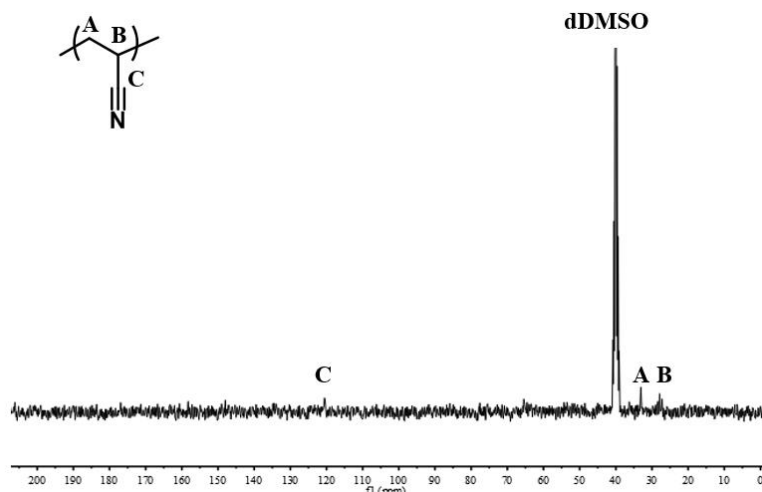
Figure 2.9 ^{13}C NMR of homopolymer PAN with labeled peaks.

^{13}C NMR was also performed on a Varian Mercury Plus 300 MHz spectrometer using 256 scans and 1 second carbon relaxation delay. ^{13}C NMR samples were prepared

with dDMSO at a concentration of 20 mg/mL. Figure 2.9 demonstrates a representative

^{13}C NMR to confirm the synthesis of homopolymer PAN, where the methylene, methine,

and cyano carbons were observed at $\delta= 33$ ppm, $\delta= 27\text{-}28$ ppm, and $\delta= 120$ ppm,

respectively.[61–63]

2.3.1.2 Gel Permeation Chromatography (GPC)

Weight average molecular weight (MW), number average molecular weight (Mn),

and dispersity (Đ) of each PAN precursor were calculated with a Waters Alliance 2695

separations module equipped with a multi-angle laser light scattering (MALLS) detector

fitted with a 20 mW power gallium arsenide laser at 690 nm from MiniDAWN Wyatt

Technology Inc., Optilab DSP interferometric refractometer from Wyatt Technology Inc.,

and two Agilent PL gel mixed C columns attached in series. All GPC samples were

prepared with 10 mg PAN copolymer in 1.5 g DMF (HPLC grade, 0.2 M LiBr) with an

injection volume of 100 µL at 60 °C with a flow rate of 0.5 mL/min. The absolute Mw

was calculated from the MALLS detector with a dn/dc value calculated from the

interferometric refractometer detector, where 100% mass recovery was assumed from

both columns.

2.3.2 Thermal Analysis

2.3.2.1 Differential Scanning Calorimetry (DSC)

Exotherm, activation energy, and collision frequency were determined with a

DSC Q200 TA Instruments equipped with nitrogen purge gas. All DSC experiments were

performed with a sample size between 1.8 to 2.2 mg PAN precursor in hermetically

sealed aluminum pans equipped with a hole punched into the lid at ramp rates of 5, 10,

and 15 °C/ min. to at least 310 °C. The hole in the DSC lid aided in the evolution of off-

gas products. This method allowed the afforded exotherms to possess only one heat flow

value for each temperature and eliminated the acquisition of non-function exotherms. The

energy of activation (E_a) was calculated in duplicate according to the Kissinger and

Flynn-Wall-Ozawa (FWO) method listed below as Equation 1 and 2, respectively, where

R was the universal gas constant, T_p was the peak exotherm temperature in Kelvin, and φ

was the ramp rate temperature in Kelvin. The collision frequency, A, was calculated for

the Kissinger and FWO method from Equation 3.[29,64–66]

$$\frac{-E_a}{R} = \frac{d\left[\ln\left(\frac{\varphi}{T_p^2}\right)\right]}{d\left(\frac{1}{T_p}\right)} \qquad\qquad\qquad \text{Equation 1}$$

$$\frac{-E_a}{R} = 1.052 * \frac{d\left[\ln(\varphi)\right]}{d\left(\frac{1}{T_p}\right)} \qquad\qquad\qquad \text{Equation 2}$$

$$A = \frac{\varphi E_a}{R T_p^2} e^{\frac{E_a}{R T_p}} \qquad\qquad\qquad \text{Equation 3}$$

2.3.2.2 Isoconversional Analysis (ICA)

Activation energy and collision frequency were also analyzed with a model-free

ICA method, where the model used the exothermic data acquired from previously

obtained E_a and A DSC results. The model-free ICA method assumed that throughout the

reaction rate an Arrhenius temperature dependence occurred and that both activation

energy and collision frequency were not constant. Instead E_a and A were treated as

functions of the degree of cure, labeled as α, as presented in Equation 4, where A was the

collision frequency, R was the universal gas constant, and T was temperature.[67] For PAN,

α was considered the progression of ring closure that can vary from 0 which represented

negligible ring closure to 1 that signified complete ring closure.

$$\ln\left(\frac{d\alpha}{dt}\right) = \ln\left(A\left(\alpha\right) * f(\alpha)\right) - \frac{E_a(\alpha)}{RT(t)} \qquad \text{Equation 4}$$

2.3.2.3 Fourier Transform Infrared Spectroscopy (FTIR)

Extent of stabilization (E_s) was determined by FTIR in transmission mode with a Thermo Scientific Nicolet 6700 FTIR equipped with a KBr beam splitter, DTGS KBr detector, nitrogen or air purge, and a collection range between 3500-500 cm^{-1}. All FTIR experimental samples were prepared by dissolving a PAN precursor into DMF (20: 80 wt. %), respectively, and then casting the solution onto a polished NaCl plate. DMF solvent was removed overnight under vacuum at 60 °C prior to running FTIR. Afterwards, the salt plate with the polymer film was placed into the Simplex Scientific Heating attachment and then set into the FTIR, where 64 scans were collected every 5 minutes under the following heating procedure: ramp from room temperature to 225 °C, 24 min. isothermal hold, ramp to 235 °C, 24 min. isothermal hold, ramp to 245 °C, 24 min. isothermal hold, ramp to 255 °C, and 24 min. isothermal hold. This heating procedure mimicked the four heating ovens during thermo-oxidation stabilization at Deakin University.[68] E_s was calculated with Equation 5, where A corresponded to the absorbance of the broad alkene peak at 1590 cm^{-1} over the absorbance of the sharp nitrile peak at 2240 cm^{-1}.[25,29,37] The unreacted CN fraction was calculated with Equation 6, where f was the ratio of absorptivity constants and was equal to 0.29.[37,69,70] The dehydrogenation index was calculated by Equation 7, where the absorbance peaks at 1350 cm^{-1} and 1454 cm^{-1} corresponded to the CH and CH$_2$ stretches, respectively.[71] Cyclization length was calculated by Equation 8, where the cyclic structure absorbance values at 1610 and 1590 cm^{-1} were compared to the nitrile peak at 2240 cm^{-1} and f equaled to 0.29.[72]

$$\text{Extent of Stabilization} = \frac{A_{1590\ cm^{-1}}}{A_{2240\ cm^{-1}}} \qquad\qquad \text{Equation 5}$$

$$\text{Unreated CN Fraction} = \frac{A_{2240\ cm^{-1}}}{A_{2240\ cm^{-1}} + f * A_{1590\ cm^{-1}}} * 100 \qquad \text{Equation 6}$$

$$\text{Dehydrogenation Index} = \frac{A_{1350\ cm^{-1}}}{A_{1454\ cm^{-1}}} \qquad\qquad \text{Equation 7}$$

$$\text{Cyclization Length} = \frac{(A_{1590\ cm^{-1}} + A_{1610\ cm^{-1}}) * f}{A_{1610\ cm^{-1}} * 3} \qquad \text{Equation 8}$$

2.3.2.4 Thermogravimetric Analysis in tandem with Mass Spectroscopy (TGA-MS)

Weight loss and gas evolution was measured using a TGA-MS TA Instruments Discovery series equipped with both nitrogen and air purge gas. All TGA-MS experiments were performed with a sample size ranging from 1.1 to 1.9 mg under the following heating procedure: ramp from room temperature to 225 °C, 24 min. isothermal hold, ramp to 235 °C, 24 min. isothermal hold, ramp to 245 °C, 24 min. isothermal hold, ramp to 255 °C, and 24 min. isothermal hold under air conditions. Afterwards the procedure was switched to nitrogen atmosphere and the sample was ramped from 255 to 800 °C at a 20 °C/min. ramp rate.

2.3.3 Thermo-Mechanical Analysis

2.3.3.1 Rheology

Rheological measurements were collected on a TA Instruments Ares G2 rheometer that was equipped with a parallel plate geometry, where the parallel plates were 40 mm and composed of Peltier plate steel. Prior to analysis, PAN copolymers were dissolved in DMSO (20: 80 wt./v %), respectively, and then tested from 25 °C to 60 °C at a 5 °C/ min. ramp rate with a 0.1 second[-1] shear rate.

2.3.4 Microstructure Analysis

2.3.4.1 X-Ray Scattering

Wide angle X-ray scattering (WAXS) experiments were conducted on a Xeuss 2.0 Xenocs system equipped with a Genix3D source operating at 30 W with a wavelength of $CuK\alpha = 0.1542$ nm for PAN precursor samples. These samples were measured under vacuum to avoid air scatter at a distance of 170 mm with an exposure time of 1 hr. Diffraction peaks and integral areas were collected with a Pilatus 1 M detector and processed using Igor 7 with Nika package. The Bragg Equation was used to calculate domain spacing (d-spacing) as depicted in Equation 9, where λ was the wavelength of $CuK\alpha$ and θ was the Bragg angle.[29,32] The Scherrer Equation, displayed in Equation 10, was used to determine lateral crystallite thickness (L_c), where K was an apparatus constant of 0.9, λ was the wavelength of $CuK\alpha$, B was the full width at half max (FWHM) in radians approximately at $2\theta = 17$, and θ was the Bragg angle.[59,73,74] The qualitative formation of structural order due to cyclic structures was investigated with the Stabilization Index (S_I) via Equation 11, where I_o and I_i were the intensities of the pristine and heated polymers at $\sim 2\theta = 17$.[73,75,76] The heat treated polymers underwent the following temperature protocol: ramp from room temperature to 225 °C followed by a 24 min. isotherm, ramp to 235 °C and 24 min. isothermal hold, ramp to 245 °C and 24 min. isothermal hold, and ramp to 255 °C and 24 min. isothermal hold under air atmosphere.

$$d = \frac{\lambda}{2sin\theta} \hspace{4cm} \text{Equation 9}$$

$$L_c = \frac{K*\lambda}{\beta*cos\,(\theta)} \hspace{4cm} \text{Equation 10}$$

$$S_I = \frac{I_0 - I_i}{I_0} * 100 \hspace{4cm} \text{Equation 11}$$

WAXS and small angle X-ray scattering (SAXS) was also performed on the white fiber bundles containing 30 filaments that were exposed to the various spinning conditions under the guidance of Dr. Peter Lynch and his team at the Australian synchrotron at Monash University. The WAXS and SAXS spectra obtained for the white fiber bundles were collected with an energy of 18 keV, camera length of 617 mm, and wavelength of 0.68880 Angstroms.

2.3.4.2 Scanning Electron Microscopy (SEM)

White fiber cross sections were imaged by SEM and prepared by two methods: (1) immersing the fiber bundles in liquid nitrogen and cutting with a room temperature razor and (2) microtoming. Prior to microtoming, the white fibers were embedded into a Technovit 7100 resin and allowed to cure 24 for hours at room temperature. Upon curing, all white fiber bundles were microtomed with a high profile diamond blade. After the fibers were cross-sectioned by either method, they were then mounted with silver paint and vacuumed overnight prior to sputter coating with 5 nm of gold in an effort to reduce fiber charging. All images were collected on a JOEL JSM 7800f at 5.0 kV.

2.3.4.3 Transmission Electron Microscopy

TEM samples were prepared and conducted at Florida State University (FSU) in collaboration with Dr. Richard Liang's research group. All fiber TEM samples were prepared with a dual beam ThermoFisher Scientific Helios G4 focused ion beam (FIB) and mounted onto a TEM grid with OmniProbe. Images of the fiber cross sectional and longitudinal areas were taken on a JOEL JEM-ARM200cF high resolution TEM at 80 kV to avoid beam damage.[77,78]

2.3.5 Mechanical Analysis

2.3.5.1 Favimat

Single fiber mechanical testing was performed on a Textecho FAVIMAT+ equipped with ROBOT2 at Deakin University's Carbon Nexus facility in Geelong, Australia. All tests were performed with a 210 cN load cell, 4 mm clamp, 25 mm gauge length, and a pretension of 1.1 cN.[28,41] All fibers were tested until failure, and mechanical properties were calculated at approximately five fibers per sample.

CHAPTER III – EFFECT OF PRECURSOR DESIGN ON THE CYCLIZATION BEHAVIOR OF PAN-BASED CARBON FIBER PRECURSORS

3.1 Abstract

Herein a study of the effect of precursor design, including comonomer selection and polymerization method, on PAN thermal ring closure was performed. All polymers were successfully synthesized either by conventional free radical, controlled batch and semi-batch Reversible Addition-Fragmentation Chain Transfer (RAFT) polymerization methods with approximately 2 mole % of NEAA, NIPAM, and NTAA comonomers. RAFT-based copolymers possessed desirable precursor structural properties including molecular weights above 100,000 g/mol and dispersity values below 1.3. The thermal behavior of each precursor was studied with FTIR, DSC, ICA, WAXS, and TGA-MS to highlight the impact of precursor design, including polymerization method and comonomer selection, on ring closure. FTIR and DSC results demonstrated that semi-batch RAFT precursors afforded increased extent of stabilization (E_s) and reduced activation energy (E_a) values as compared to FR precursors. These results suggested that well-defined semi-batch RAFT precursors possess increased ring closure to yield an overall increased graphitic structure and, ultimately, will increase tensile strength compared to their FR counterparts. Further ICA analysis determined that E_a and collision frequency (A) varied as cyclization progressed and invalidated the use of the Kissinger method. Additionally, ammonia and water emissions from TGA-MS provided insights into the thermo-oxidative stabilization mechanism of PAN precursors, where cyclization and dehydrogenation were found to occur simultaneously.

3.2 Results and Discussion

3.2.1 Polymerization of FR and RAFT Precursors

Nine copolymers with ~ 2 mole % of various acrylamide-based comonomers were synthesized by free radical, batch RAFT, and semi-batch RAFT polymerization methods and were abbreviated according to Table 3.1, where a tenth homopolymer precursor was synthesized as a control. All precursors were successfully synthesized and analyzed by ^{1}H NMR, where a representative ^{1}H NMR of copolymers with each acrylamide comonomer was presented in Figure 2.8 of Chapter II and was used to determine copolymer composition according to the aforementioned method.[35] The amount of comonomer incorporation varied from 1.9 to 2.4 mole %, which was in good agreement with the targeted 2 mole % as displayed in Table 3.2. The incorporation of only 2 mole % comonomer was selected as this value is within the typical total comonomer incorporation range and will afford high carbon yields. Additionally, incorporating 2 mole % of comonomer is below the suggested 8 mole % comonomer maximum in literature, where the use of higher comonomer concentrations is expected to limit carbon yields and mechanical properties within the final black fiber.[1,2,12,41]

Table 3.1 Precursor nomenclature and abbreviation.

Comonomer	Polymerization Method	Abbreviation
N-ethyl acrylamide	Free Radical	NEAA FR
N-ethyl acrylamide	Batch RAFT	NEAA BR
N-ethyl acrylamide	Semi-Batch RAFT	NEAA SB
N-isopropylacrylamide	Free Radical	NIPAM FR
N-isopropylacrylamide	Batch RAFT	NIPAM BR
N-isopropylacrylamide	Semi-Batch RAFT	NIPAM SB
N-tert-butylacrylamide	Free Radical	NTAA FR
N-tert-butylacrylamide	Batch RAFT	NTAA BR
N-tert-butylacrylamide	Semi-Batch RAFT	NTAA SB

Table 3.1 (Continued).

No comonomer added	Free Radical	Homopolymer FR

Table 3.2 ^{1}H NMR and GPC results for all PAN-based precursors.

Precursor	Comonomer Incorporation[a] (mole %)	MW[b] (g/mol)	Mn[b] (g/mol)	Đ[b] (MW/Mn)
NEAA FR	2.7	205,900	148,100	1.39
NIPAM FR	1.9	218,700	173,700	1.30
NTAA FR	2.4	196,900	141,400	1.39
NEAA BR	2.1	138,800	114,400	1.21
NIPAM BR	2.2	164,000	141,200	1.17
NTAA BR	2.2	186,200	144,600	1.29
NEAA SB	2.0	188,000	168,300	1.12
NIPAM SB	2.4	210,500	190,000	1.11
NTAA SB	2.3	179,700	144,200	1.25
Homopolymer FR	0	204,500	167,800	1.22

[a]The mole % of acrylamide-based comonomer incorporated into the PAN copolymer backbone was analyzed by ^{1}H NMR. [b] The weight average molecular weight (MW), number average molecular weight (Mn), and dispersity (Đ) was determined by GPC.

DMF GPC analysis afforded the weight average molecular weight (MW), number average molecular weight (Mn), and dispersity (Đ) of each PAN copolymer, which are listed in Table 3.2. Dispersity was calculated as the ratio of MW to Mn. The refractive index shoulders present within NEAA SB, NIPAM FR, and NIPAM FR may suggest a lack of control at lower molecular weight fractions. All PAN polymers possessed molecular weights well above the targeted 100,000 g/mol benchmark recommended for successful white fiber spinning of high performance carbon fiber.[38–40] The higher molecular weight precursors, above 100,000 g/mol, that were prepared here will likely lead to improved fiber mechanical properties as increased copolymer molecular weight will increase white fiber density and reduce the amount of defects or inhomogeneities

within the fiber.[40,79] All dispersity values of precursors prepared by RAFT polymerization were 1.29 or less.

Interestingly, the dispersity values of NEAA FR, NIPAM FR, NTAA FR, and homopolymer FR were lower than anticipated, especially the Đ of 1.22 for homopolymer FR. The GPC mono-modal refractive index traces displayed in Figure 3.1 indicated the presence of one polymer product after synthesis to suggest minimal chain transfer for both RAFT and FR precursors.[62] These low Đ values that were reported in Table 3.2 may stem from the GPC measurements being performed on precursors after precipitation thereby removing polymers that significantly deviated in Mw. A similarly low Đ value of 1.33 was reported by Rwei and coworkers with a PAN precursor prepared by solution free radical polymerization. Furthermore, Rwei and coworkers speculated that the Trommsdorff effect could influence Đ values due to inadequate heat dissipation within the reaction solution, where the diffusion of macro-radicals that could participate in chain transfer and termination was hindered.[62]

During the synthesis of the ten precursors within this chapter, it was noted that FR polymerizations became more viscous as reaction time progressed in comparison to RAFT polymerizations. Increased viscosity and gelation can occur in conventional solution free radical polymerizations due to intermolecular chain transfer between polymer chains to afford long chain branching.[80] It was thought that the increased viscosity within each FR precursors was due to the formation of long chain branches, despite the mono-modal RI traces and decreased dispersity values from GPC. Results from Bol'bit and coworkers determined that long chain branches were still present in solution free radical polymerization with decreased Đ values as compared to emulsion

polymerization.[81] Additionally, Bol'bit et al. discussed that as conversion increased, chain mobility decreased due to an increase in copolymer chain entanglement points, which hindered the macro-radical to participate in termination as similarly discussed by Rwei and coworkers.[62,81] Therefore, the reduced Đ values here were thought to be due to the presence of long chain branches within the free radical precursor, which increased viscosity and entanglement points as the reaction progressed as well as limited macro-radical termination. However, the diffusion of small monomers to grow the polymer chain was not inhibited as high MW polymers were observed in Table 3.2.
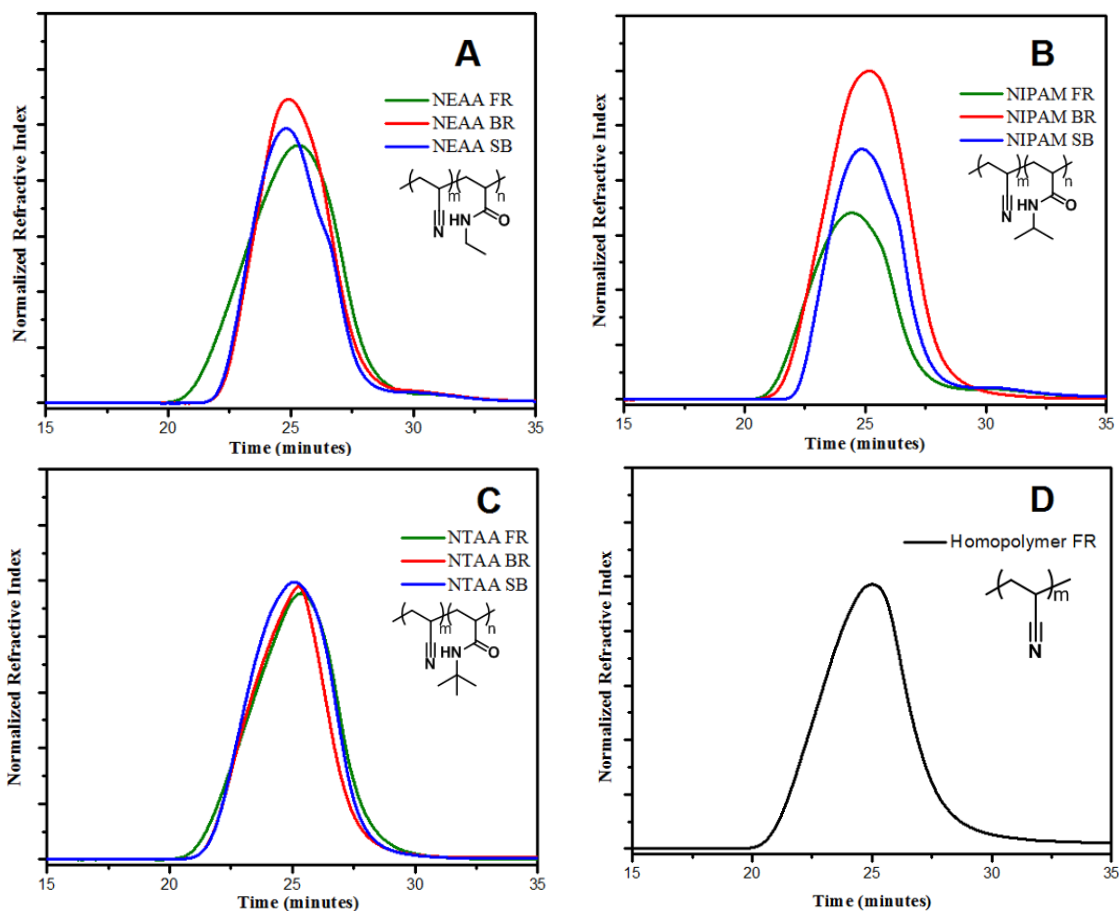
Figure 3.1 RI GPC traces for A) poly(AN-co-NEAA) B) poly(AN-co-NIPAM) C) poly(AN-co-NTAA) and D) Homopolymer precursors polymerized by FR, BR, or SB methods.

42

3.2.2 WAXS Diffraction Patterns and Microstructure Properties

WAXS was performed on all pristine, i.e. non-heated precursors, to investigate the PAN microstructure including crystalline and amorphous domains. The 2D diffraction patterns and 1D 2θ plots were collected and displayed in Figure 3.2 and 3.3, respectively. In Figure 3.3, the distinct peak at $\sim 2\theta = 17°$ was attributed to the (100) reflection of the hexagonal crystal lattice of PAN and the broad amorphous peak was observed $\sim 2\theta = 25.5°$.[37,73,74,82,83] The peak at $\sim 2\theta = 17°$ was due to the strong intra-molecular dipole-dipole interactions of the nitrile pendent groups along the copolymer backbone.[84] Intensity values were normalized to the respective sample thickness in Figure 3.3, as a thicker sample would scatter more and lead to increased intensity values.

SB
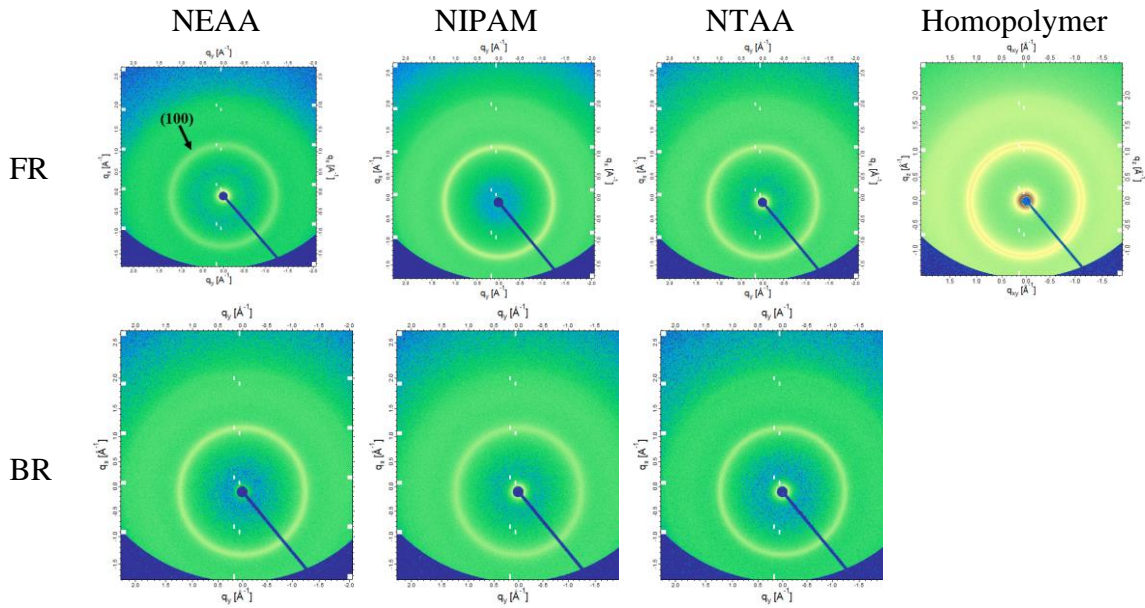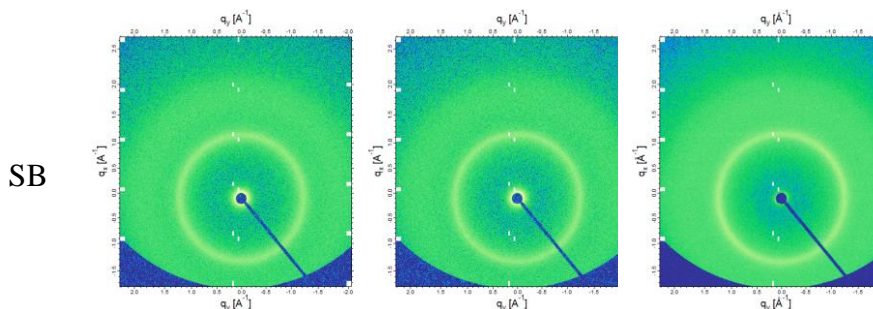
Figure 3.2 WAXS diffraction patterns of pristine PAN copolymer precursors.
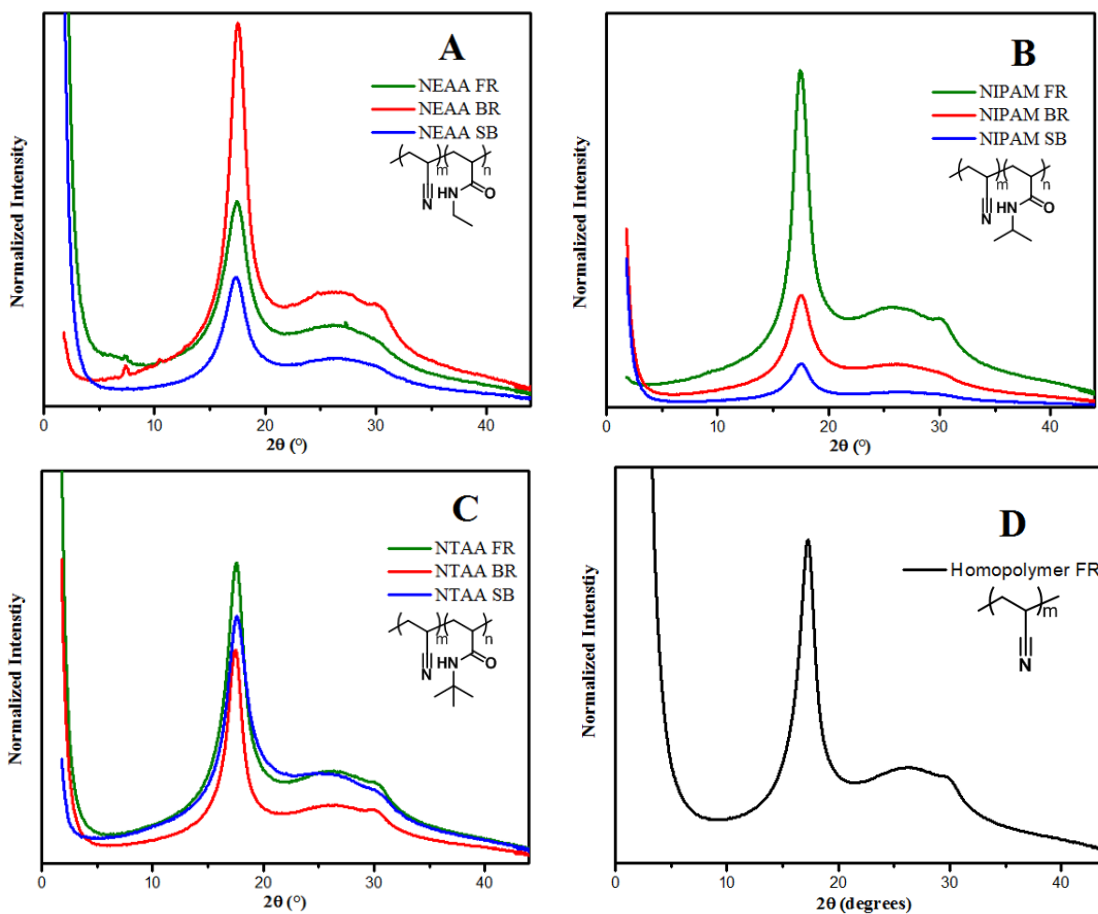
Figure 3.3 Plot of 2θ vs. intensity for A) poly(AN-co-NEAA) B) poly(AN-co-NIPAM) and C) poly(AN-co-NTAA) and D) Homopolymer precursors prepared by FR, BR, or SB methods.

The domain spacing (d-spacing) and crystallite thickness (L_c) were calculated via the Bragg and Scherrer Equations and recorded in Table 3.3, where the Bragg Angle (θ) and full width at half max (FWHM) were used in these calculations.[29] The domain spacing values were similar to literature findings of 0.52 nm, whereas the crystallite sizes

44

were larger than expected.[37,73] The increase in crystallite size is likely due to the high molecular weight of each precursor, where increased precursor molecular weights would also increase the amount of steric repulsion of the nitrile groups along the polymer backbone to afford an increase in crystallite size.[20,85] Additionally, the increased crystallite size is also suggested to be due to the incorporation of bulky acrylamide comonomers that increased steric repulsion as well. From the WAXS data, the presence of the (100) hexagonal crystal lattice reflection indicative of PAN precursors was confirmed as this reflection was observed as a band in WAXS diffraction pattern in Figure 3.2 and in Figure 3.3 at ~ $2\theta = 17°$. Continued WAXS analysis will be reported in Chapter IV to investigate the structural changes within the crystallites as precursors were exposed to thermo-oxidative stabilization conditions.

Table 3.3 WAXS data of pristine PAN copolymer precursors.

Precursor	2θ (°)	FWHM	d-spacing (nm)	L_c (nm)
NEAA FR	17.43	0.1653	0.509	50.81
NEAA BR	17.53	0.1185	0.506	70.87
NEAA SB	17.43	0.16031	0.509	52.38
NIPAM FR	17.43	0.1126	0.509	74.60
NIPAM BR	17.51	0.1568	0.506	53.55
NIPAM SB	17.51	0.1493	0.506	56.25
NTAA FR	17.60	0.1316	0.504	63.83
NTAA BR	17.51	0.1113	0.506	75.46
NTAA SB	17.60	0.1334	0.504	56.25
Homopolymer FR	17.27	0.1315	0.513	5.06

3.2.3 Thermal Behavior of PAN Precursors

After the successful polymerization and structural confirmation of the ten precursors prepared with various acrylamide comonomers and polymerization methods, their thermal behavior was examined. The thermal ring closing behavior of each precursor was analyzed via FTIR, DSC, and TGA-MS to further elucidate the effect of precursor design on ring closing efficiencies. The knowledge gained from the interdependencies of precursor design and thermal behavior will aid in the selection of which comonomer(s) and polymerization method(s) will afford superior ring closing structures that is anticipated to improve fiber morphologies and mechanical properties.

3.2.3.1 FTIR Cyclization Behavior

Real-time FTIR was used to track the ring closure of PAN throughout thermo-oxidative stabilization conditions, where the extent of cyclization also known as E_s, length of cyclization, unreacted acrylonitrile fraction, and dehydrogenation index was calculated according to literature.[25,28,29,37,72,86] A representative *in situ* FTIR plot of homopolymer FR that was exposed to thermo-oxidative stabilization (TOS) heating conditions under nitrogen and air atmosphere is illustrated in Figure 3.4. This heating procedure ranges from room temperature to 255 °C and is well within the TOS range utilized throughout processing stabilized carbon fiber.[87]
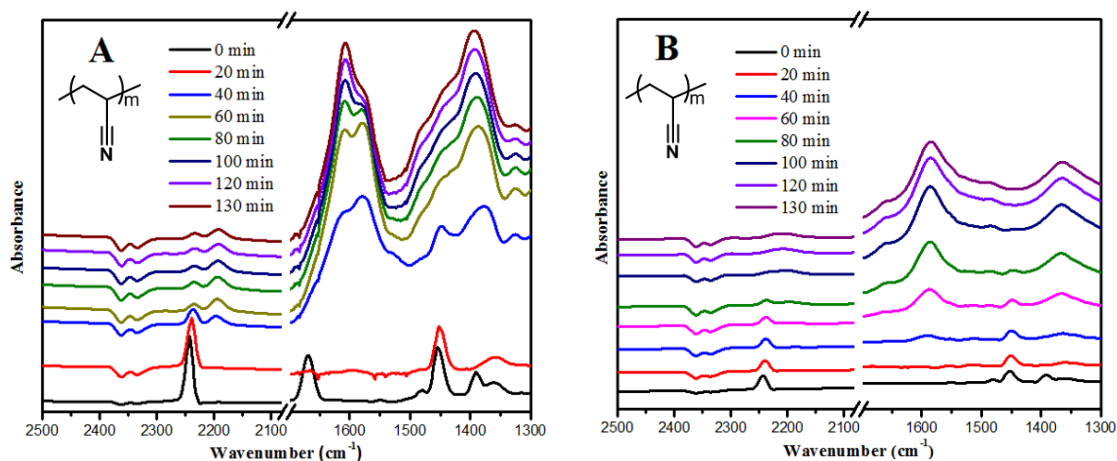
Figure 3.4 Representative FTIR spectra throughout TOS conditions under A) nitrogen and B) air.

Prior to heating at 0 min., a pronounced peak at approximately 2240 cm^{-1} was observed, which corresponded to the nitrile peak from the acrylonitrile groups along the polymer backbone in Figure 3.4 A) and B). Additionally, the lack of a peak at 1590 cm^{-1}, at 0 min. in Figure 3.4, suggested that negligible ring closure had occurred prior to heating under nitrogen or air atmosphere as this peak corresponds to the formation of C=C, C=N, and N-H bonds. As the polymer film was heated, a broad peak at approximately 1590 cm^{-1} appeared at 40 min. and indicated that ring closure had begun.[9,37,88] Furthermore, at 40 min. a small band at 2195 cm^{-1} formed and was indicative of the α, β- unsaturated nitrile groups.[89–91] As temperature increased, the band at 1590 cm^{-1} continued to increase in intensity, while the band at 2240 cm^{-1} gradually decreased. This plot highlighted that as temperature and time progressed, the ring closure along the polymer backbone continued as well.
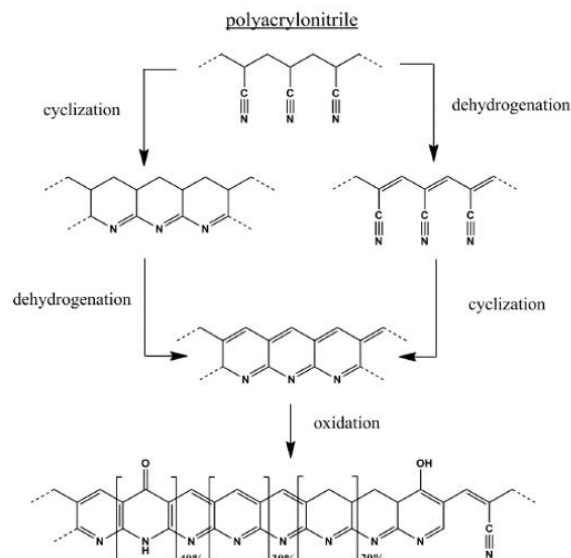
Figure 3.5 Ring closure of PAN during thermo-oxidative stabilization.[48]

The influence of TOS atmosphere (nitrogen or air) on the ring closure mechanism of PAN was also investigated by FTIR. The ring closure mechanism of PAN during TOS can be observed in Figure 3.5.[48] Under inert atmosphere, dehydrogenation cannot occur as oxygen is required for this reaction to ensue; therefore, it is effectively removed and the PAN ring closing mechanism is attributed to cyclization and oxidation only.[46] Then upon ring closing under air, the PAN mechanism can proceed via dehydrogenation, cyclization, and oxidization.[46,48] During dehydrogenation the CH_2 band at 1454 cm^{-1} was consumed and converted into a CH moiety, which was detected at 1350 cm^{-1} in Figure 3.4.[71] From Figure 3.4 B as time increased, the CH_2 stretch reduced and the CH peak increased to signify that dehydrogenation had occurred. This trend was not observed under nitrogen atmosphere as anticipated due to the lack of oxygen required for water to be released.

From FTIR, the extent of stabilization, also known as E_s, values were calculated and plotted in A1, B1, and C1 of Figure 3.6 under both air and nitrogen atmosphere. In

48

general, the unitless E_s values can be thought of as the relative amount of ring closure via cyclization or dehydrogenation that occurred in the polymer chains, where increased E_s values signify a desirable ring-closed graphitic structure which may lead to improved stabilized and carbonized fibers. Under inert atmosphere, E_s values rapidly increased around 25 min. and then gradually plateaued; whereas, under air atmosphere the E_s values increased to a maximum and rapidly decreased. These variations in E_s behavior suggested that under inert conditions, complete ring closure was not achieved; whereas, under air conditions, the sharp decrease after the E_s maxima may have implied that ring closure was complete and could not progress further, likely due to a lack of available pendent nitrile groups or mobility within the structure to continue to ring close. Pendent nitrile availability after exposure to TOS conditions under both N_2 and air was investigated by calculating the unreacted nitrile % as depicted in A2, B2, and C2 in Figure 3.6. Under oxidative conditions, the unreacted CN fractions were lower and possessed higher maximum E_s values as compared to each respective copolymer under inert atmosphere, confirming that oxidative conditions increased the amount of ring closure.

49
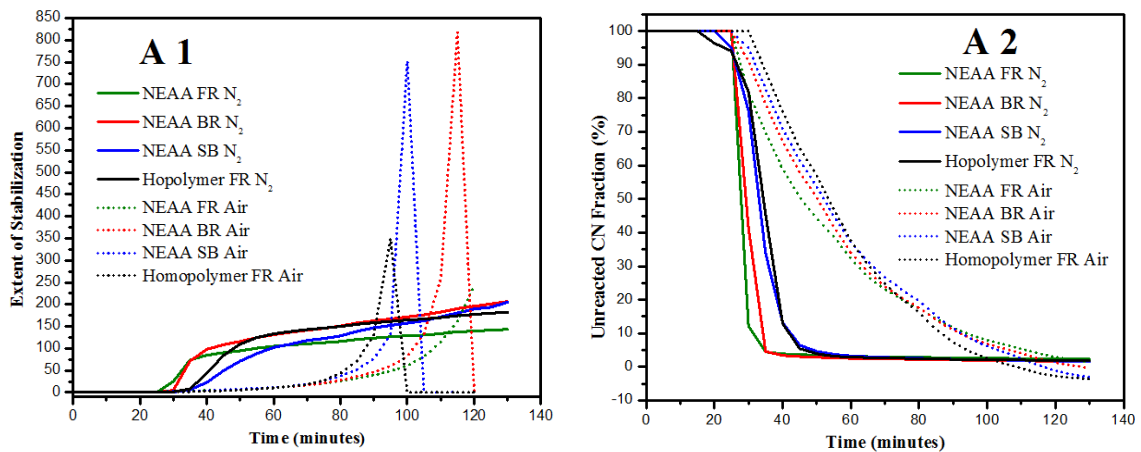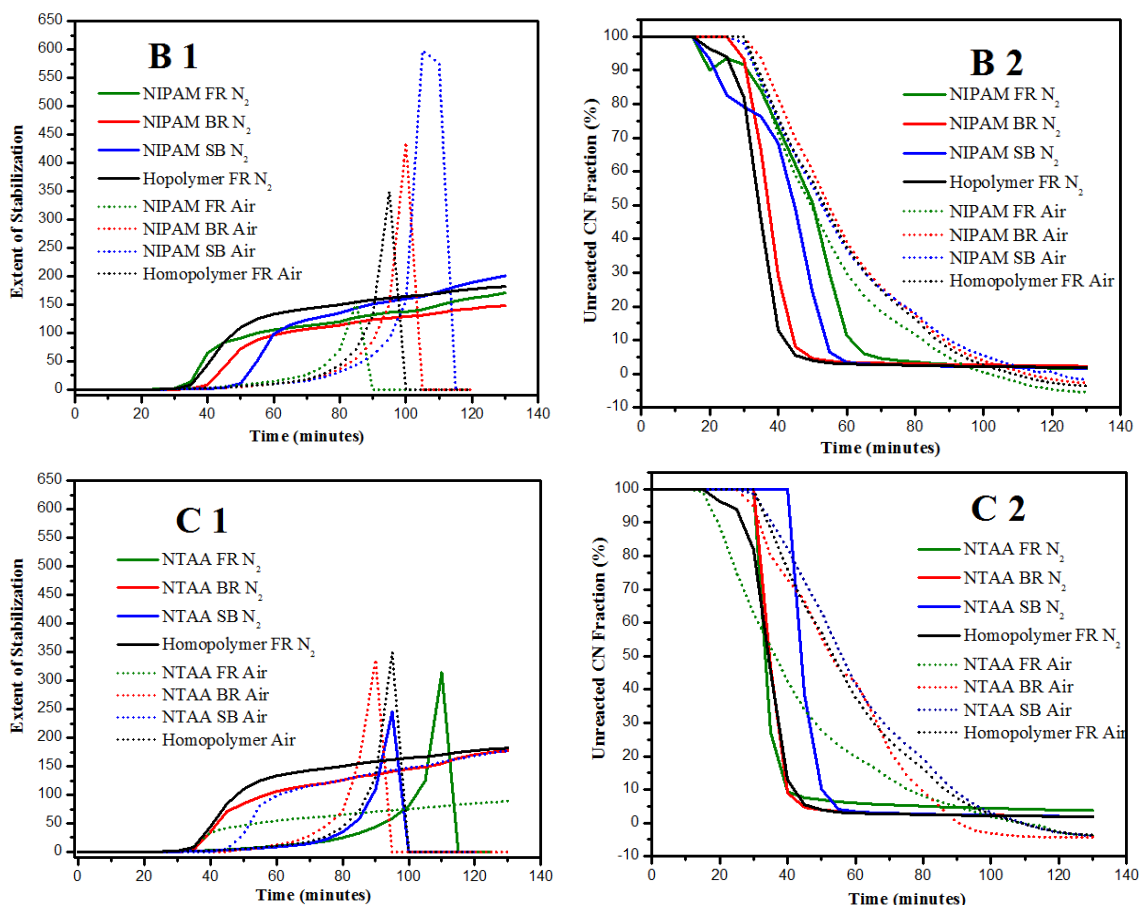
Figure 3.6 FTIR results for 1) E_s and 2) Unreacted CN Fraction nitrogen for A) poly(AN-co-NEAA) B) poly(AN-co-NIPAM) and C) poly(AN-co-NTAA) precursors as compared to the Homopolymer FR.

E_s values under atmospheric conditions were also significantly higher due to the ability of the precursor to ring close via dehydrogenation and oxidation reactions which resulted in an overall increased graphitic structure as compared to ring closure under inert atmosphere. The dehydrogenation index was calculated for precursors exposed to inert and oxidative conditions as listed in Table 3.4, where the values noted were recorded from the end of the heating profile. Additionally, Table 3.4 summarized all FTIR data by reporting the maximum E_s values and unreacted CN fraction values under both purge gas conditions. Here, negative dehydrogenation values indicated that minimal dehydrogenation occurred. These negative dehydrogenation index values were expected

50

for the FTIR trials conducted under nitrogen due to the lack of oxygen required for dehydrogenation. Increased dehydrogenation index values under oxidative conditions were recorded for FR to indicate more dehydrogenation occurred than in BR or SB precursors. However, SB precursors afforded higher E_s values than FR precursors under inert conditions and oxidative conditions, with the exception of NTAA SB. Therefore, more cyclization reactions occurred which may be the result of decreased dispersity that allowed for more neighboring CN moieties to cyclize. It is anticipated that white fibers spun, oxidized, and carbonized from SB precursors would afford increased black fiber tensile strength values due to the increased E_s values, suggesting that the carbon fiber structure would be more graphitic in nature because of an increase in cyclized rings.

Table 3.4 Summary of FTIR data under nitrogen and air conditions for PAN copolymers.

Precursor	E_s	Unreacted CN Fraction (%)	Dehydrogenation Index
NEAA FR N_2	143.3	2.4	-0.8
NEAA BR N_2	206.7	1.6	-1.2
NEAA SB N_2	205.0	1.7	-6.3
NIPAM FR N_2	170.7	1.5	-0.7
NIPAM BR N_2	145.0	2.3	-1.4
NIPAM SB N_2	200.0	1.7	-2.5
NTAA FR N_2	89.3	3.7	-0.4
NTAA BR N_2	177.1	1.9	-3.7
NTAA SB N_2	177.1	1.9	-11.0
Homopolymer FR N_2	181.8	1.9	-0.2
NEAA FR Air	243.0	1.4	28.4
NEAA BR Air	818.2	-0.3	21.8
NEAA SB Air	753.0	-3.1	22.4
NIPAM FR Air	154.2	-5.4	43.4
NIPAM BR Air	435.8	-2.7	26.2
NIPAM SB Air	575.6	-1.7	17.4
NTAA FR Air	313.9	-3.8	26.7
NTAA BR Air	336.2	1.0	44.9
NTAA SB Air	244.7	-3.8	14.4
Homopolymer FR Air	349.2	-3.6	13.3

Interestingly, NEAA and NIPAM SB copolymers that were exposed to air and N_2 displayed higher E_s values than homopolymer FR, where it was anticipated that homopolymer FR would possess the highest E_s value as ring closure is not impeded by comonomers. However, cyclization of homopolymer PAN is known to possess a high heat of exotherm due to the lack of heat dissipation via the ionic ring closing mechanism afforded by acidic comonomers.[8,9,25,26] This rapid evolution of heat likely caused polymer degradation via chain scission within homopolymer FR precursor and afforded a lower E_s value in comparison to SB copolymers.[39,45] The exotherm of homopolymer FR will be examined via DSC to further investigate the cause of its reduced E_s value.

3.2.3.2 DSC Cyclization Behavior and Kinetic study of E_a and A

The cyclization behavior of each precursor including exotherm, activation energy also denoted as E_a, and collision frequency also known as A was performed by DSC. Figure 3.7 displays the overlaid exotherms of each precursor at 10 °C/min. under nitrogen atmosphere. The exothermic behavior of a traditional acidic comonomer is broad and affords multiple exothermic events due to ring closure proceeding through both ionic and free radical mechanisms; conversely, neutral comonomers typically possess a single sharp exothermic peak signifying a free radical closing mechanism. The broad and multi-modal exothermic behavior of acidic comonomers was not observed in Figure 3.7, which suggested that all acrylamide containing copolymers exhibited neutral comonomer exothermic behavior rather than acidic.[9,92] Previous research suggested that the incorporation of the NIPAM comonomer would lead to an ionic ring closing mechanism

through the available amide functionality; however, the mono-modal exotherm curve in this report signified that the free radical ring closure mechanism dominated.[35] It was suspected that strong nucleophilicity of the amide moiety may have inhibited the comonomer's ability to participate in the ionic ring closing mechanism traditionally exhibited by acidic comonomers.[20]
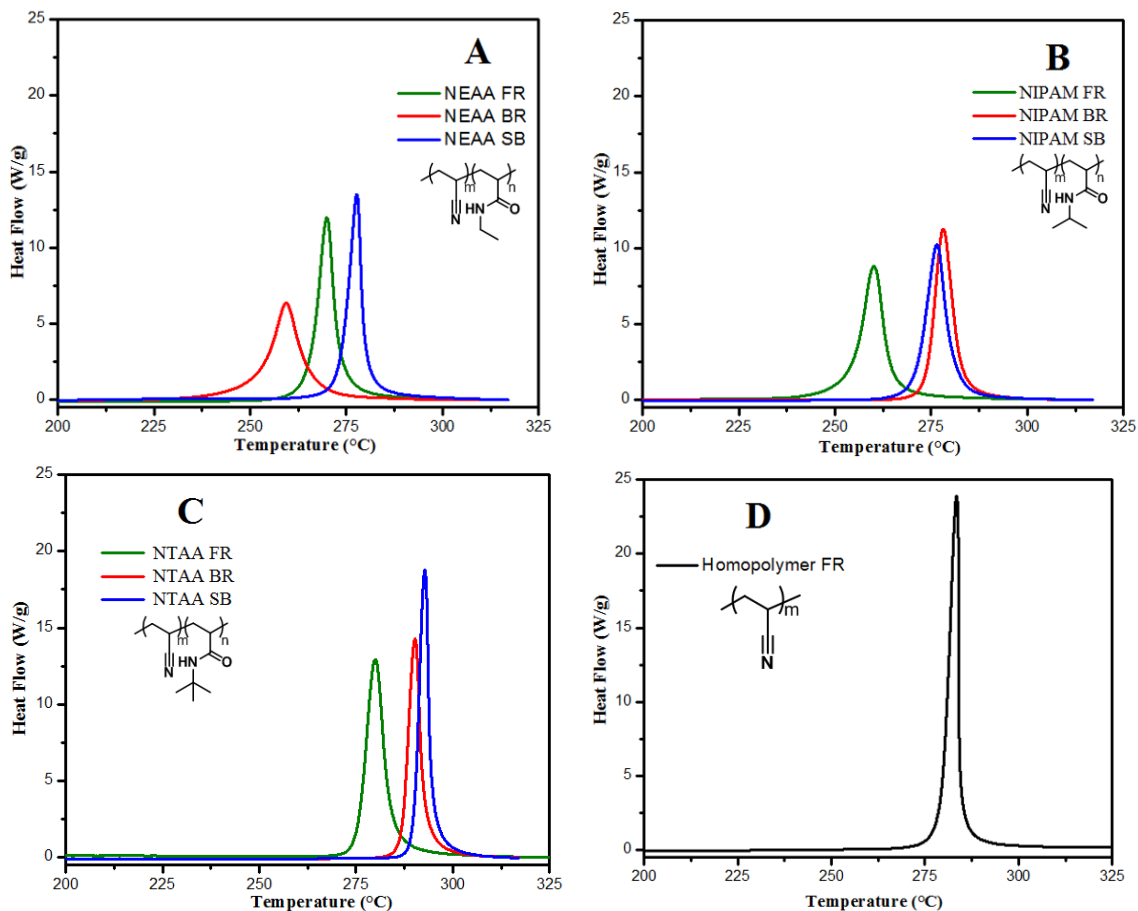
Figure 3.7 DSC exotherm curves for A) poly(AN-co-NEAA) B) poly(AN-co-NIPAM) C) poly(AN-co-NTAA) and D) Homopolymer precursors heated at 10 °C/min.

From Figure 3.7, FR precursors with the exception of NEAA FR possessed lower exothermic temperatures as compared to their RAFT counterparts. The lower molecular weight of NEAA BR may have reduced the exotherm temperature. These lower exotherm temperatures indicated that cyclization would occur earlier in FR precursors than RAFT

53

highlighting that the polymerization method could have a significant influence on thermal behavior such as exotherm due to MW and Đ variations inherent to the polymer backbone. No apparent trend in exotherm behavior was noted for BR precursors possibly due to compositional drift or a compositional gradient of comonomers along in the PAN copolymer backbone that can occur in batch polymerization.[44] This compositional gradient may lead to morphological defects and thus decreased mechanical properties; therefore, BR precursors will likely be removed from consideration for white fiber spinning.[20]

It is reasonable to consider that earlier onset temperatures would yield precursors with increased graphitic structure due to earlier cyclization; however, this consideration did not hold true for the FR precursors. The impurities within the FR copolymers are believed to have caused the reduced cyclization onset temperature, and afforded increased cyclization according to DSC.[37] These impurities can arise from unwanted intermolecular or intramolecular chain transfer to the polymer which would yield either long or short chain branching, respectively. Branching is known to occur in conventional free radical polymerizations. These long chain branches hinder the reputational motion of the polymer and can eventually cause unwanted gelation.[37,80] The reduced E_s values, from FR copolymers, suggested that overall cyclization was reduced. Therefore, by coupling the DSC and FTIR results, these impurities are hypothesized to be: (1) a point from which cyclization could propagate to lead to a reduced exotherm onset temperature and (2) a point which could inhibit the extent of PAN ring closure. Future rheology experiments to investigate the nature of these impurities is necessary as solution prepared FR copolymers can possess long polymer chain branches of high molecular weight

54

fractions and gels, likely due to free radical mechanism that affords increased Đ, which is anticipated to reduce the processability of these precursors when spun into fiber and the overall graphitic structure of PAN upon ring closure.[37,81,93]

Both NEAA and NIPAM containing precursors possessed lower cyclization temperatures ranging from about 255 to 280 °C, whereas the NTAA containing precursors cyclized at higher temperature range of 275 to 300 °C. This cyclization temperature difference may be due steric bulk of the tert-butyl group requiring more energy to allow for cyclization to occur or the NEAA and NIPAM may possess similar reactivity ratios to yield similar polymer architectures that ring close at comparable temperatures. Additionally, the bulky tert-butyl pendent group on NTAA yielded increased onset cyclization temperatures, whereas the less bulky ethyl and isopropyl groups in NEAA and NIPAM, respectively, lead to similar cyclization onset temperatures. These exotherm results demonstrated that both NEAA and NIPAM precursors cyclized at earlier temperatures than NTAA copolymers which could lead to both NEAA and NIPAM copolymers possessing more cyclized structures in the final fiber morphology, increasing overall tensile strength. FTIR analysis supported these findings, particularly with NIPAM SB and NEAA SB, where these precursors possessed higher E_s values than NTAA SB. Although, this trend was not observed for FR precursors likely due to the presence of impurities as previously discussed.

The heat release rates were also calculated by integrating the heat release from each exothermic event and dividing by the time difference between the exothermic offset and onset in Figure 3.8, where the commercially available BlueStar white fiber heat release rate was approximated from results by Khayyam and coworkers.[56] A lower heat

release rate signified a controllable cyclization, alleviated localized heat release, and reduced probability of premature heat degradation via chain scission within the copolymer backbone.[8,26] From Figure 3.8, homopolymer FR yielded the highest heat release rate as expected due to cyclization occurring rapidly over a short amount of time, which further suggested that chain scission may have occurred and afforded a reduced E_s value from FTIR as compared to other RAFT-based precursors. The heat release rate for BR precursors seemed to be higher than FR precursor but lower than SB precursors with the exception of NEAA BR. It is believed that the lower molecular weight of NEAA BR in comparison to NEAA FR and NEAA SB, reduced the heat release rate of NEAA BR. SB precursors possessed higher heat release rates as compared to FR counterparts. The higher exothermic intensities and heat release rates are likely caused by a greater amount of molecular alignment of the PAN polymer chains due to a decrease in Đ values, which lead to higher E_s values. Additionally, all acrylamide containing precursors possessed high heat release rates as compared to commercially available BlueStar which further suggested that these comonomer behavior exhibited neutral comonomer behavior. Careful selection of SB precursors will be necessary as these high exothermic intensities and heat release values can rupture polymer chains and lead to morphological defects in the fiber, reducing mechanical properties.[26]
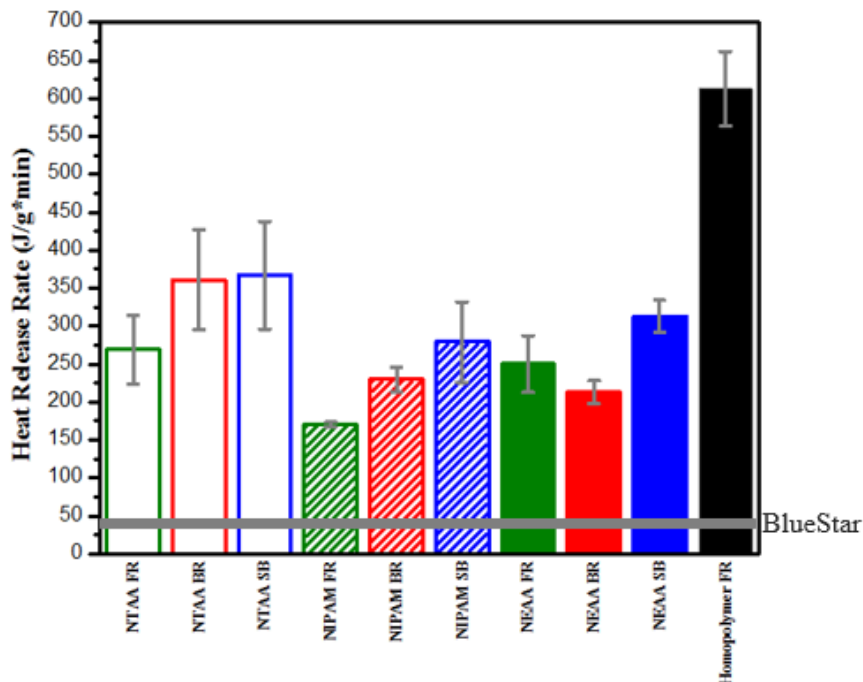
Figure 3.8 Heat release rate for PAN copolymers and Homopolymer FR.

A kinetic study of E_a and A was conducted by DSC and analyzed with the

Kissinger and Flynn-Wall-Ozawa (FWO) method, where ramp rates of 5, 10, 15 °C/min.

were used, and the calculated values are listed in Table 3.5. The E_a and A values from the

Kissinger and FWO method agreed well with each other. SB RAFT precursors afforded

equal or lower E_a and A values than the FR-based precursors, which was similar to

previous findings.[37] NEAA SB and NTAA SB also exhibited significantly lower E_a

values as compared to the E_a of 139.22 kJ/mol for BlueStar.[56] The lower E_a values for SB

precursors implied that the cyclization reactions occur more readily to afford an overall

increase in graphitic structure upon heating due to the reduced energy barrier. These

lower E_a values complimented both the E_s and heat release values from FTIR and DSC to

highlight that the reduced E_a values in SB precursors allowed for increased cyclization as

noted by the increased DSC heat release rates and FTIR E_s values. The increased

collision frequencies in the FR precursors may be due to the impurities or long polymer

chain branches that FR polymerizations are known to possess, which would give rise to more cyclization sites.[37,81,88] Additionally, all FR precursors had higher molecular weights as compared to their respective BR or SB precursors which also may have increased the number of cyclization sites and A factor.

Table 3.5 Activation energies and collision frequencies determined by the FWO and Kissinger methods.

Precursor	FWO Method		Kissinger Method	
	E_a (kJ/mol)	A (sec^{-1})	E_a (kJ/mol)	A (sec^{-1})
NEAA FR	96.7	2.7×10^{15}	92.6	6.9×10^{14}
NEAA BR	178.8	4.2×10^{30}	179.2	5.9×10^{30}
NEAA SB	96.7	8.4×10^{13}	92.6	1.7×10^{13}
NIPAM FR	200.8	4.0×10^{40}	202.4	1.9×10^{41}
NIPAM BR	149.6	3.8×10^{28}	148.1	4.7×10^{28}
NIPAM SB	157.6	1.8×10^{28}	156.7	1.8×10^{28}
NTAA FR	98.7	2.2×10^{14}	94.5	4.7×10^{13}
NTAA BR	120.2	3.4×10^{17}	117.2	1.2×10^{17}
NTAA SB	93.4	3.9×10^{12}	89.4	7.2×10^{11}
Homopolymer FR	144.6	1.2×10^{24}	143.0	1.0×10^{24}

It is important to acknowledge the limitations of the Kissinger and FWO methods as both of these methods calculate a single composite E_a value, and more specifically the Kissinger method assumes that E_a does not vary. Within this chapter, the Kissinger method was applied with caution until the assumption that E_a did not vary was made apparent.[94] It is reasonable to assume that during thermo-oxidative stabilization, multiple E_a values would be present due to several simultaneous or near simultaneous reactions ie cyclization, dehydrogenation, and oxidation. Therefore, a model-free iso-conversional analysis method, also known as ICA, was used to investigate if E_a and A varied under TOS conditions as well as to determine if the Kissinger assumption held true. This model

was developed by Anders et al. and allowed the variables E_a an A to vary with respect to α and only assumed that the reaction rate obeyed an Arrhenius type temperature dependence, where α was considered the progression of PAN ring closure or cure that can vary from 0 which represented negligible ring closure to 1 that signified complete ring closure. Additionally, this method does not require any previous knowledge of the mechanism, which is beneficial as the thermo-oxidative stabilization mechanism is complex.[67] The model-free ICA method was applied to the exotherm data gathered from DSC and compared in Figure 3.9 for homopolymer FR. The model-free ICA method was found to fit the experimental data well throughout cure progression, depicted by the comparison of the solid to dotted lines in Figure 3.9 A and the high R^2 value throughout cure in Figure 3.9 B.
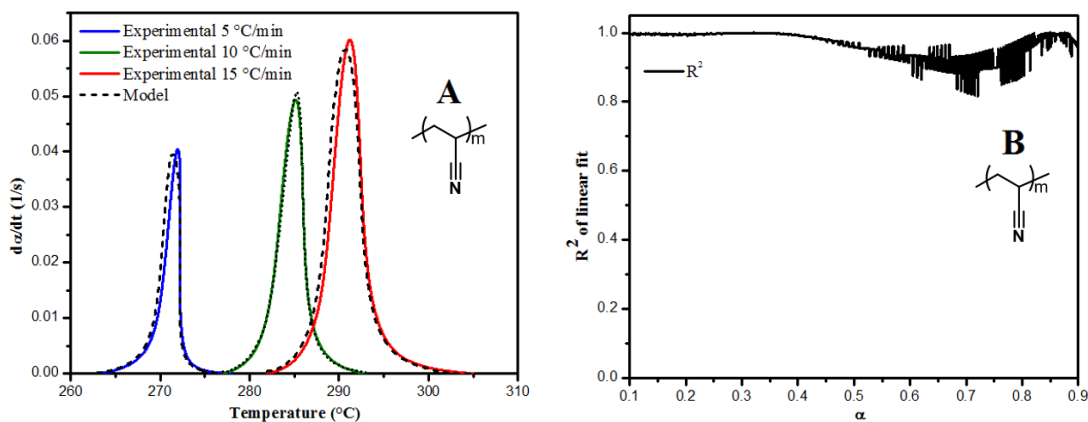
Figure 3.9 Representative results of the model-free ICA method A) fit of the model in comparison to experimental data and B) R^2 linear fit as cure progressed.

From the model, a plot of E_a and A versus α was graphed in Figure 3.10 and highlighted that both E_a and A does indeed vary as α increased. This variation in E_a and A invalidated the use of the Kissinger method as the assumption that E_a remained constant does not hold true. Interestingly, for all copolymers and homopolymer FR precursors, E_a and A varied in a similar manner, which suggested that these changes in E_a and A were a

result of the cyclization that occurs during TOS rather the free radical or ionic ring closing mechanism. The ionic ring closure cannot occur in homopolymer FR due to the lack of acidic comonomers; therefore, these Ea and A variation were not indicative of ionic ring closure.
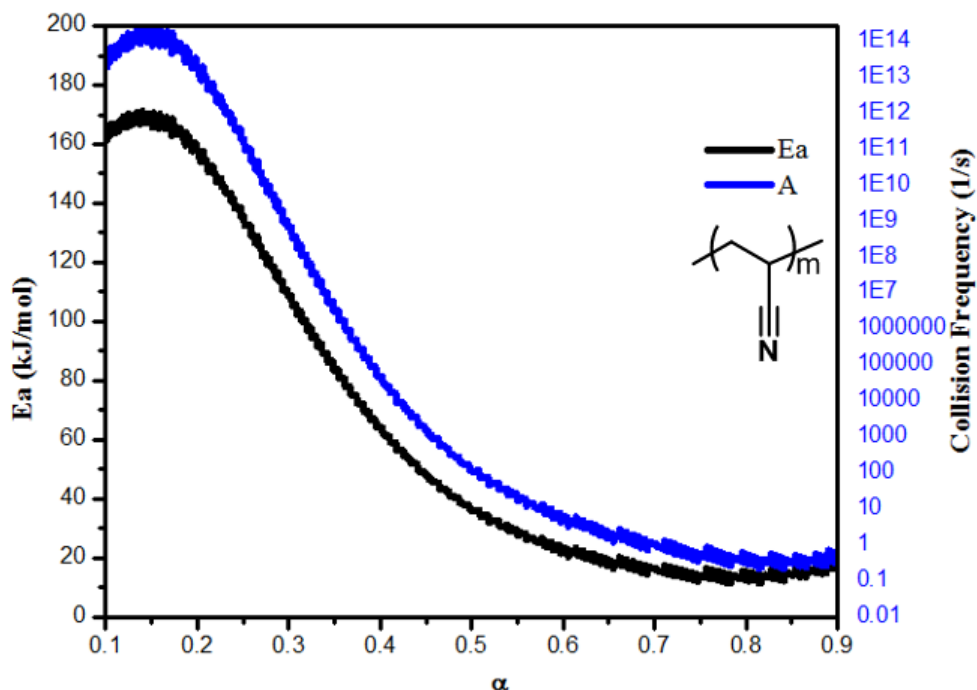
Figure 3.10 Representative Ea and A of the model-free ICA method for Homopolymer FR.

The order of the dehydrogenation, cyclization, and oxidation during TOS has been debated in literature.[54,95] The use of a nitrogen atmosphere eliminated dehydrogenation from occurring as an oxygen atmosphere is required for dehydrogenation.[46] The initial increase in E_a followed by a sudden decrease may suggest that the cyclization reaction is difficult at first but once a small molecule is released, the cyclization mechanism becomes easier and E_a is reduced. Even though cyclization in theory does not produce off-gas products, ammonia has been reported to be released and was evolved throughout the TGA-MS experiments below.[46] At increased α values,

activation energy and collision frequency was reduced likely due to the pendent nitrile availability being severely restricted at the end of cyclization. Further research to investigate the influence of an oxygen atmosphere in DSC is needed to determine its effect on exotherm, E_a, and A.

3.2.3.3 TGA-MS Off-Gas Evolution

TGA-MS was used to provide insights into the TOS mechanism for these novel acrylamide containing copolymers. Here, oxygen atmosphere was used from room temperature to 255 °C and once above 255°C an inert atmosphere was used up to 800 °C to best simulate fiber TOS and low temperature carbonization conditions.[28,68,71] Figure 3.11 illustrated a representative TGA-MS chromatogram of homopolymer FR with 2, 17, 18, and 27 amu, which corresponded to the following common PAN evolution products: hydrogen, ammonia, water, and hydrogen cyanide, respectively.[47,58] These selected masses of interest were readily apparent in the TGA-MS, whereas other typical PAN off-gas products such as diatomic nitrogen and carbon monoxide at 28 amu were not distinct due to the use of nitrogen atmosphere. TOS occurs from 180 to 300 °C and is comprised of dehydrogenation, cyclization, and oxidation reactions. Water and ammonia are known byproducts of dehydrogenation and cyclization, respectively. In principle, cyclization should not afford an off gas product; however, when imine functional groups were proposed as a possible terminating structure of PAN, then ammonia was linked to cyclization as these end imine groups would emit ammonia upon further heating.[46,47,58] Within the stabilization range of 180 to 300 °C, water and ammonia emissions were detected indicating that cyclization and dehydrogenation occurred simultaneously. From 300 °C to 380 °C, dehydrogenation and cyclization continued and signified

intermolecular crosslinking between neighboring polymer chains.[11] Hydrogen cyanide gas was observed as a broad peak above 300 °C and was reported by Meinl et al.to be the result of degradation when hydrogen cyanide and ammonia gases were released jointly.[58] Lastly, hydrogen was steadily increased above 500 °C and is a typical product release during carbonization as the graphitic structure continues to fuse upon heating.[1]
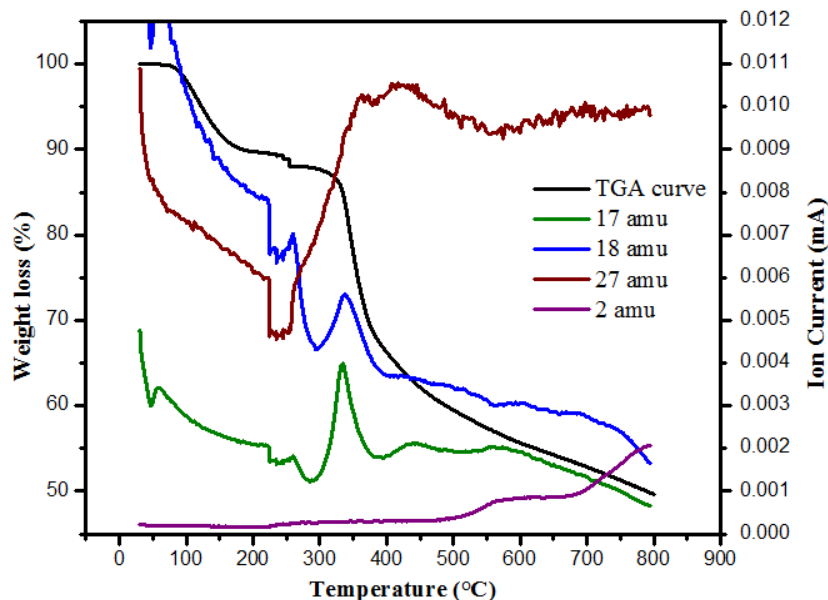
Figure 3.11 Representative TGA-MS chromatogram of Homopolymer FR.

The selected masses of 2, 17, 18, 27 amu from each precursor were integrated, summed, and listed in Table 3.6 along with TGA-MS char yield. Homopolymer FR possessed the highest summed gas emissions, heat evolution rate, and exotherm intensity to signify that more dehydrogenation and cyclization byproducts were evolved throughout the DSC exotherm than other precursors. The TGA-MS data suggested an overall improved graphitic structure; but, FTIR and DSC highlighted that polymer degradation likely occurred as indicated by the lowered E_s value and increased heat release rate. It was expected that SB precursors would possess lower gas emissions than

FR precursors and afford increased char yields, which was observed for NEAA

containing precursors in Table 3.6. However, this trend was not observed for NIPAM or

NTAA, likely due to other off-gas products such as nitrogen and carbon monoxide that

could not be accounted for. All char yields were between approximately 45 to 54 %,

which is similar to commercial PAN fiber carbon yields ~ 50 %.[96] NEAA containing

precursors and NTAA SB exhibited the highest char yields between approximately 52 to

54 % suggesting that these precursors were more stable after TOS and low temperature

carbonization that is beneficial for fiber processing and PAN structure. [35,37]

Table 3.6 Summed TGA-MS gas emissions and char yield.

Precursor	Summed Gas Emissions (mA*°C)	Char Yield (%)
NEAA FR	0.060	53.78
NEAA BR	0.080	52.73
NEAA SB	0.026	53.67
NIPAM FR	0.016	51.62
NIPAM BR	0.028	46.82
NIPAM SB	0.011	50.90
NTAA FR	0.051	45.04
NTAA BR	0.055	48.29
NTAA SB	0.038	53.96
Homopolymer FR	0.107	49.64

3.3 Conclusions

From this chapter, the interdependencies of copolymer composition including

comonomer selection and polymerization method on their respective thermal behavior

were examined by measuring ten key precursors. Utilizing a semi-batch RAFT

polymerization method, well-defined PAN architectures with lower Đ values were

synthesized. It is believed that this well-defined SB architecture allowed for increased

cyclization due to the polymer chains being more aligned and afforded increased E_s

values, exotherm intensities, and heat release values with reduced E_a values as compared to free radical counterparts. SB RAFT precursors also possessed a more consistent exotherm behavior as compared to batch RAFT precursors which was attributed to compositional drift or a compositional gradient along the polymer backbone that would then lead to morphological defects and thus decreased mechanical properties.[20,44] This inconsistent thermal behavior and propensity for compositional drift led to the elimination of batch RAFT precursors from being further investigated or selected for white fiber spinning in Chapter V.

The incorporation of NEAA, NIPAM, and NTAA comonomers also highlighted that these acrylamide comonomers expressed neutral comonomer exotherm behavior and participated in the free radical ring closing mechanism as evident by the single exotherm peak in DSC. Further investigation of the effect of comonomer incorporation on thermal ring closure behavior of SB RAFT precursors will be examined in Chapter IV before selecting which comonomer(s) and comonomer concentration(s) should be utilized for fiber scale up in Chapter V.

CHAPTER IV – INFLUENCE OF ACRYLAMIDE COMONOMER
CONCENTRATION ON SEQUENCE BEHAVIOR AND CYCLIZATION OF PAN-
BASED CARBON FIBER PRECURSORS

4.1 Abstract

The effects of increasing NEAA, NIPAM, and NTAA comonomer concentration from 2 to 4 to 6 mole % on polyacrylonitrile (PAN) precursor architecture and thermal ring closure was investigated. The copolymer architecture was determined by reactivity ratios via the Fineman-Ross, Kelen-Tudos, and non-linear least squares methods (NLLS). Reactivity ratios of NEAA or NTAA and acrylonitrile were ≤ 1 as calculated by the NLLS method and supported the development of a favorable alternating copolymer architecture. Thermal cyclization was measured by FTIR, DSC, and WAXS. As the concentration of each comonomer increased, the acrylonitrile sequence length, extent of stabilization measured by FTIR, and heat release rate monitored by DSC, decreased. This data signified that increased acrylamide comonomer concentration reduced the amount of cyclization sites and hindered the overall ring closed graphitic structure upon heating. Additionally, as each copolymer was heated to 255 °C, the semi-crystalline morphology of PAN was affected, where crystallite size and d-spacing increased as compared to each respective pristine copolymer. Knowledge regarding the relationships between precursor design including polymerization method, comonomer selection, and comonomer concentration on PAN ring closing behavior from Chapter III and IV was used to down-select 3 precursors (2 mole % NIPAM FR, 2 mole % NIPAM SB, and 2 mole % NTAA SB) for white fiber spinning, oxidation, and eventual carbonization in Chapter V.

4.2 Results and Discussion

Herein, copolymers were prepared via semi-batch RAFT (SB) with acrylamide comonomer concentrations of 2, 4, and 6 mole %. These comonomer amounts were selected as they were below the 8 mole % comonomer target for carbon fibers.[2] This chapter will focus on the effect of comonomer concentration on copolymer architecture and cyclization behavior to down-select three precursors for fiber spinning, oxidation, and carbonization.

4.2.1 Sequence Distribution of PAN-based Precursors

4.2.1.1 Reactivity Ratios

The reactivity ratios were calculated by the Fineman-Ross, Kelen-Tudos, and the non-linear least squares methods to investigate the copolymer architecture of acrylonitrile (AN) with either NTAA or NEAA comonomer. The reactivity ratio of NIPAM was not calculated as previous research with the group had already determined it; however, the effect of NIPAM concentration on the cyclization behavior was discussed.[20] The reactivity ratios of monomer one, AN, and monomer two (NTAA or NEAA) are defined in Equations 1 and 2, where k_{11}, k_{12}, k_{22}, k_{21} are the rate constants for homo-propagation and cross propagation of acrylonitrile and NTAA or NEAA, respectively. The experimental determination of reactivity ratios from the graphical Fineman-Ross and Kelen-Tudos methods was considered an initial guide to understanding the PAN copolymer architectures with various acrylamides and was performed in accordance with Moskowitz and coworkers.[35,97] The Fineman-Ross and Kelen-Tudos methods were selected as they are widely used for the determination of reactivity ratios of PAN copolymerizations.[32,35,98,99] However, the more appropriate NLLS method accounted for

error within the experimental data and therefore the NLLS results were emphasized.[97] The following calculations are for the NLLS method as it is widely accepted as the most accurate method in determining reactivity ratios, where the guess values required for the NLLS method were the reactivity ratios calculated by the Fineman-Ross and Kelen-Tudos methods. All reactivity ratio experiments were subjected to the aforementioned batch RAFT polymerization procedure without the usage of a syringe pump, where the appropriate amount of NTAA or NEAA was charged directly into the reaction vessel.

$$r_1 = \frac{k_{11}}{k_{12}} \qquad\qquad \text{Equation 1}$$

$$r_2 = \frac{k_{22}}{k_{21}} \qquad\qquad \text{Equation 2}$$

Equations 1 and 2 were used to calculate the instantaneous co-polymerization defined by Equation 3 (Mayo-Lewis Equation), where F_1 and f_1 correspond to the mole fraction of monomer one in the copolymer and feed, respectively. The NLLS is defined by Equation 4, where n is the number of compositional data points and σ is the standard deviation for F_1. The objective of Equation 4 was to minimize the difference between the fitted data in the Mayo-Lewis Equation (Equation 3) and the real data to obtain the global minimum which is the weighted sum of squares error.[35,100]

$$F_1 = G(f_1, r_1, r_2) = \frac{r_1 f_1^2 + f_1(1-f_1)}{r_1 f_1^2 + 2f_1(1-f_1) + r_2(1-f_1)^2} \qquad \text{Equation 3}$$

$$SSE(r_1, r_2) = \sum_{i=0}^{n} \left(\frac{F_{1i} - G(f_{1i}, r_1, r_2)}{\sigma}\right)^2 \qquad \text{Equation 4}$$

The F_1 and f_1 compositions are recorded in Table 4.1 and 4.2, where F measurements were determined via ^{1}H NMR. All copolymer reactions were quenched at five hours or less to limit conversion under 10 % in an effort to avoid compositional drift that tends to occur as conversion increases.[35,100] ^{1}H NMR confirmed that conversion was

below 10 % prior to quenching each reaction. As higher concentrations of NEAA (> 40 mole %) were incorporated, unwanted foaming occurred as the reaction solution was filtered after precipitation. To collect the precipitates of the more concentrated NEAA copolymers, the precipitated reaction solution was slowly vacuum filtered over several hours. The cause of this foam remains unclear; however, during filtration air may have been incorporated into the solution to generate foam. Additionally, three attempts to prepare 80 mole % NEAA were unsuccessful as no polymer was collected, despite the conversion being ~ 9 %.

Table 4.1 Composition of the final poly(AN-co-NTAA) copolymer and monomer feed.

f_{AN}	f_{NTAA}	F_{AN}	F_{NTAA}
0.95	0.05	0.937	0.063
0.90	0.10	0.876	0.124
0.80	0.20	0.739	0.261
0.60	0.40	0.659	0.341
0.40	0.60	0.388	0.612
0.20	0.80	0.189	0.811

Table 4.2 Composition of the final poly(AN-co-NEAA) copolymer and monomer feed.

f_{AN}	f_{NEAA}	F_{AN}	F_{NEAA}
0.90	0.10	0.880	0.120
0.80	0.20	0.723	0.277
0.60	0.40	0.573	0.427
0.40	0.60	0.352	0.648

The reactivity ratios determined by all methods were found to be in agreement with one another and are summarized in Table 4.3 and 4.4, where r_1 and r_2 from the Fineman-Ross, Kelen-Tudos, and NLLS methods varied from ± 0.10 and ± 0.30, respectively. The copolymer compositions calculated by each reactivity ratio method and

experimental data were compared in Figure 4.1. Obtaining the copolymers with NEAA

and NTAA content above 60 mole % was difficult and took multiple attempts due to the

low quantity of polymer within the reaction solution.

Table 4.3 Reactivity ratios of monomer one (AN) and monomer two (NTAA).

Reactivity Ratio Method	r_1	r_2
Kelen-Tudos	0.69	0.77
Fineman-Ross	0.72	1.07
Non-linear Least Squares	0.79	0.85

Table 4.4 Reactivity ratios of monomer one (AN) and monomer two (NEAA).

Reactivity Ratio Method	r_1	r_2
Kelen-Tudos	0.74	1.18
Finemas-Ross	0.78	1.32
Non-linear Least Squares	0.69	1.03
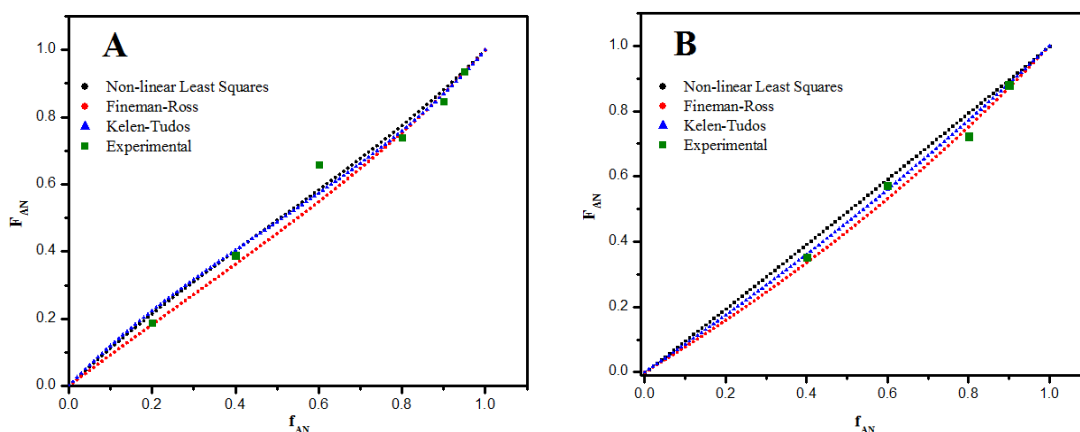
Figure 4.1 Copolymer and monomer composition of experimental data compared to the calculated reactivity ratio methods of A) NTAA and B) NEAA.

The reactivity ratios between AN and NTAA were below 1 for the NLLS method

and confirmed that both monomers preferred to cross-propagate with one another rather

than homo-propagate.[97] The reactivity ratios for AN and NTAA were also approximately

equal and suggested that both monomers would cross-propagate into the copolymer

backbone at similar rates. The reactivity ratios of AN and NIPAM, as previously calculated by Moskowitz and coworkers with the NLLS method, were 0.39 and 0.72, respectively, and indicated that poly(AN-co-NIPAM) copolymers preferred to cross-propagate similarly to AN and NTAA.[35] The r_1 and r_2 values calculated from the NLLS method for AN and NEAA were ≤ 1, where the reactivity ratio for NEAA was greater than AN to signify that NEAA was more reactive than AN. From these reactivity ratios, poly(AN-co-NEAA) copolymers would also afford the favorable alternating copolymer architecture.[97]

This alternating copolymer architecture is ideal as homo-propagation or a reactivity ratio much greater than one is undesirable, because it will create an architecture where several comonomers will be arranged closely together along the polymer backbone, which will disrupt the semi-crystalline morphology to a greater extent and produce more fiber morphological defects. As these reactivity ratios determined that NEAA, NIPAM, and NTAA preferred to add to acrylonitrile, no acrylamide comonomers were eliminated from white fiber down-selection yet, as it was previously decided that comonomers that possessed reactivity ratios >> 1 would be removed from consideration. Therefore, the effect of comonomer concentration on the number average sequence length of acrylonitrile, or the run number of AN, was investigated to gain further insights into the influence of these comonomers on the copolymer architecture.

4.2.1.2 Number average sequence length

Number average sequence length of acrylonitrile was conducted with the NLLS reactivity ratios and based upon Mayo-Lewis theory as discussed by Çatalgil-Giz and coworkers.[101] The probability that the propagating acrylonitrile (AN) chain terminus

would add to acrylonitrile monomer, expressed as P_{ANAN}, is displayed in Equation 5. By assuming full conversion, the number average sequence length of acrylonitrile, $<N_{AN}>_n$, was calculated by Equation 6.

$$P_{ANAN} = \frac{r_{AN}f_{AN}}{f_{AN}(r_{AN}-1)+1}$$ Equation 5

$$<N_{AN}>_n = \frac{1}{1-P_{ANAN}}$$ Equation 6

The average sequence length of acrylonitrile with NTAA or NEAA acrylamide-based comonomers with increasing mole % of 2, 4, and 6 was calculated and listed in Table 4.5 and 4.6, respectively. The incorporation of comonomer had a drastic effect on $<N_{AN}>_n$ as anticipated and noted in Table 4.5 and 4.6. The average sequence length of acrylonitrile with the incorporation of 2 mole % NTAA was 39.71, and the addition of 6 mole % NTAA decreased the $<N_{AN}>_n$ to 13.38 (33 %). More explicitly, the increased NTAA mole % of 2 to 6 mole % reduced the run of AN monomer units along the copolymer backbone (from roughly 40 to 13) before a single NTAA comonomer was added into the polymer chain. This decrease in $<N_{AN}>_n$ is anticipated to reduce the unfavorably high pyridine ring strain that occurs as pendent acrylonitrile groups ring close upon heating.

Ring strain was reported to increase as consecutive pyridine rings were formed until a critical value was reached, typically above 7 pyridine rings, and resulted in chain rupture.[35,102] Here, it is highlighted that ring strain will be alleviated as the concentration of NTAA increased, where 6 mole % of NTAA afforded the lowest acrylonitrile sequence length (approximately 13), which was unfortunately still above the highest recorded pyridine sequence length of 7. Further increase of NTAA incorporation to 10

mole % would result in a $<N_{AN}>_n$ of 8.11 which is closer to the critical consecutive pyridine limit of 7; however, higher incorporations of comonomer is anticipated to negatively affect final fiber mechanical properties.[9] Previous research by Moskowitz et al. determined the reactivity ratios and $<N_{AN}>_n$ for NIPAM and AN comonomers and recorded that poly(AN-co-NIPAM) (95:5) copolymers possessed an $<N_{AN}>_n$ of approximately 8.[35] Here, the poly(AN-co-NIPAM) (94:6) copolymer was successfully synthesized and analyzed to investigate the thermal properties of a precursor that possessed a $<N_{AN}>_n$ of 7.11 and corresponds to the maximum limit of consecutive conjugated pyridine structures.

Table 4.5 Average number sequence length of poly(AN-co NTAA) compositions.

Average Number Sequence Length	poly(AN-co-NTAA) (98:2)	poly(AN-co-NTAA) (96:4)	poly(AN-co-NTAA) (94:6)
AN	39.71	19.96	13.38
NTAA	1.02	1.04	1.05

Table 4.6 Average number sequence length of poly(AN-co NEAA) compositions.

Average Number Sequence Length	poly(AN-co-NEAA) (98:2)	poly(AN-co-NEAA) (96:4)	poly(AN-co-NEAA) (94:6)
AN	34.81	17.56	11.81
NEAA	1.26	1.69	2.55

4.2.2 NMR and GPC Results

Table 4.7 highlights both the [1]NMR and DMF GPC results acquired from each precursor containing NEAA, NIPAM, and NTAA comonomers. All dispersity values were below 1.3 and molecular weights were above 100,000 g/mol except for 6 mole % NEAA SB and 6 mole % NIPAM SB. Several attempts to synthesize 6 mole % NEAA

SB and NIPAM SB with molecular weights $\geq$ 100,000 g/mol were performed. However, at 6 mole % of NEAA and NIPAM, molecular weight was hindered and were below the traditional molecular weight range of typical PAN precursors of 70,000 to 100,000g/mol.[37,74] Careful consideration of these low molecular weight precursors will be performed upon further understanding their thermal behavior to decide if these precursors should be selected for white fiber spinning.

Table 4.7 ^{1}H NMR and GPC results for SB precursors.

Precursor	Comonomer Incorporation[a] (mole %)	MW[b] (g/mol)	Mn[b] (g/mol)	Đ[b] (MW/Mn)
2 mole % NEAA SB	2.0	188,000	168,300	1.117
4 mole % NEAA SB	4.3	140,300	117,400	1.195
6 mole % NEAA SB	6.2	61,010	51,010	1.196
2 mole % NIPAM SB	2.4	210,500	210,500	1.108
4 mole % NIPAM SB	3.8	197,500	154,400	1.279
6 mole % NIPAM SB	5.8	68,740	56,610	1.214
2 mole % NTAA SB	1.9	140,900	113,700	1.239
4 mole % NTAA SB	3.5	178,800	152,600	1.172
6 mole % NTAA SB	7.1	154,700	133,000	1.164

[a] In the final copolymer composition, the mole % of acrylamide-based comonomer incorporated into the copolymer backbone was analyzed by ^{1}H NMR. [b] The weight average molecular weight (MW), number average molecular weight (Mn), and dispersity (Đ) was determined by GPC.

4.2.3 Thermal Behavior

Insights gained into the interrelationships between copolymer architecture and thermal behavior will be used to ultimately down-select precursors for white fiber spinning. Thermal behavior mimicked thermo-oxidation stabilization conditions and was examined by FTIR, DSC, and WAXS to determine extent of stabilization (E_s), unreacted

CN fraction, exotherm, activation energy (E_a), and microstructure as NEAA, NIPAM, or NTAA comonomer concentration increased within each respective copolymer.

4.2.3.1 FTIR

E_s and unreacted CN fraction values were calculated according to the aforementioned method in Chapter II and plotted in Figure 4.2, where 2 mole % comonomer contained the highest E_s value and as comonomer content increased, E_s values decreased.[25,37] This result was expected as the number average sequence length for 2 mole % comonomer was calculated to be higher than precursors containing 4 or 6 mole % comonomer and suggested that cyclization reactions decreased as $<N_{AN}>_n$ decreased. From Figure 4.2, it was also noted that as unreacted CN fraction decreased, E_s values increased to highlight that the pendent nitrile groups along the copolymer backbone were ring closing.
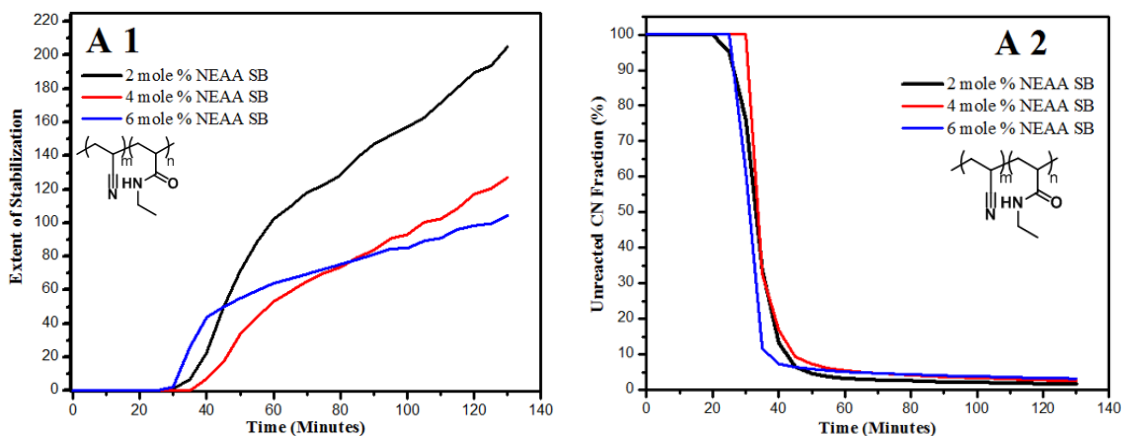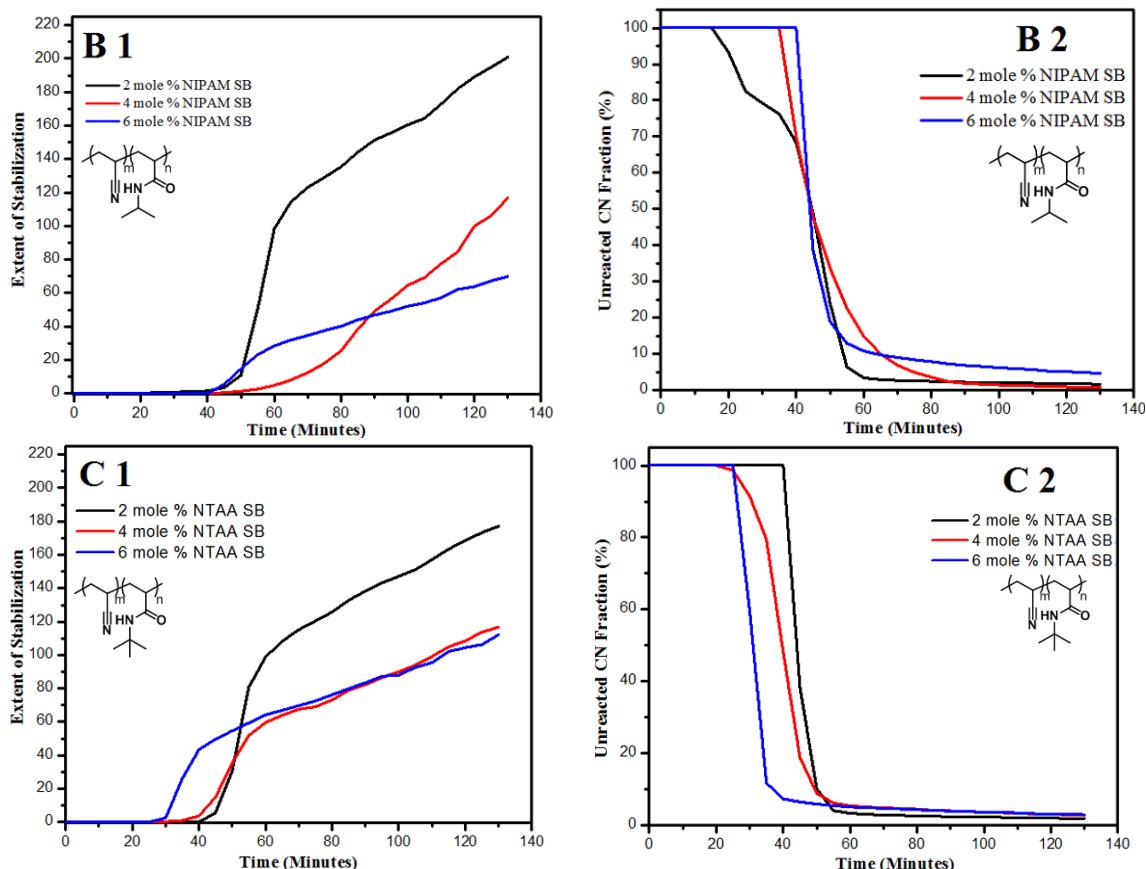
Figure 4.2 1) E_s and 2) unreacted CN fraction for A) poly(AN-co-NEAA) B) poly(AN-co-NIPAM) and C) poly(AN-co-NTAA) precursors with increasing comonomer mole %.

Table 4.8 FTIR data compared to average number sequence length.

Precursor	E_s value	Cyclization Length	$<N_{AN}>_n$
2 mole % NEAA SB	205.03	19.82	34.81
4 mole % NEAA SB	127.12	12.62	17.56
6 mole % NEAA SB	104.42	10.09	11.81
2 mole % NIPAM SB	200.84	19.41	20.11
4 mole % NIPAM SB	116.79	11.29	10.36
6 mole % NIPAM SB	69.90	6.76	7.11
2 mole % NTAA SB	177.11	17.12	39.71
4 mole % NTAA SB	116.66	11.28	19.96
6 mole % NTAA SB	112.15	10.84	13.38

Cyclization length was also calculated via FTIR after each precursor had been

exposed to the aforementioned heating procedure and was summarized along with final

E_s and $<N_{AN}>_n$ values in Table 4.8.[72] For all precursors except for 6 mole % NIPAM SB, the cyclization length was above the maximum length of 5 to 7 consecutive conjugated pyridine rings. From Table 4.8, increased comonomer concentration hindered cyclization length and led to decreased E_s values, which further supported the previous findings from the calculated $<N_{AN}>_n$ values. Both 2 mole % NEAA and NIPAM had final E_s values ~ 200, whereas the final E_s value for the respective NTAA copolymer was below 200 to suggest a less graphitic structure. The less graphitic structure of 2 mole % NTAA may lead to an increased fiber defects and a reduction in fiber tensile strength.

Interestingly, the cyclization lengths determined for NIPAM precursors corresponded well to the $<N_{AN}>_n$ values calculated from the reactivity ratios from Moskowitz et al.[35] The cyclization length for NTAA precursors were lower than the calculated $<N_{AN}>_n$. Cyclization lengths appeared to plateau around 20; it is possible that above 20 ring closed structures, ring strain or the atactic nature of PAN did not allow for further cyclization. Theoretically, homopolymer PAN would possess the highest cyclization length if premature polymer chain scission did not occur; however, the cyclization length of homopolymer PAN from Chapter III was only 17.86 and Fu and coworkers did not surpass the 20 plateau limit.[72]

4.2.3.2 DSC

Exotherm, heat release rate, activation energy, and collision frequency were investigated by DSC at 5, 10, and 15 °C/min. ramp rates. The exotherm and heat release rate of each precursor with increasing comonomer concentration at 10 °C/min. ramp rate is depicted in Figure 4.3. All exotherms were mono-modal as previously noted in Figure 3.5 to support free radical ring closing mechanism that occurs in homopolymer PAN.[9,26]

For NEAA containing precursors, a decrease in exotherm and heat release rate was observed for the 2 and 6 mole % NEAA SB precursors, whereas the 4 mole % NEAA SB possessed a heat release rate than was lower expected. This decrease in heat release rate in comparison to other NEAA precursors was due to the broader exotherm of 4 mole % NEAA SB that lead to a reduced heat release rate. For NIPAM and NTAA-based precursors, both exotherm intensity and heat release rate decreased as comonomer concentration increased. This reduction in exotherm and heat release rate is due to the decrease in AN sequence length and overall amount of cyclization and dehydrogenation reactions that can occur as supported by FTIR. Even though increasing comonomer concentration will help alleviate significant amount of heat release over a short period of time, it will also incorporate more defects into the ultimate black fiber and reduce fiber mechanical properties as more neutral comonomer sites within the copolymer backbone will not be able to ring close.[9] Therefore, selection of copolymers with higher comonomer concentrations, such as 6 mole %, may need to be removed from consideration for spinning into white fiber as they will disrupt cyclization more than 2 and 4 mole % comonomer and introduce flaws in the black fiber.
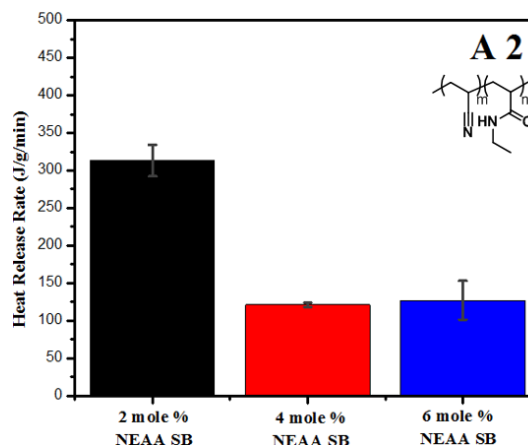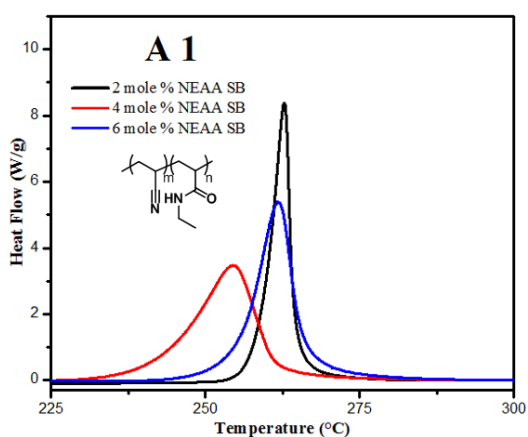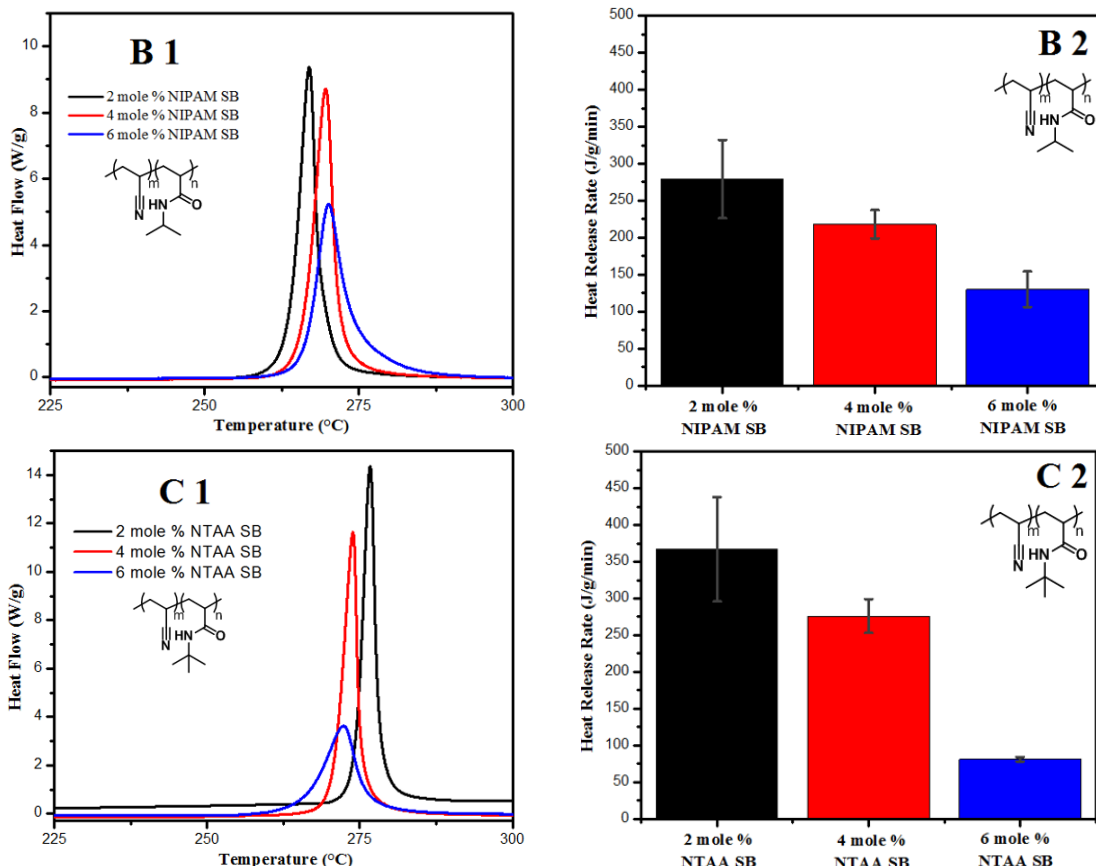
Figure 4.3 1) Exotherm 2) and heat release rate for A) poly(AN-co-NEAA) B) poly(AN-co-NIPAM) and C) poly(AN-co-NTAA) copolymers with increasing comonomer mole %.

Activation energies and collision frequencies were also calculated by the FWO method as the Kissinger assumptions were proven to not hold true after examination of the ICA model-free method in Chapter III. These activation energies and collision frequencies at 10 °C/min. are compiled in Table 4.8. The effect of activation energy on comonomer concentration remains unclear in literature, where past references have reported that E_a has increased, decreased, or remained unchanged with incorporation of a neutral comonomer.[69,103–105] Here, all of the E_a trends that have been reported in literature were recorded for these well-defined precursors as comonomer concentration increased. Activation energy of the 2 and 4 mole % NEAA SB and NIPAM precursors decreased as

comonomer concentration increased. This trend may be due to the inert comonomer disrupting the crystalline domains within the semi-crystalline PAN microstructure to increase the overall amorphous fraction. Cyclization occurs more often within the amorphous fraction and would increase the amount of cyclization sites and yield a reduced E_a.[103] However, an increase in comonomer can also reduce the number of cyclization sites by decreasing the $<N_{AN}>_n$ and give an increased E_a value as recorded for 4 and 6 mole % NEAA SB. For NTAA SB precursors, no trend between E_a and comonomer concentration was observed as similarly reported by Hao and coworkers possibly due to a combination of an increase and decrease in E_a causing a negligible change in E_a.[103]

Table 4.9 Activation energies determined by the FWO method.

Precursor	E_a (kJ/mol)
2 mole % NEAA SB	96.7 ± 3.0
4 mole % NEAA SB	64.8 ± 0.9
6 mole % NEAA SB	117.3 ± 0.5
2 mole % NIPAM SB	157.6 ± 34.0
4 mole % NIPAM SB	136.8 ± 20.6
6 mole % NIPAM SB	80.3 ± 1.6
2 mole % NTAA SB	93.4 ± 2.1
4 mole % NTAA SB	84.3 ± 10.3
6 mole % NTAA SB	91.7 ± 1.8

4.2.3.3 WAXS

WAXS was also performed on both pristine and heat treated precursors to understand the influence of comonomer mole % and TOS conditions on the PAN crystallites. During stabilization, the amorphous and crystalline fractions within the PAN precursor morphology will be affected by temperature and the presence of oxygen. In

general, stabilization will begin in the amorphous region where the crystalline fraction will remain mostly intact. As temperature increases, stabilization will begin to occur in the crystalline region and break down the crystal structure leading to unstable PAN chains. This unstable state, due to the gradual amorphitization of the crystalline structure, can allow for oxygen to be incorporated into the PAN backbone.[23,24,73,103]

From Figure 4.4 and 4.5, the (100) reflection of the hexagonal crystal lattice, due to the intra-molecular dipole-dipole interactions from the nitrile groups in the pristine PAN, was observed at ~ $2\theta = 17$ °.[84] An additional reflection at ~ $2\theta = 29$ ° from the (110) reflection was easily observed in Figure 4.5; however, this band was difficult to discern in the WAXS diffraction pattern.[37,59,73] The (110) reflection corresponded to the spacing between closely associated polymer chains.[106] Prior to heating, the sharp and intense band at ~ $2\theta = 17$ ° of the pristine precursors suggested an increased percent crystallinity and crystallite size as compared to the heated samples. Upon heating, this band became broader and/or decreased in intensity as comonomer concentration increased as displayed in Figure 4.5. This variation in the (100) reflection upon heating inferred that as comonomer concentration increased, the crystallinity was reduced and afforded an increased amorphous fraction.[24]
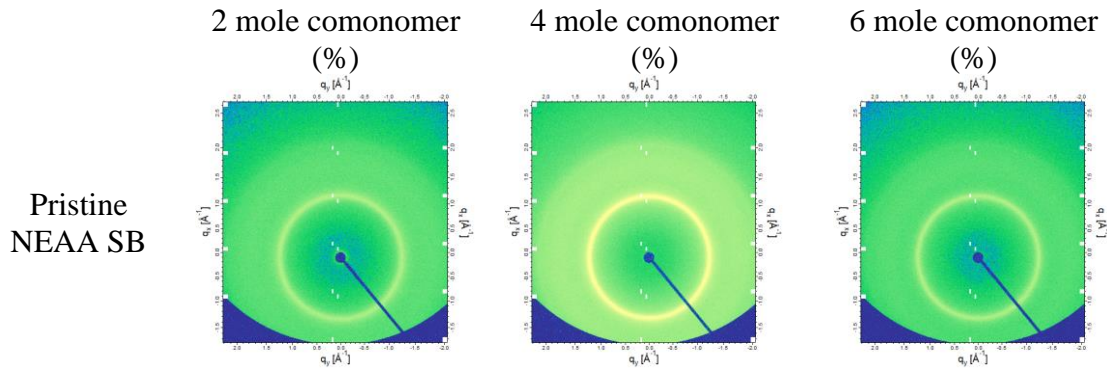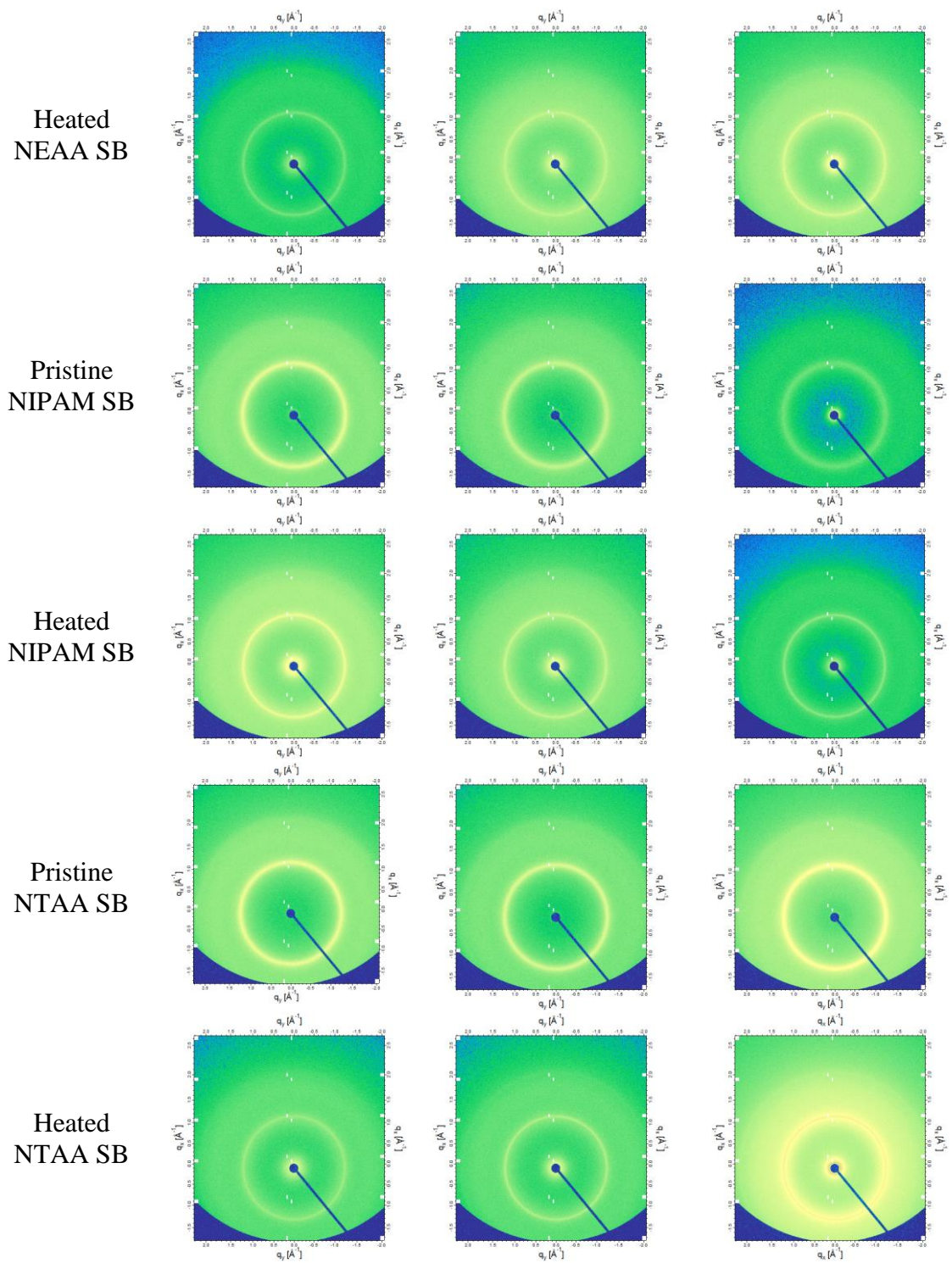
Figure 4.4 WAXS diffraction patterns of pristine and heated precursors.
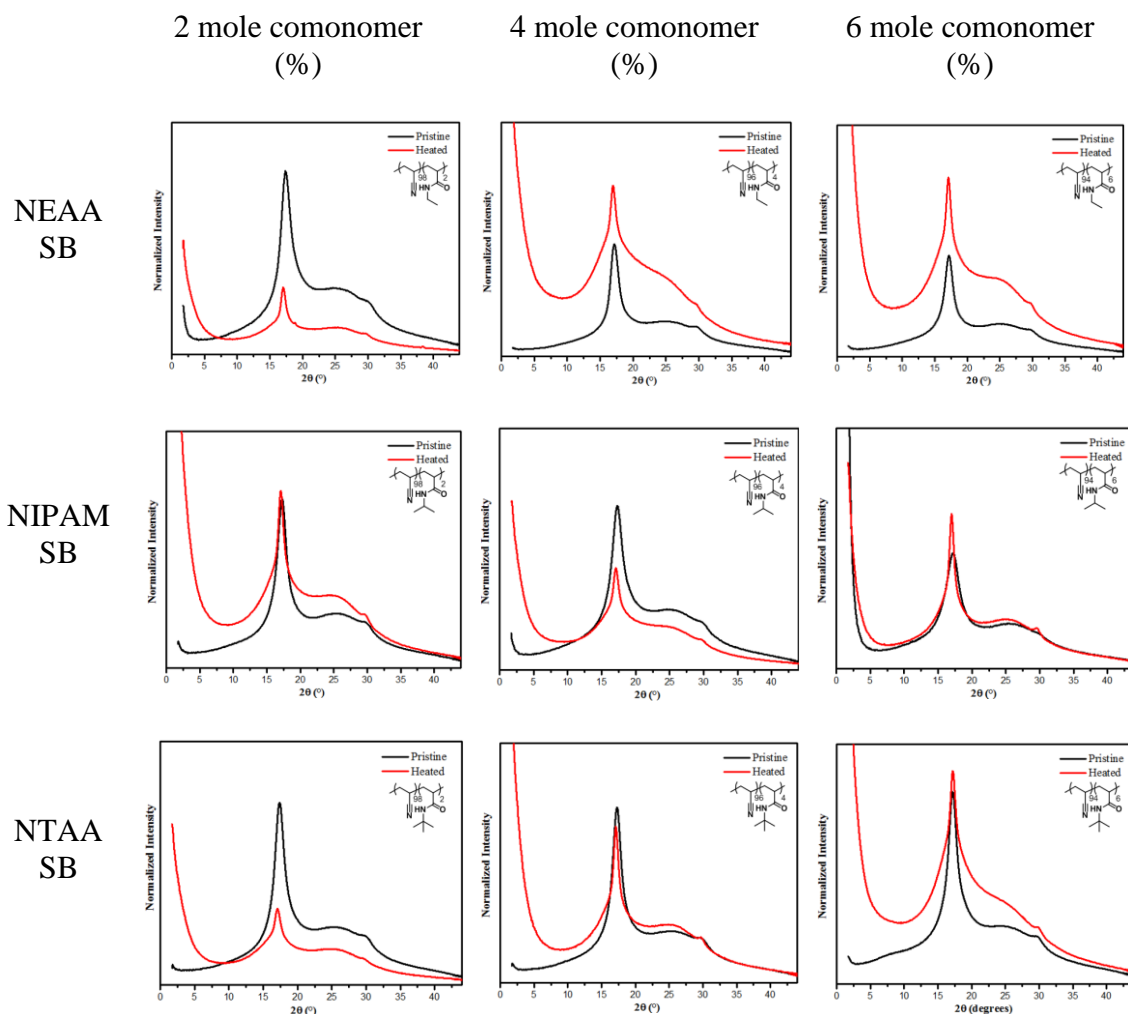
Figure 4.5 Plot of 2θ vs. intensity for pristine and heated precursors with increasing comonomer concentration.

The d-spacing and crystallite size was calculated by the Bragg and Scherrer equations for the pristine and heated precursors at the (100) reflection at ~ 2θ = 17° and was listed in Table 4.10. After heating to 255 °C, the crystallite thickness (L_c) and interplanar spacing increased as compared to the pristine copolymers. The increase in L_c and d-spacing is thought to be the detectable result of the PAN molecules that have interacted with oxygen. As these samples were exposed to air during heating, dehydrogenation and oxidation reactions likely affected the crystal structure.[73] Here, the samples were only heated to 255 °C, which was below the observed exotherm peak

maximum from DSC for NIPAM and NTAA copolymers. Therefore, ring closure had not significantly progressed in these copolymers suggesting that the increase in L_c and d-spacing may be due to a small amount of dehydrogenation occurring within the amorphous region of the PAN morphology, rather than amorphitization of the crystal structure. During amorphitization, an increase in d-spacing and decrease in crystallite size was expected to indicate an unstable crystal structure.[73] Evidence to support amorphitization was not recorded likely due not an insufficient amount of heat (255 °C) that was applied to the precursors.

Table 4.10 Summary of WAXS data for pristine and heated precursors.

Pristine Precursors			Heat Treated Precursors		
Entry	D spacing (nm)	Lc (nm)	D spacing (nm)	Lc (nm)	S_I (%)
2 mole % NEAA SB	0.511	4.65	0.521	7.68	63.4
4 mole % NEAA SB	0.516	5.34	0.521	5.59	-51.8
6 mole % NEAA SB	0.513	5.33	0.518	8.24	-77.1
2 mole % NIPAM SB	0.513	5.35	0.518	7.89	39.0
4 mole % NIPAM SB	0.513	4.48	0.518	6.98	37.8
6 mole % NIPAM SB	0.516	3.99	0.521	9.34	-34.1
2 mole % NTAA SB	0.511	4.84	0.518	6.27	58.1
4 mole % NTAA SB	0.513	5.30	0.518	8.50	10.9
6 mole % NTAA SB	0.516	5.31	0.516	6.27	-10.9

Additionally, Table 4.10 displayed the stabilization index (SI) values that were calculated to evaluate the development of cyclic ring closed structures after exposure to

TOS conditions.[76] The calculated SI values for the 6 mole % comonomers were negative due to the higher intensity values of these heated precursors in comparison to their respective pristine precursors.[73,75] As the stabilization reactions have not progressed significantly, especially for the NIPAM and NTAA copolymers, the heat applied provided enough energy to disrupt the boundary between the amorphous and crystalline regions which afforded increased crystallization and decreased stabilization values.[29,73] Interestingly, both SI and E_s results decreased with increasing comonomer content which may suggest that crystallites are disrupted as comonomer concentration increased. Further WAXS research at higher temperatures would aid in understanding the effect of comonomer concentration on PAN crystallite structure.

4.2.4 Down-selection of Carbon Fiber Precursors for White Fiber Spinning

Previous insights on the interdependencies of precursor design including polymerization technique, comonomer selection and concentration on the thermal behavior of PAN precursors from Chapters III and IV were used for the down-selection of carbon fiber precursors for white fiber spinning, thermo-oxidative stabilization, and eventual carbonization at Deakin University in Geelong, Australia under the guidance of Dr. Joselito Razal's research group. In particular, the heat release rate and extent of stabilization results obtained from DSC and FTIR, respectively, under nitrogen conditions were focused on to aid in the careful selection of precursors to be taken to Deakin University. Lower heat release rates are ideal for the spun white fiber to survive TOS and carbonization conditions, while higher E_s values would provide an overall more graphitic structure. Even though increasing comonomer concentration will help alleviate significant amount of heat release over a short period of time, precursors with lower

comonomer concentrations are thought to afford fibers with less defects due to their increased graphitic structure and ultimately improve the tensile strength values of the ultimate black fiber.[1,2,9] Therefore, lower comonomer concentrations will be down-selected for white fiber spinning in the effort to increase fiber tensile strength. The DSC and FTIR results are compiled in Figure 4.6, where the hypothesized precursors that would afford improved tensile strength due to their increased E_s values were circled. However, not all five precursors (2 mole % NTAA SB, 4 mole % NTAA SB, 2 mole % NEAA SB, 2 mole % NIPAM FR, and 2 mole % NIPAM SB) that are believed to generated increased tensile strength fibers could be spun into white fiber.
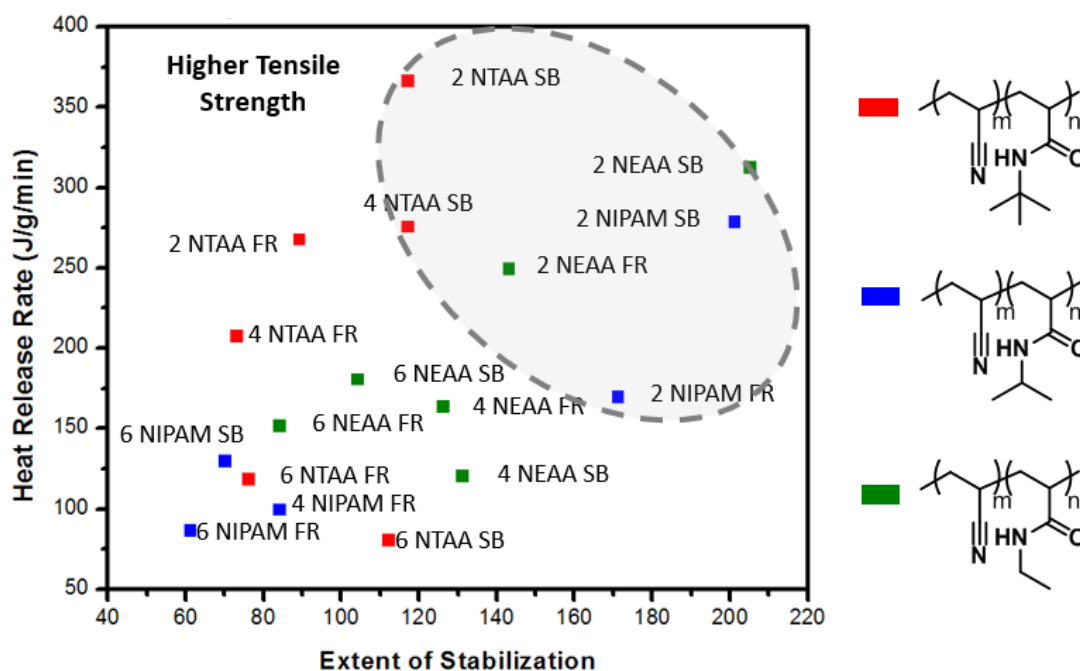
Figure 4.6 Summary of DSC and FTIR data from Chapters III and IV.

Dr. Joselito Razal's research group also impressed the criteria that 7 to 10 g of each precursor was the minimum amount required for their multifilament white fiber spin line. Additionally, the limited time at Deakin University allowed for the spinning of only 3 precursors from WRG. Preparing 7 to 10 grams of RAFT precursors containing higher

85

mole concentrations (4 and 6 mole %) of comonomer proved to be difficult as soxhlet extraction did not fully remove the ethylene carbonate solvent and molecular weight tended to suffer at higher comonomer content. Figure 4.7 displayed all the precursors that could be prepared at the required amount for white fiber spinning and which precursors would theoretically possess higher tensile strength from solely examining the precursor thermal data. Precursors, 2 mole % NIPAM FR, 2 mole % NIPAM SB, and 2 mole % NTAA SB, demonstrated improved ring closure from thermal data which suggested superior tensile strengths; therefore, these precursors were down-selected for white fiber spinning in an effort to further understand how to improve tensile strength via precursor design and fiber processing as the current PAN-based fibers only exhibit a mere 10% of their theoretical tensile strength potential.[2,8]
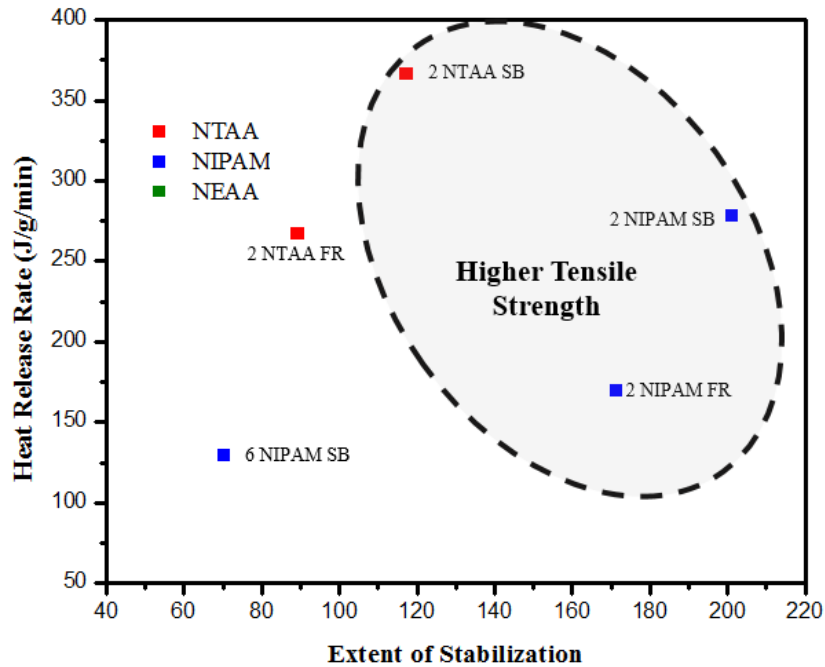
Figure 4.7 Down-selected precursors with higher tensile strength.

4.3 Conclusions

The three down-selected precursors for white fiber spinning, oxidation, and carbonization were 2 mole % NIPAM FR, 2 mole % NIPAM SB, and 2 mole % NTAA SB upon investigating the influence of acrylamide comonomers on copolymer architecture and thermal ring closure. Reactivity ratios of acrylonitrile and NEAA, NIPAM, or NTAA were both ≤ 1, as determined by the non-linear least squares method, and suggested favorable alternating copolymer architecture. As comonomer concentration increased, the average acrylonitrile sequence length, extent of stabilization, cyclization length, heat release rate, and stabilization index all decreased to suggest that thermal ring closure is dependent on comonomer concentration. It is hypothesized that as comonomer concentration is increased, the amount of cyclization sites among the polymer backbone decreased to afford a reduced ring closed graphitic structure; therefore, a comonomer concentration of 2 mole % was selected for fiber processing to increase the final carbon fiber graphitic morphology. [9]

Previous collaborations with WRG and University of Kentucky have highlighted the white fiber spinning capabilities of 2 mole % NIPAM FR. Previous white fiber spinning knowledge will be expanded upon in Chapter V by introducing various white fiber spinning parameters to the 3 down-selected precursors to highlight which spinning conditions affect the development of fiber morphology. The understandings gained from white fiber spinning will allow us to select key white fibers with superior properties to be oxidized and eventually carbonized. The insights gained from Chapters III, IV, and V will provide crucial understandings on the effect of precursor design on thermal ring closure as well as successfully prepare white, oxidized, and carbonized fibers in an effort

to link precursor design to ultimate fiber morphology and properties- an area in which

minimal precedent exists.[9]

CHAPTER V –TRANSFORMATION AND ELUCIDATION OF DOWN-SELECTED

POLYACRYLONITRILE CARBON FIBER PRECURSORS INTO WHITE AND

BLACK FIBER

5.1 Abstract

Two RAFT-based precursors (2 mole % NIPAM SB and 2 mole % NTAA SB) that displayed promising graphitic structure and one free radical precursor (2 mole % NIPAM) were down-selected for white fiber spinning. Careful selection of white fiber spinning parameters, including coagulation conditions and total fiber draw, afforded circular white fibers with diameters of approximately 12 µm or less by scanning electron microscopy (SEM). Additionally, SEM and transmission electron microscopy (TEM) detected increased white fiber defects as total fiber draw increased, which resulted in decreased white fiber break stress values. Interestingly, RAFT-based white fibers also exhibited more consistent break stress and Young's modulus than free radical-based white fibers and suggested more regular RAFT-based white fiber morphologies. Afterwards, all white fibers were exposed to thermo-oxidative stabilization conditions, where time, tension, and temperature parameters were considered to be of vital importance. Upon imaging the oxidized fibers by TEM and SEM, defects that were detected by SEM in the white fibers translated to defects observed in the oxidized fibers. FTIR highlighted that the ring closure within respective oxidized fibers increased as oxidation temperatures also increased. Future work includes carbonization of the previously oxidized fibers, and characterization of black fiber morphologies and mechanical properties.

5.2 Results and Discussion

5.2.1 White Fiber Spinning

White fibers were spun from 3 down-selected precursors from Chapters III and IV alongside the commercially available Goodfellow PAN precursor (99 AN: 1 MA), where GoodFellow PAN was prepared by free radical polymerization and served as a control for the purposes of this investigation. This control was labeled as Goodfellow FR. All four precursors were spun under various conditions, where the draw down ratio (DDR) and gear pump speed (GPS) were varied in an effort to understand how these spinning conditions would affect both physical and mechanical white fiber properties.

Figure 5.1 displayed a schematic of the white fiber spin line used at Deakin University, where the DDR ratio was controlled by the uptake roller labeled as 8, and the GPS was the rate at which the polymer dope labeled as 1 entered the coagulation bath. Draw ratio was calculated as the velocity of the uptake roller labeled as 8 in Figure 5.1, over the velocity of the first roller which was always set to 1 m/min.[60] As DDR was increased from 20 to 25 to 30 m/min., it was hypothesized that white fiber diameters and defects would be reduced to afford highly oriented white fibers with improved black fiber mechanical properties. As the DDR increased, the gear pump speed was kept constant at 0.33 m/min. It is also reasonable to assume that at some elevated DDR, white fiber morphology is negatively affected due to fiber breakage; therefore, it is important to understand under which spinning conditions these defects will occur.
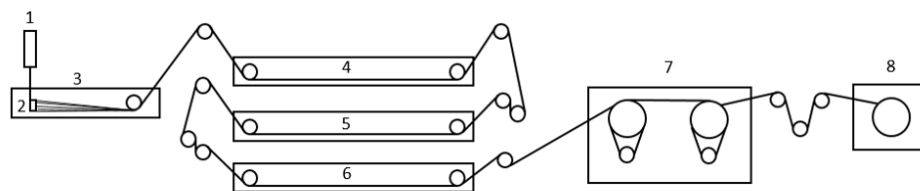
1 – Spinning Solution set at
    a gear pump speed
2 –Spinneret
3 – Coagulation Bath

4-6 – Washing Baths
7 – Heated Godet
8 – Uptake Roller set at
    a draw down ratio

Figure 5.1 Schematic of the white fiber spin line at Deakin University.

Additionally, gear pump speed, also known as volumetric pump rate, controlled the flow of polymer dope within the coagulation bath and was regulated to ensure a consistent flow. Herein, volumetric pump rate was varied from 0.16, 0.22, and 0.33 m/min. to determine a GPS that afforded a consistent dope flow within the coagulation bath as a standard protocol for these precursors, including GPS and DDR, was unavailable as these precursors have never been spun at Deakin University. As GPS varied, the DDR was kept constant at 25 m/min. The volumetric pump rate is known to affect diffusion of solvent and non-solvent within the coagulation bath as a result of influencing shear rate within the spinneret, labeled as 2 in Figure 5.1.[40] The interdependencies between volumetric pump rate on coagulation and white fiber properties within these precursor-based dopes is not well understood; therefore, variations in volumetric pump rate were performed to investigate the effect of spinneret shear rate on white fiber properties.

The spinning conditions including draw and coagulation during the formation of white fibers is vital for the morphological development of final black carbon fiber since white fiber is the final form of the PAN copolymers prior to thermo-oxidative stabilization and carbonization.[11] To afford superior PAN white fibers, a delicate balance

91

between processing conditions, including DDR and GPS, and precursor design must be met in order to obtain white fibers that possess the following favorable characteristics: diameters between 10 to 12 µm, circular cross-sections, a small number of voids, low comonomer content, carbon yields above 50 %, and high mechanical properties.[38,39,51,107,108] Herein, white fiber spinning of RAFT and FR-based precursors provided key insights on the effect of precursor design and processing conditions on white fiber morphology and mechanical properties.

5.2.1.2 Dope rheology and spinnability

A polymer dope is typically comprised of 15 to 30 wt. % PAN copolymer dissolved into a good solvent such as DMSO and is fed through a spinneret into a coagulation bath, where an ideal spinnable dope viscosity for typical wet spinning is about 50 Pa*s.[40] All polymer dopes were carefully prepared by dissolving the 7 to 10 g of precursor into DMSO (20 wt. /v %), respectively, as not to introduce contaminants or excess water from the DSMO solvent. Dope preparation is crucial as gelled polymers, contaminants, air, and water can cause spinneret blockages, fiber breakage, and voids within the fiber.[40,48] After polymer dissolution, the dope appeared transparent and free from large gels or contaminants as observed in Figure 5.2 A, where it is important to keep in mind that the presence of micro-gels cannot be detected by the naked eye.
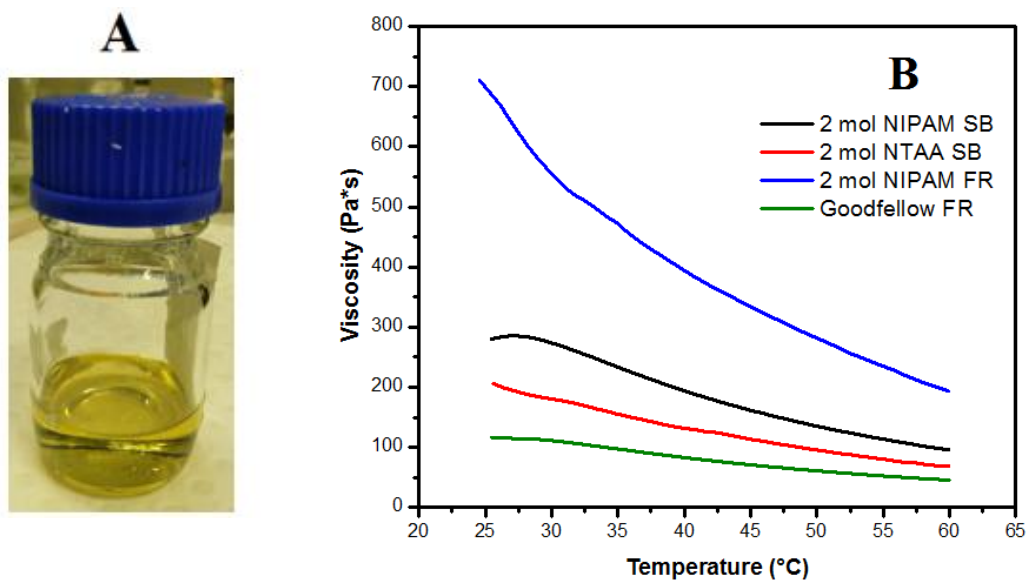
Figure 5.2 Spinning dope solution A) after dissolving precursor overnight B) rheology data.

Rheological measurements of each PAN precursor were collected on a TA Instruments Ares G2 rheometer at Deakin University that was equipped with a 40 mm parallel plate geometry, where the results are graphed in Figure 5.2 B. The dope viscosities of the 2 mole % NIPAM FR precursor were higher than either RAFT-based precursors, as expected from previous findings by Jackie and coworkers that reported the low dispersity values of RAFT caused reduced viscosities.[41] These reduced RAFT viscosities would additionally allow for spinnable dopes with higher polymer concentrations to effectively widen the white fiber processing window as gelation or high viscosities would not occur until higher polymer concentrations. Spinning a polymer dope with higher polymer concentration is advantageous as it increases the probability of spinning dense, non-hollow white fibers.[41]

Goodfellow FR possessed the lowest viscosity measurements of the prepared precursors as depicted in Figure 5.2 B. This lower viscosity occurred due to the lower molecular weight of about 190,000 g/mol, whereas all other precursors had molecular

weights that ranged between 174,700 to 274,000 g/mol as determined by DMF GPC in

Table 5.1. As molecular weight varied for each precursor due to batch-to-batch variation,

it was difficult to determine if the reduced RAFT viscosities were due to decreased

dispersity or molecular weight as viscosity will increase with molecular weight.[40,109] All

dope viscosities in Figure 5.2 B were above the typical spinning viscosity of 50 Pa*s due

to the increased molecular weight values being well above the typical 100,000 to 120,000

g/mol range.[40] These increased dope viscosities, especially 2 mole % NIPAM FR, may be

difficult to spin into white fiber as the spinning solution may clog the spinneret. It would

be convenient to develop a method to eliminate batch-to-batch variation in molecular

weight during precursor synthesis which will be further investigated in Chapter VI.

Future work to determine the optimum viscosity for these precursors is needed as dope

viscosity can affect white fiber properties including defects.[41]

Table 5.1 Precursor molecular weights and dispersity values determined by DMF GPC.

Precursor	Molecular Weight (g/mol)	Đ
2 mole % NIPAM FR	229,300-299,300	1.278-1.286
2 mole % NIPAM SB	174,700-210,500	1.160-1.171
2 mole % NTAA SB	188,000-274,000	1.176-1.201
Goodfellow FR	194,300	1.624

These four polymer dopes were heated at 65 °C, deaerated, filtered, and spun

under similar white fiber spinning conditions with a constant coagulation bath

concentration of DMSO and H_2O (70: 30 v/v) and a coagulation bath temperature of 60

°C as either DDR or GPS varied. Commonwealth Scientific and Industrial Research

Organization (CSIRO) and literature precedent suggested that a higher coagulation bath

concentration would lead to circular, dense white fibers that are desirable for high

performance carbon fiber.[57,110] The copolymer dope was heated at 65 °C in an effort to eliminate die swell at the spinneret and jet inconsistencies within the coagulation bath.[50,57] The coagulation bath temperature of 60 °C was selected as a preliminary white fiber spinning trial with 20 grams of RAFT-based PAN precursor, graciously provided by CSIRO, resulted in white fiber breakage and inconsistencies at 50 and 55 °C. This preliminary trial was beneficial as the 7 to 10 grams of each USM precursor only afforded ~ 20 mL of polymer spinning solution, which limited the amount of spinning parameters that could be altered before all the dope solution was used.

An image of the white fibers containing the NIPAM and NTAA-based precursors spun at 20 DDR and 0.33 GPS are displayed in Figure 5.3. The appearance or luster of white fiber is a quick and qualitative method to rank the quality of white fiber, where highly lustrous fibers imply superior physical and mechanical properties.[38,40] The luster on the white fibers in Figure 5.3 signified that these fibers possessed improved fiber properties, such as a circular shape and fewer surface defects, in comparison to white fibers drawn at higher 25 or 30 m/min. DDR values, which lacked this lustrous appearance.
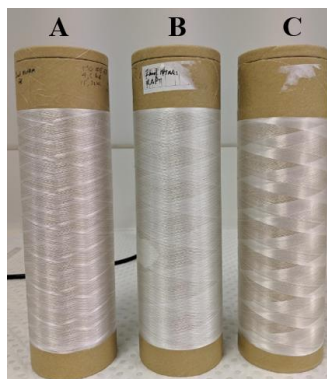
Figure 5.3 White fibers spun at 20 DDR and 0.33 GPS containing A) 2 mole % NIPAM FR B) 2 mole % NTAA SB and C) 2 mole % NIPAM SB precursors.

Table 5.2 highlighted which precursors could and could not afford white fibers under a given DDR or GPS processing conditions. Interestingly, both copolymer PAN precursors that were prepared via free radical methods could not withstand higher DDRs of 30 m/min.; however, RAFT-based white fibers could be drawn and molecularly oriented more so than FR white fibers, highlighting that precursor design does affect fiber spinnability. Increased molecular orientation of the RAFT copolymer chains in the white fiber could lead to improved graphitic structure upon stabilization and therefore increasing the fiber tensile strength.[40] The white fiber shape, density, diameter, and mechanical properties will be measured to investigate the influence of DDR and GPS spinning conditions on RAFT and FR-based PAN copolymer precursors.

Table 5.2 White fiber spinnability of each precursor as DDR or GPS varied.

	Goodfellow FR	2 mole % NIPAM FR	2 mole % NIPAM SB	2 mole % NTAA SB
20 DDR	YES	YES	YES	YES
25 DDR	YES	YES	YES	YES
30 DDR	NO	NO	YES	YES
0.16 GPS	NO	YES	YES	YES
0.22 GPS	NO	YES	YES	YES
0.33 GPS	YES	YES	YES	YES

5.2.1.3 Density

White fiber density measurements were performed on a Ray-Ran Auto density gradient apparatus containing degassed deionized water and sodium bromide solution, where the density gradient ranged from 1.05 to 1.35 g/cm^3. All measurements were performed in duplicate at 23 °C. White fiber samples were prepared by taking three 30 filament tows of a respective white fiber and tying the tows together into three knots, dipping the tied tows into acetone, and dabbing the solvent off with a Kimwipe. Three

tows were used during preparation as using one tow would float and stick to the glass column. Table 5.3 depicted the average density and standard deviation results for each white fiber spun under various spinning conditions.

Table 5.3 White fiber density results.

	Density of Goodfellow FR (g/cm^3)	Density of 2 mole % NIPAM FR (g/cm^3)	Density of 2 mole % NIPAM SB (g/cm^3)	Density of 2 mole % NTAA SB (g/cm^3)
20 DDR	1.168 ± 0.001	1.176 ± 0.0003	1.176 ± 0.001	1.171 ± 0.0003
25 DDR	1.171 ± 0.002	1.172 ± 0.002	1.177 ± 0.002	1.173 ± 0.0001
30 DDR	N/A	N/A	1.177 ± 0.0001	1.172 ± 0.003
0.16 GPS	N/A	1.172 ± 0.003	1.178 ± 0.00002	1.173 ± 0.001
0.22 GPS	N/A	1.175 ± 0.0001	1.182 ± 0.004	1.171 ± 0.001
0.33 GPS	1.171 ± 0.002	1.172 ± 0.002	1.177 ± 0.002	1.173 ± 0.0001

White fibers spun from Goodfellow PAN and 2 mole % NIPAM FR possessed density measurements ranging from 1.168 to 1.176 g/cm^3, while the density of white fibers spun from RAFT-based precursors were from 1.171 to 1.182 g/cm^3 to suggest that precursor design and spinning conditions affect fiber density, as expected. These density measurements were in accordance to PAN density of 1.17 g/cm^3 and suggested that RAFT-based white fibers were more dense and contained less defects such as cavities and voids possibly due to reduced dispersity values and improved spinning conditions.[9,41,74]

The lowest DDR of 20m/min. yielded the lowest density values for each respective precursor with the exception of 2 mole % NIPAM FR. It was expected that as DDR increased, fiber diameter would be reduced and afford increased fiber density values. It is also important to note that the spinning conditions for each precursor were not optimized and the ideal spinning conditions to yield dense round fibers will vary

according to each precursor. Therefore, it was not surprising that the spinning conditions that afforded the highest white fiber density measurements for 2 mole % NIPAM FR at 20 DDR were not identical to the processing conditions necessary for increased density values for 2 mole % NIPAM SB at 0.22 GPS. SEM and TEM microscopy will further aid in the identification of defects within white fibers spun from FR or RAFT-based precursors.

5.2.1.4 SEM Diameter and Morphology

White fiber diameter measurements are important values to obtain prior to oxidation and carbonization as fiber tensile strength is affected by fiber diameter, where advantageous white fiber diameters are within 10 to 12 µm.[38] White fiber diameters ~ 10 to 12 µm will then be reduced to diameter of ~ 5 to 6 µm upon carbonization due to the typical ~ 50 % char yield of commercially available PAN fibers.[39,96] These small carbonized fiber diameters (~ 5 µm) have been reported to increase fiber tensile strength due to a lack of fiber defects.[40,79,111] Therefore, white fibers spun with diameters larger than 10 to 12 µm will likely not be selected for oxidization or carbonization as the amount of fiber defects could be increased. White fiber diameters were measured by the microscopy method, where individual fiber bundles were prepared and measured under SEM as displayed in Table 5.4. Here, at least 3 fiber measurements were calculated for white fiber diameters.

Table 5.4 SEM white fiber diameter measurements as spinning conditions varied.

	Diameter of Goodfellow FR (µm)	Diameter of 2 mole % NIPAM FR (µm)	Diameter of 2 mole % NIPAM SB (µm)	Diameter of 2 mole % NTAA SB (µm)
20 DDR	11.8 ± 1.3	10.0 ± 1.0	11.6 ± 0.6	10.9 ± 1.1
25 DDR	9.8 ± 1.2	10.5 ± 1.0	8.84 ± 0.2	10.3 ± 0.5
30 DDR	N/A	N/A	6.5 ± 0.5	7.5 ± 0.7
0.16 GPS	N/A	Not recorded	7.1 ± 0.5	7.6 ± 0.9
0.22 GPS	N/A	9.0 ± 0.8	9.6 ± 0.2	8.3 ± 0.5
0.33 GPS	10.1 ± 0.9	10.5 ± 1.0	11.7 ± 0.4	10.3 ± 0.5

From Table 5.4, the expected trend of decreased diameter values were recorded as DDR increased for GoodFellow FR, 2 mole % NIPAM SB, and 2 mole % NTAA SB. The diameter of 2 mole % NIPAM FR slightly increased with increased DDR likely due to the limited amount of diameter measurements recorded. Several white fibers possessed lower diameters than the white fiber diameter limit of 10 to 12 µm; however, theoretically if these fibers can withstand the oxidation and carbonization process, then these fibers will afford higher strength values due to a more dense graphitic structure, where decreased white fiber diameters due to increased DDR have been reported to afford increased tensile strength values.[40,111] Additionally, white fibers spun at 20 DDR were close or within the desired white fiber diameter range of 10 to 12 µm and were highly considered for oxidation as these fibers also possessed density values similar to PAN. Further SEM and TEM images of white fibers cross-sectional and longitudinal areas will aid in the down-selection of which white fibers will be selected for both oxidation and carbonization.

SEM was also used to examine the cross-section of each white fiber spun under different processing conditions to investigate fiber shape, diameter, and presence of

defects. Multiple SEM sample preparation methods, including sectioning under liquid

nitrogen and microtoming, were attempted to determine which procedure would provide

a white fiber cross-section without damaging the area of interest. Both methods were

initally thought to have afforded an undamaged cross-sectional image. SEM images

obtained from Goodfellow FR and 2 mole % NIPAM FR, under multiple spinning

conditions, can be observed in Table 5.5.

Table 5.5 SEM images for white fibers spun from Goodfellow FR and 2 mole % NIPAM
FR precursors under various spinning conditions.
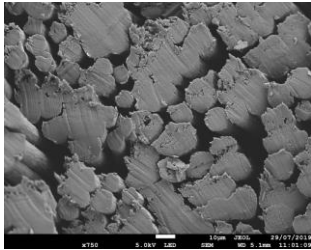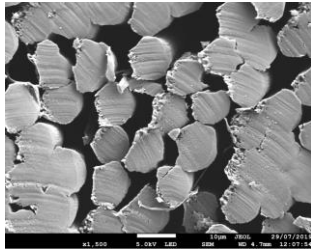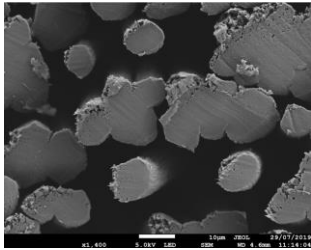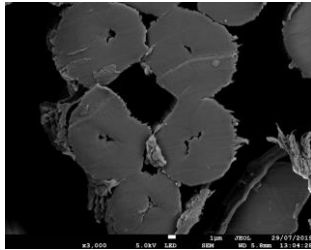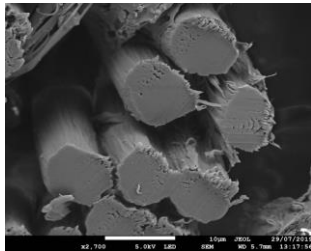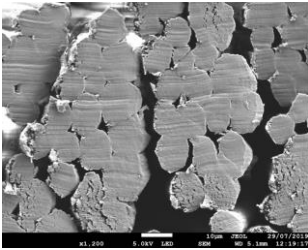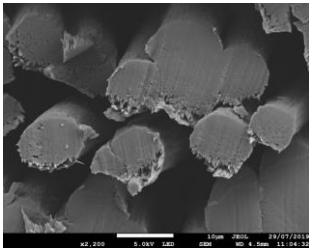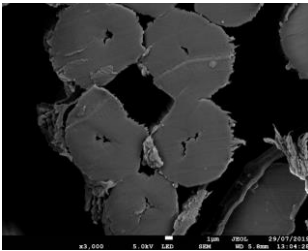
	Goodfellow FR	2 mole % NIPAM FR
20 DDR		
25 DDR		
30 DDR	N/A	N/A
0.16 GPS	N/A	

Table 5.5 (Continued).

0.22 GPS	N/A	
0.33 GPS		

Primarily, these SEM images highlighted that circular white fibers were obtained under certain spinning conditions for precursors prepared by free radical polymerization techniques. All Goodfellow FR spinning conditions that afforded white fibers were circular; whereas, a few possibly bean-shaped fibers were observed in 2 mole % NIPAM FR at 20 DDR. The circular shape of the white fibers indicated that coagulation bath temperature and concentration conditions were satisfactory. However, the presence of white fiber voids suggested that spinning conditions were not optimized as coagulation bath conditions were selected from a preliminary spinning trial with RAFT-based precursor from CSIRO. The location and shape of voids within PAN-based white fibers can aid in selecting which spinning parameter needs to be adjusted or if the copolymer dope needs to be prepared more judiciously. White fiber defects can arise from (1) phase separation that occurs in the coagulation bath and subsequent washing, (2) minor

deformities in the spinneret which allow coagulation bath contents to enter the fiber via surface defects, and (3) dope impurities or gases.[40]

Further SEM imaging as observed in Figure 5.4 highlighted that these white fiber defects within Goodfellow FR and 2 mole % NIPAM FR at 20 DDR were primarily located close to the fiber surface. It was suspected that white fiber defects on the fiber surface was due to poor phase separation within the coagulation or washing baths. Decreasing coagulation rate by reducing the coagulation bath temperature below 60 °C and slow washing is anticipated to aid phase separation and the elimination of white fiber voids.[38,40,110,112] Additionally, white fibers from 2 mole % NIPAM FR precursor spun at 25 DDR and 0.33 GPS in Table 5.5 afforded a loose core structure, where voids were located in the center of the white fibers. This loose core structure can be also attributed to high coagulation rates and is expected to lead to reduced black fiber mechanical properties.[40]

A) Goodfellow FR
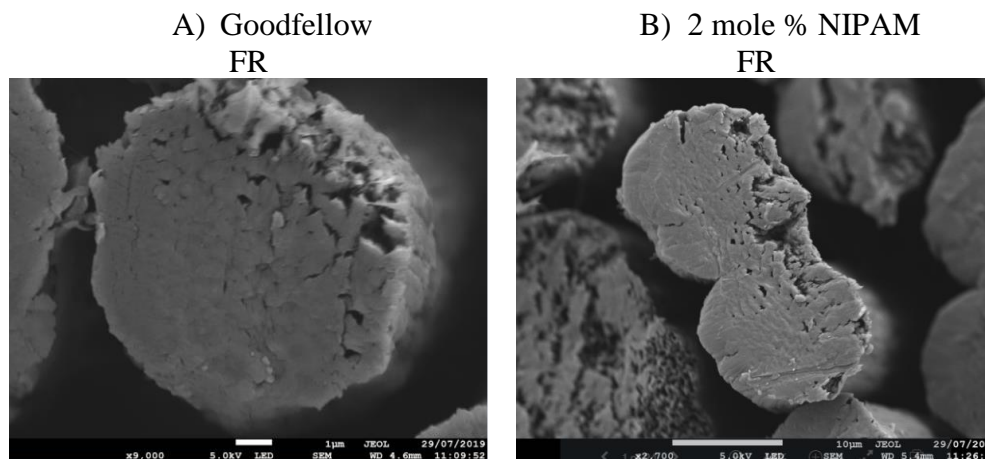
B) 2 mole % NIPAM FR

Figure 5.4 White fiber surface defects for A) Goodfellow FR and B) 2mol NIPAM FR.

SEM images were collected for white fibers spun from RAFT-based precursors and can be observed in Table 5.6, where the white fibers were circular and possessed fewer defects within the fiber core and surface than identified in white fibers spun from

FR precursors in Table 5.5. The reduced voids within the RAFT-based white fibers were hypothesized to be due to reduced dispersity values as well as spinning parameters that were closer to optimum conditions. These RAFT-based white fibers were anticipated to afford improved white and black fiber mechanical properties and will be investigated herein.

Table 5.6 SEM images for white fibers spun from 2 mole % NIPAM SB and 2 mole % NTAA SB precursors under various spinning conditions.
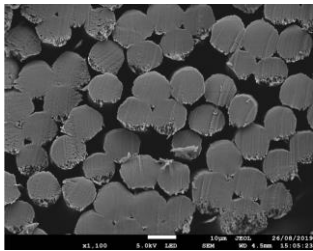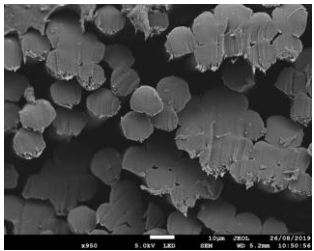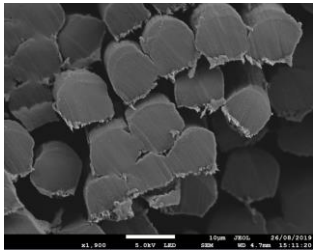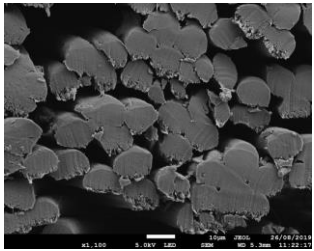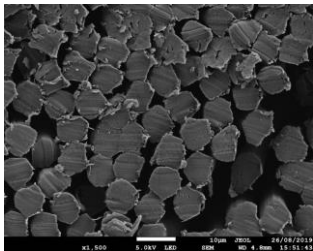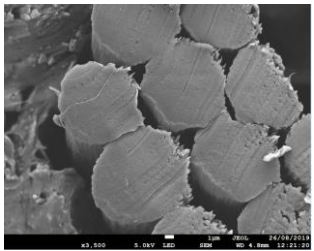
	2 mole % NIPAM SB	2 mole % NTAA SB
20 DDR		
25 DDR		
30 DDR		

Table 5.6 (Continued).

0.16 GPS		
0.22 GPS		
0.33 GPS		

A)   B)   C)
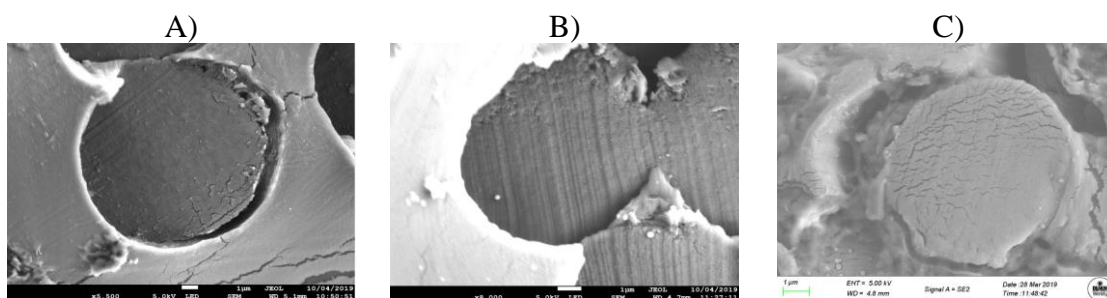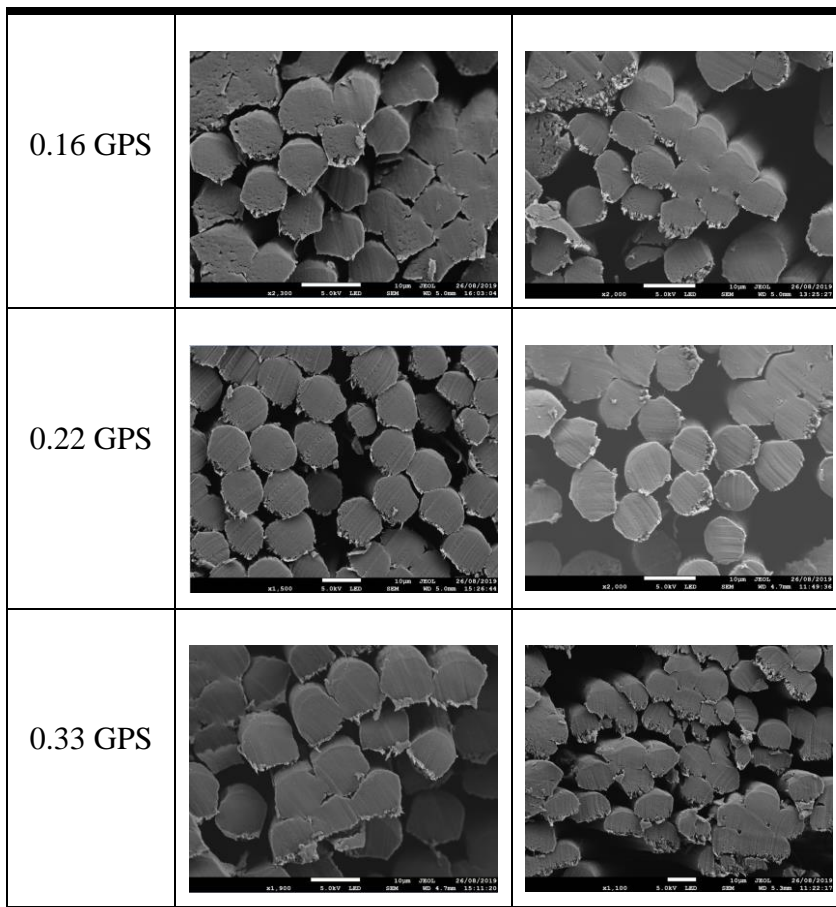
Figure 5.5 SEM images for 2 mole % NIPAM SB as DDR increased from A) 20 to B) 25 to C) 30 m/min.

An interesting phenomenon was recorded in SEM for 2 mole % NIPAM SB, where the appearance of cracks within the white fiber increased at 30 DDR as highlighted in Figure 5.5. It is unclear if these cracks are artifacts from microtoming or if the DDR

limit that the PAN copolymer could withstand was surpassed; thus leading to fiber breakage. However, the white fibers that contained these micro-cracks possessed similar density measurements to white fibers that lacked these features, where it was expected that if these defects were indicative of the fiber morphology, then it would lead to reduced density measurements. These density measurements suggested that the micro-cracks could be artifacts of microtoming. Careful examination of the white fiber mechanical properties will be performed to further investigate the cause of these white fiber defects at 30 DDR. Additionally, future fiber SEM preparation will avoid the use of microtoming, as sectioning the fibers under liquid nitrogen led to undamaged cross-sectional fibers.

5.2.1.5 TEM

TEM was kindly performed by Dr. Richard Liang's research group at Florida State University, where only 2 mole % NIPAM SB white fibers spun at 20, 25, and 30 DDR were imaged due to limited instrumentation time. Figure 5.6 highlighted the white fiber cross-sectional TEM images and corresponding Fast Fourier Transform (FFT) obtained from this collaboration, where the formation of the short graphitic folds within the PAN turbostratic morphology, originally suggested by Johnson in 1987, was observed.[14] A few needle-like crystals were perceived in the high magnification TEM images and were circled in Figure 5.6. The FFT images qualitatively displayed the amorphous halo within the PAN microstructure of each respective white fiber. It was difficult to determine the presence of other typical microstructure features including crystalline bands within the FFT images; therefore, WAXS was performed later on.

A) 2 mole % NIPAM SB at 20 DDR   B) 2 mole % NIPAM SB at 25 DDR   C) 2 mole % NIPAM SB at 30 DDR
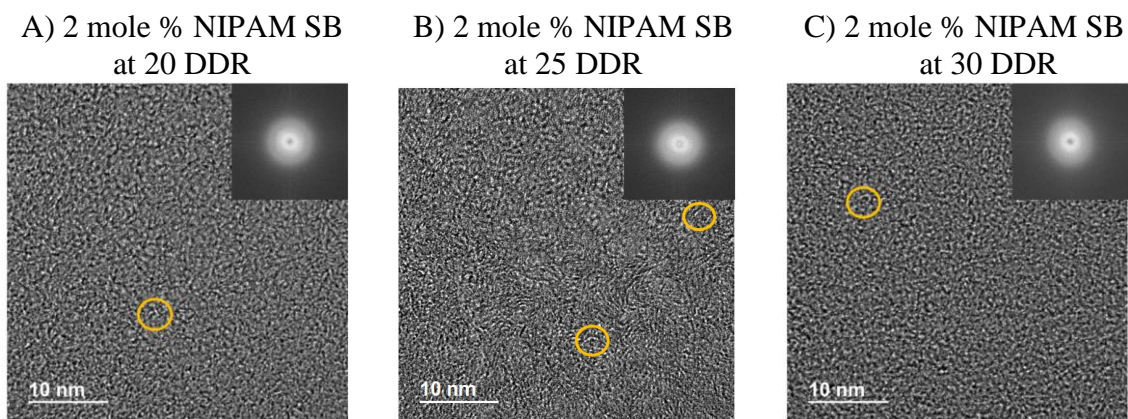
Figure 5.6 TEM and FFT images of white fiber cross-sections for 2 mole % NIPAM SB at A) 20 B) 25 and C) 30 DDR with needle-shaped defects circled in yellow.

Interestingly, at 25 and 30 DDR pores were observed in the white fiber cross-sectional images as recorded in Figure 5.7. These circular pores suggested that either the dope was not sufficiently degassed and caused air to be encapsulated into the fiber or residual solvent remained within the fiber. It was anticipated that the presence of these pores would afford reduced density values; however, from the density measurements from Table 5.3 the density was not affected by these voids.

A) 2 mole % NIPAM SB at 25 DDR   B) 2 mole % NIPAM SB at 30 DDR

106
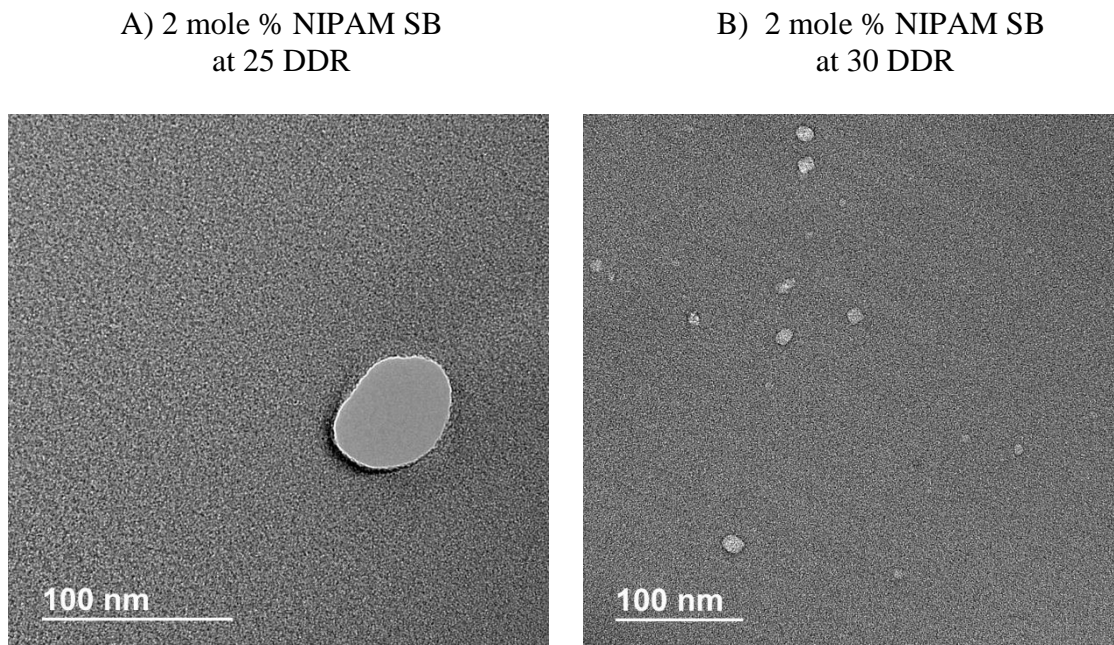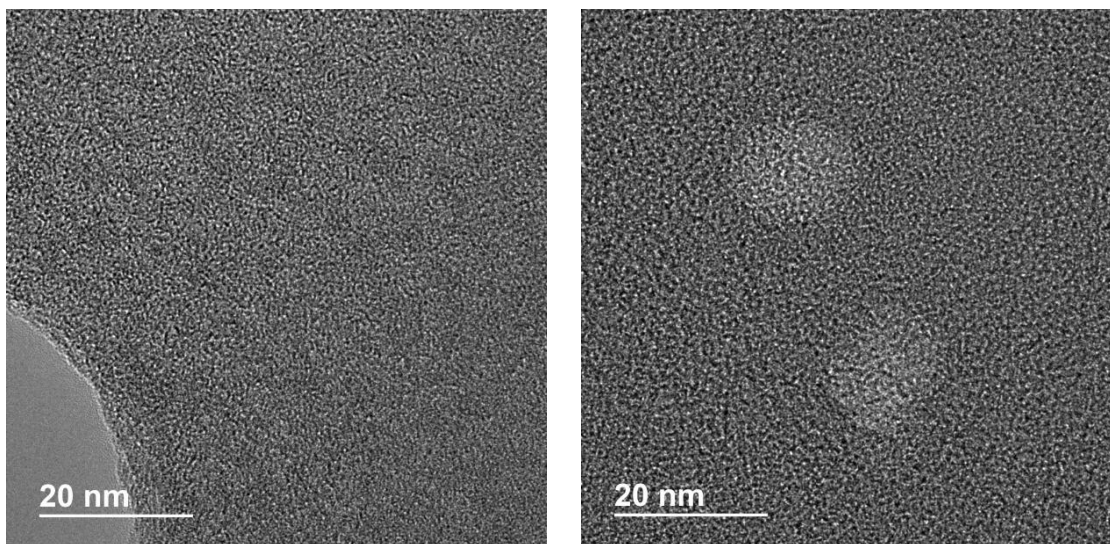
Figure 5.7 TEM images of 2 mole % NIPAM SB at A) 25 and B) 30 DDR.

TEM was also performed of the longitudinal direction of 2 mole % NIPAM SB at 20, 25, and 30 DDR, where the ion beam milling direction was perpendicular to the fiber direction as highlighted in Figure 5.8 and resulted in striations within the TEM image. These striations in the milled direction are referred to as the "curtain effect" and are due to fiber preparation.[113,114] This "current effect" was observed in Figure 5.8 C and should not be confused with polyacrylonitrile chain alignment within the white fiber sample. Several pores were observed for the 2 mole % NIPAM SB at 30 DDR in both the cross-sectional and longitudinal directions in Figures 5.7 B and 5.8 C, respectively. These defects are anticipated to afford reduced white and black fiber tensile strength properties as tensile strength is controlled by the presence of morphological defects within the fiber such as pores and crystallites. For improved tensile strength properties, a white fiber with limited pores and crystallites is highly desired as defect-laden white fiber morphology will affect black fiber morphologies.[4] White fibers that were spun at 25 and 30 DDR

exhibited white fiber morphological defects in both SEM and TEM; therefore, these white fibers will likely be removed from consideration for oxidation.

A) 2 mole % NIPAM SB at 20 DDR   B) 2 mole % NIPAM SB at 25 DDR

C) 2 mole % NIPAM SB at 30 DDR
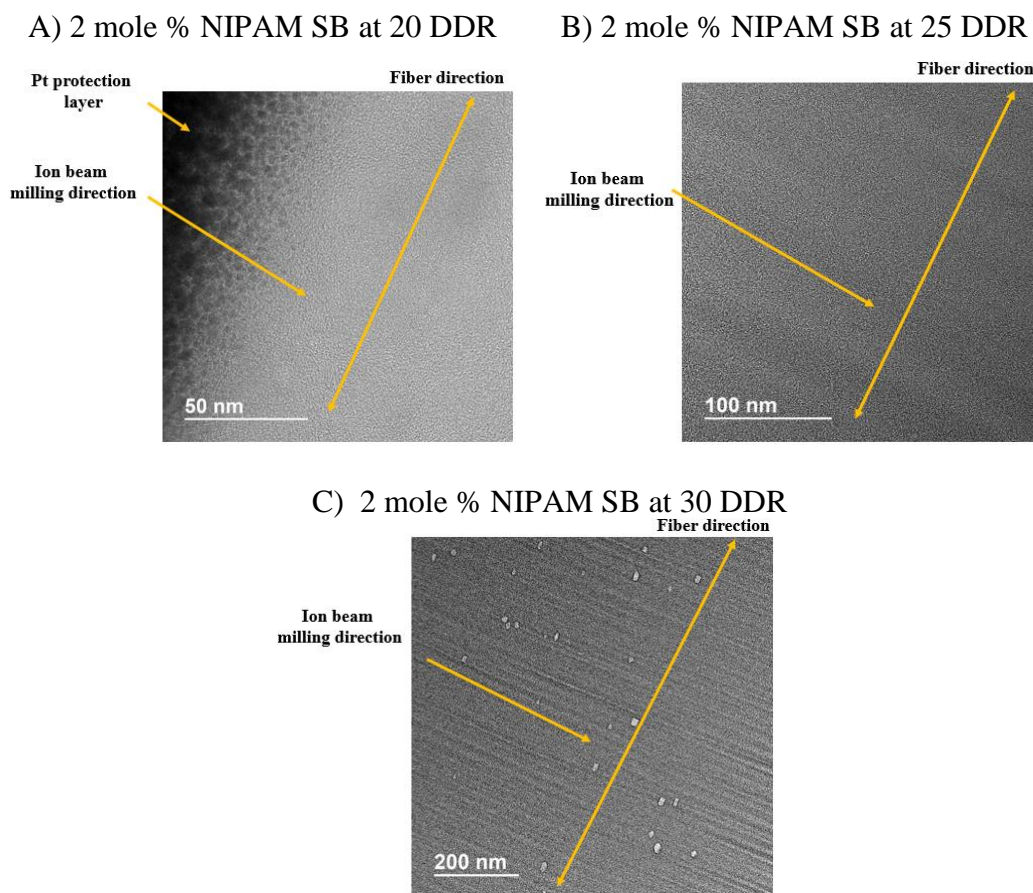
Figure 5.8 TEM and FFT images of white fiber prepared in the longitudinal direction for 2 mole % NIPAM SB at A) 20 B) 25 and C) 30 DDR.

5.2.1.6 WAXS

WAXS was performed on each 30 filament fiber bundle that was exposed to various spinning conditions under the guidance of Dr. Peter Lynch and his team at the Australian synchrotron at Monash University. A representative WAXS image of a RAFT-based white fiber was highlighted in Figure 5.9 A, where all RAFT precursor, regardless of spinning conditions, afforded similar WAXS diffractograms. From these WAXS diffractograms, distinct bands at 3 and 5 Å^{-1} that corresponded to the (110) and (100)

crystal lattice planes, respectively, were clearly observed and expected from PAN-based white fibers. The (100) crystal plane was indicative of the intra-molecular dipole-dipole interactions from the pendent PAN nitrile groups, while the (110) band is attributed to the crystallographic planes in PAN. It is anticipated that upon carbonization in the low temperature oven, the (002) and (004) bands will appear due to the parallel stacking of hexagonal carbon sheets in black fiber.[8,84,106,115]

A) RAFT White Fiber   B) 2 mole % NIPAM FR White Fiber
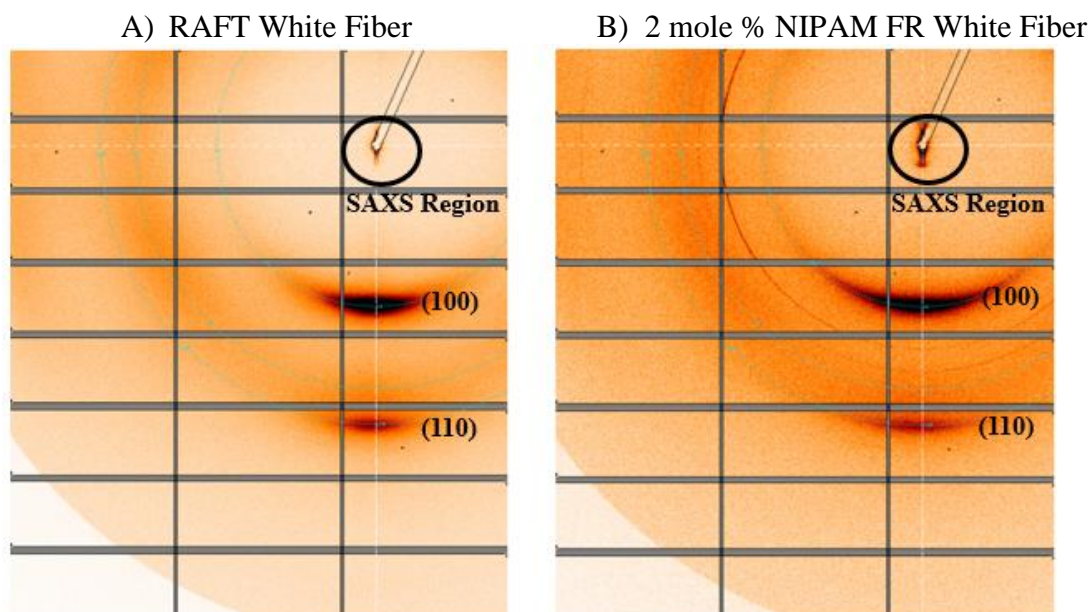
Figure 5.9 WAXS patterns for A) RAFT and B) 2 mole % NIPAM FR white fibers.

More importantly, 2 mole % NIPAM FR-based white fibers possessed additional bands closer to the beamstop in the small angle X-ray scattering (SAXS) region as depicted in Figure 5.9, which was not observed for RAFT-based white fibers and suggested that free radical-based white fibers would exhibit SAXS variations as compared to their RAFT counterparts. Notably, these SAXS bands within FR-based white fibers highlighted that the microstructure of white fibers spun from precursors prepared by traditional free radical polymerization methods are indeed different than white fibers spun from RAFT-based precursors. This promising preliminary data further

confirmed that precursor design affected white fiber microstructure. These SAXS bands, which suggest the presence of larger, possibly even micron size defects with the white fiber. This SAXS data agreed well with the SEM data for FR-based white fibers, where an increase in fiber defects was also recorded. Future work that continues to analyze both WAXS and SAXS of white fibers will be able to confirm of presence of defects ranging in size, to further elucidate the effect of controlling the PAN precursor copolymer architecture on white fiber morphologies and mechanical properties.

5.2.1.7 Mechanical Properties

Single white fiber mechanical testing including break stress and modulus was performed on a Textecho FAVIMAT+, where the average and standard deviation of each mechanical property was calculated from at least 5 replicates under each spinning condition. A typical force versus elongation curve was plotted in Figure 5.10 from the Textecho Favimat+ instrument, where representative results for 2 mole % NIPAM FR-based white fibers and RAFT-based white fibers were displayed as A) and B), respectively. Clearly from Figure 5.10, white fibers prepared from free radical precursors possessed more variation in the break stress values than exhibited in SB RAFT-based white fibers. This data suggested that SB RAFT-based white fiber morphology was more consistent than free radical-based white fiber morphology, which further supported by the previous SEM data in Table 5.5, Table 5.6, and Figure 5.4, where SB RAFT white fibers possessed less defects than free radical-based white fibers.

A) White fiber from 2 mole %
   NIPAM FR precursor

B) White fiber from SB RAFT
   precursor
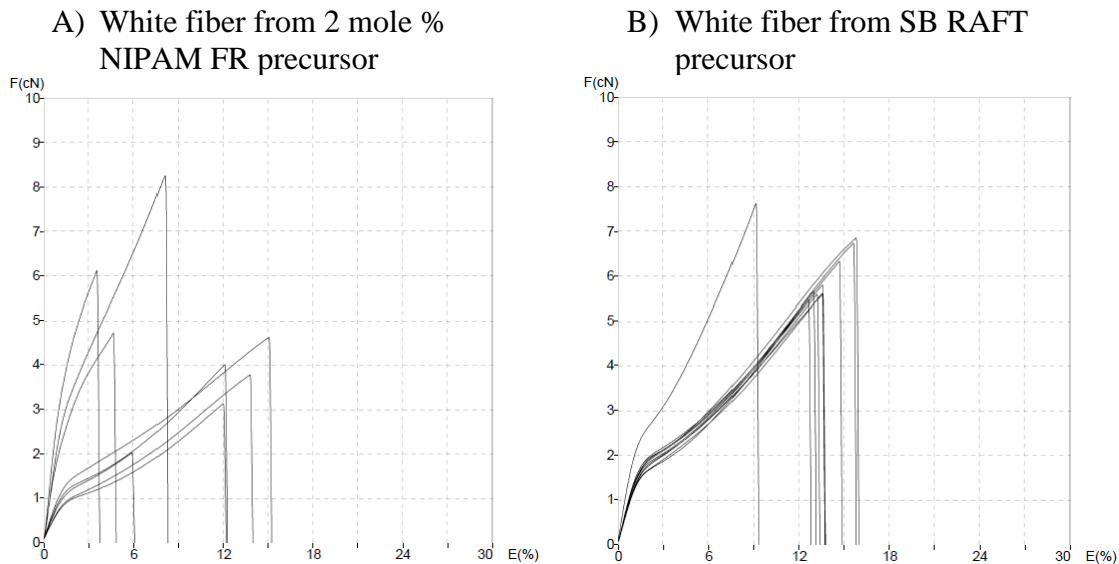
Figure 5.10 Representative white fiber Textecho Favimat+ data from A) free radical-based precursor and B) RAFT-based precursors.

It is important to understand that aforementioned morphologies and defects during the spinning of white fiber will affect mechanical properties and will subsequently affect the black fiber morphologies and mechanical properties. Therefore, careful investigation and understanding of white fiber spinning conditions on white fiber morphologies and mechanical properties is crucial to obtaining high performing carbon fiber. A trade-off between high tensile strength and high modulus carbon fiber exists, where high tensile strength, as a result of limited fiber defects, typically possess reduced tensile modulus properties. Conversely, high tensile modulus carbon fibers, from high crystallinity and crystallite alignment along the fiber direction, affords reduced tensile strength.[2,4,6]

Here, the break stress and Young's modulus were investigated and recorded in Table 5.7 and 5.8, respectively, in order to further understand the effect of white fiber spinning conditions on white fiber morphologies and to anticipate which spinning conditions would afford high tensile strength or modulus carbon fibers. This knowledge

111

will be beneficial for the down-selection of white fibers for oxidation and eventual

carbonization.

Table 5.7 Favimat break stress values for white fibers spun under various conditions.

	Break Stress of Goodfellow FR (GPa)	Break Stress of 2 mole % NIPAM FR (GPa)	Break Stress of 2 mole % NIPAM SB (GPa)	Break Stress of 2 mole % NTAA SB (GPa)
20 DDR	0.46± 0.24	0.53 ± 0.04	0.40 ± 0.02	0.44 ± 0.08
25 DDR	1.12 ± 0.34	0.49 ± 0.14	0.31 ±0.05	0.34 ± 0.08
30 DDR	N/A	N/A	0.16 ± 0.03	0.18 ± 0.04
0.16 GPS	N/A	0.20 ± 0.04	0.12 ± 0.03	0.14 ± 0.03
0.22 GPS	N/A	0.31 ± 0.13	0.23 ± 0.06	0.19 ± 0.04
0.33 GPS	1.12 ± 0.34	0.49 ± 0.14	0.31 ± 0.05	0.34 ± 0.08

Table 5.8 Favimat Young's modulus for white fibers spun under various conditions.

	Young's Modulus of Goodfellow FR (GPa)	Young's Modulus of 2 mole % NIPAM FR (GPa)	Young's Modulus of 2 mole % NIPAM SB (GPa)	Young's Modulus of 2 mole % NTAA SB (GPa)
20 DDR	12.94 ± 8.43	8.97 ± 0.79	8.33 ± 0.45	7.93 ± 0.45
25 DDR	30.31 ± 5.10	10.07 ± 1.89	7.27 ± 0.29	6.78 ± 0.47
30 DDR	N/A	N/A	4.06 ± 0.30	3.77 ± 0.19
0.16 GPS	N/A	5.86 ± 1.72	3.28 ± 0.24	3.90 ± 0.80
0.22 GPS	N/A	10.82 ± 7.10	5.23 ± 0.81	3.92 ± 0.25
0.33 GPS	30.31 ± 5.10	10.07 ± 1.89	7.27 ± 0.29	6.78 ± 0.47

From Table 5.7, white fiber spun at 20 DDR and 0.33 GPS afforded the highest

break stress values, respectively. Increased DDR values were anticipated to reduce white

fiber diameter, and increase both density and break stress values; however, the presence

of defects including pores and crystallites that were observed in both SEM and TEM led

to reduced break stress values at higher DDR values. Increasing DDR was also predicted

to increase crystal alignment along the fiber axis and therefore afford an increased

Young's modulus.[40,107] However, the Young's modulus listed in Table 5.8 did not increase upon increasing DDR for both RAFT-based white fibers. It is believed that SB RAFT-based white fibers drawn at either 25 or 30 DDR afforded over-stretched white fibers which lead to PAN fiber breakage; therefore, these spinning conditions afforded both reduced break stress and Young's modulus as over-stretching the fibers increased white fiber defects and hindered polymer chain alignment within the fibers. The break stress and Young's modulus for Goodfellow FR-based white fibers at 25 DDR and 0.33 GPS was significantly higher than the white fibers spun from USM precursors. This difference was not expected and may have occurred due to the limited Favimat data, where literature reports at least 45 replicates for each white fiber.[68,71] Future work includes increasing the amount of fiber replicates to further examine the cause of the higher break stress values in Goodfellow FR. Additionally, the upper limit of fiber stretching for FR-based white fibers was at 25 DDR, as fibers could not be spun at 30 DDR.

Previous unpublished research in the Wiggins Research Group has spun white fibers from 2 mole % NIPAM FR precursor under the expertise of Dr. Matthew Weisenberger at University of Kentucky (UK) and analyzed the white fiber mechanical properties including break stress. A comparison of the break stress of the white fibers spun at the UK, and the white fibers spun at Deakin University at 20 DDR and 0.33 GPS spinning conditions were displayed in Figure 5.11, where previous research also performed mechanical analysis on the commercially available BlueStar and Jilin white fibers. Interestingly, the free radical-based white fibers spun at UK afforded increased break stress values as compared to the Deakin University white fibers, thus suggesting

that the spinning conditions at UK were superior. This break stress comparison

highlighted that white fiber spinning conditions of the same precursors influenced fiber

mechanical properties significantly. Additionally, the RAFT-based white fibers spun at

Deakin University yielded break stress values were comparable to the commercially

available BlueStar white fibers. We anticipated that RAFT-based white fibers would

surpass the mechanical properties of commercially available white fibers as these are

prepared by free radical polymerization; however, the spinning conditions for these

RAFT fibers were not optimized. It is expected that future work in adjusting white fiber

spinning parameters such as coagulation bath temperature and concentration to reduce

coagulation rate will improve white fiber morphology and mechanical properties.

Figure 5.11 Break stress mechanical properties from white fibers obtained from A)
Deakin University and B) University of Kentucky.
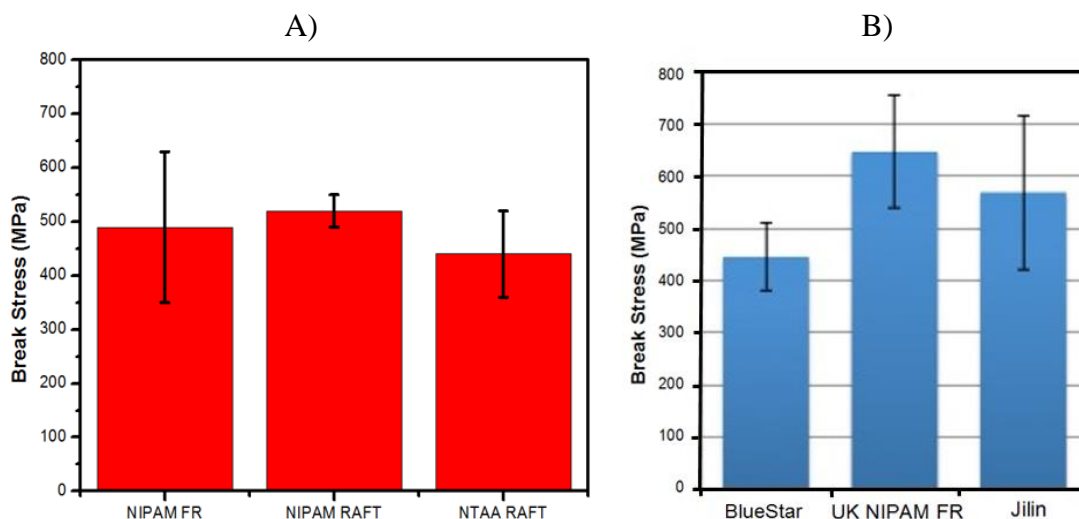
5.2.2 Oxidized Fiber

Results from white fiber spinning highlighted that white fibers spun at 20 DDR

and 0.33 GPS afforded circular fibers with favorable fiber diameters, densities, and

morphologies. Four white fibers (Goodfellow FR, 2 mole % NIPAM FR, 2 mole %

NIPAM SB, and 2 % mole NTAA SB) spun at 20 DDR and 0.33 GPS were down-selected for oxidation using a carbon fiber simulator at Carbon Nexus in Geelong, Australia. Fourteen processing parameters have been found to affect the structure of the stabilized fibers on an industrial carbon fiber line; therefore, the careful selection of oxidation parameters is not trivial. However, three main oxidation processing parameters which affect all white fiber precursors are time, temperature, and tension. These three key parameters are referred to as TTT.[56] Here, a careful balance of TTT was attempted during oxidation with two separate trials that possessed different TTT profiles in an effort to obtain stabilized fibers that lack a skin-core morphology and possessed increased ring closure.

5.2.2.1 Oxidation Trial 1

Eight white fiber tows containing 30 filaments each for a total of 240 filaments were oxidized for each of the four selected white fibers. Preparing 240 filaments for each oxidized fiber was performed to ensure that enough fiber would be available for FTIR, SEM, TEM, and carbonization. The time and temperature processing conditions used in preparing all oxidized fibers were the following: ramp from room temperature to 225 °C followed by a 24 min. isothermal hold, ramp to 235 °C, 24 min. isothermal hold, ramp to 245 °C, 24 min. isothermal hold, ramp to 255 °C, and 24 min. isothermal hold. The fan air speed was set to 80 %; however, future work to understand the influence of air fan speed and temperature ramp rates would be beneficial as these parameters also affect ring closure. These time and temperature conditions were used to mimic oxidation conditions in Chapter III and IV and afforded high ring closure via FTIR under oxidative conditions. The tension used for preparing each oxidized fiber is displayed in Table 5.9. Tension

values were set below the maximum force required to break 240 filaments of white fiber as determined from the single filament Favimat+ data.

Table 5.9 Tension values used to prepare each oxidized fiber.

Oxidized Fiber	Tension (Kg)
Goodfellow FR	1.50
2 mole % NIPAM FR	1.80
2 mole % NIPAM SB	1.40
2 mole % NTAA SB	1.50

Upon oxidation and removal of the oxidized fibers from the simulator, the stabilized fibers varied in color as observed in Figure 5.12, where the color ranged from white to yellow to dark brown, and back to yellow and white. This color change was expected as oxidation is known to cause white fiber to undergo various shades of yellow, reddish brown, and eventually black.[1] While the cause of these color changes is not well-understood, some hypothesize that the black color is due to the formation of the ring closured structure that contains C-N bonds.[39] Based on this conjecture, black oxidized fibers in Figure 5.12 were not obtained and suggested that significant ring closure along the PAN backbone did not occur. FTIR will be performed to examine the amount of ring closure after oxidation.
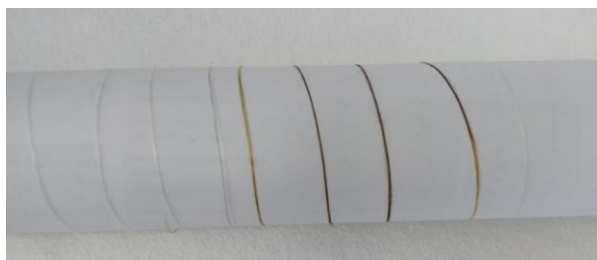
Figure 5.12 Color variation in oxidized fibers.

5.2.2.1.2 SEM and TEM for Oxidation Trial 1

Florida State University was able to examine the morphology of the oxidized fiber

prepared from the 2 mole % NIPAM SB precursor under both SEM and TEM. The SEM

images can be observed in Figure 5.13, where there is a platinum layer deposited around

the outside of the fiber which should not be considered to be indicative of the oxidized

fiber morphology. From these SEM images, a few pores were observed in the middle and

edge of the fiber. These pores are likely the result of defects that translated from the

white fiber, as previously observed in SEM images of the white fiber, to the oxidized

fibers which may ultimately become present in the final carbonized fiber and reduce

tensile strength.
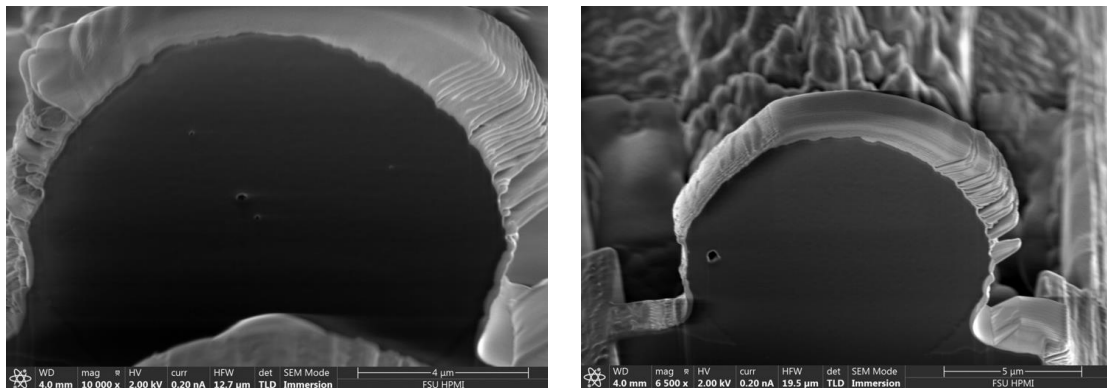
Figure 5.13 SEM images of oxidized fibers from 2 mole % NIPAM SB precursor.

TEM was also performed and displayed in Figure 5.14 at various scale lengths,

where the typical graphitic folds within the turbostratic morphology of PAN was

observed.[14] Minimal crystallites and pores were observed within the TEM images, which

suggested the oxidized fiber did not possess nanometer size defects or inhomogeneities.

The extent of ring closure for each oxidized fibers was performed via FTIR to determine

if the fibers were sufficiently stabilized.
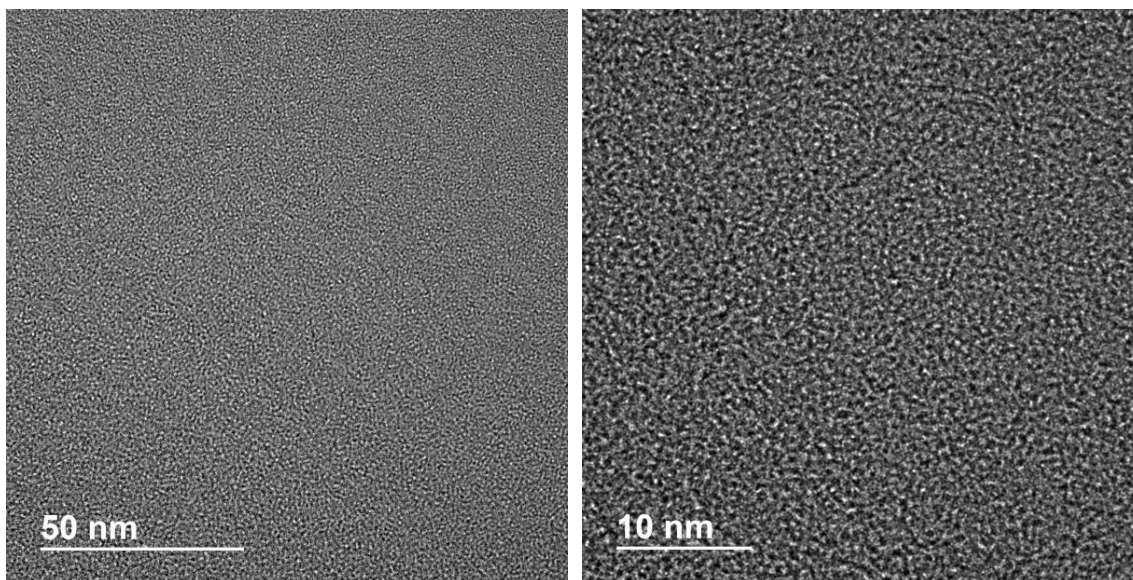
Figure 5.14 TEM images of oxidized fibers from 2 mole % NIPAM SB precursor.

5.2.2.1.3 FTIR for Oxidation Trial 1

FTIR was performed on the oxidized fibers, where special care was taken to analyze the darkest portion of the fibers, consistently. A representative FTIR plot of an oxidized fiber can be observed in Figure 5.15, where the peaks of interest are labeled. From the FTIR, the reacted nitrile % was calculated by comparing the alkene peak at 1590 cm^{-1} and the alkyne peak at 2240 cm^{-1} according to Nunna and coworkers.[28] Additionally, the dehydrogenation index was determined from the CH stretch at 1350 cm^{-1} and the CH$_2$ band at 1451 cm^{-1} with Equation 7 in Chapter II.[28] These calculated values from FTIR were listed in Table 5.10. Both the reacted nitrile % and dehydrogenation index values were lower than expected and suggested that insufficient ring closure occurred, which agreed with the lack of black color in the oxidized fibers. From Table 5.10, it was noted that at least 80 % of pendent nitrile groups within the copolymer backbone were still available for ring closure after subjecting these fibers to oxidative conditions. If these oxidized fibers, with such limited cyclized rings, were to be

118

carbonized, the fibers would rupture due to thermal shock and would render no fiber at the end of carbonization.
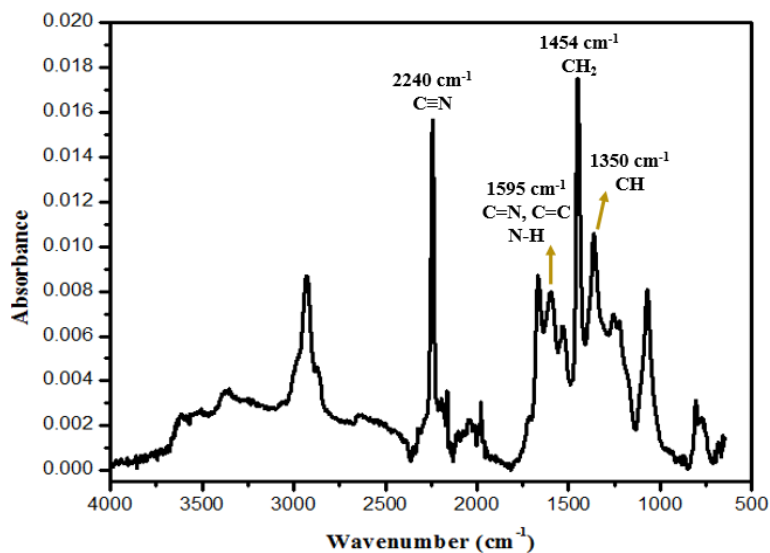
Figure 5.15 Representative FTIR of an oxidized fiber.

Table 5.10 Results from oxidized fibers.

Oxidized Fiber	Reacted Nitriles (%)	Dehydrogenation Index
Goodfellow FR	13.72	0.50
2 mole % NIPAM FR	6.74	0.49
2 mole % NIPAM SB	7.86	0.48
2 mole % NTAA SB	9.90	0.34

A qualitative burn test which is typically subjected to oxidized fibers in order to determine if an oxidized fiber would survive carbonization was attempted with the four down-selected oxidized fibers. This burn test was performed according to Tshai and workers, where one tow of oxidized fibers (30 filaments) was used.[116] In order to pass the burn test, the oxidized fibers must not burn when placed into a flame.[1] Upon immediate exposure to the flame, the oxidized fiber would break and shrink, which made it difficult to determine if the oxidized fiber burned. Additionally, one tow of white fiber was

119

exposed to the same burn test conditions and yielded similar results where white fiber was anticipated to burn. It was thought that using a small tow size of only 30 filaments limited one's ability to use the burn test.

FTIR results from the oxidized fibers suggested that the TTT conditions selected were not ideal due to the low reacted nitrile %. Upon re-examining the DSC results from Chapter IV and collaborating with Deakin University, oxidation conditions with higher temperatures should be selected in the next carbon fiber simulator trial. From the previous DSC experiments (ramp at 10 °C/min. to 325°C), NIPAM and NTAA began ring closure at 275 and 255 °C, respectively. Therefore, setting the highest oxidation temperature to 255 °C did not provide sufficient heat and energy to ring close a significant amount of nitrile groups within NIPAM and NTAA-based precursors.

5.2.2.2 Oxidation Trial 2

As the majority of the three USM down-selected white fibers were consumed in the first oxidation trial, additional precursor (2 mole % NIPAM FR, 2 mole % NIPAM SB, and 2 mole % NTAA SB) was prepared according to similar methods and sent to Deakin University to spin a sufficient amount of white for the second oxidation trial.

After white fiber spinning, according to the analogous 20 DDR and 0.33 GPS processing conditions, thirty white fiber tows containing 30 filaments each for a total of 720 filaments were oxidized for each of the three USM selected white fibers. Goodfellow FR was not spun under these same conditions into white fiber due to time restraints. Here, temperature was increased when preparing all oxidized fibers according to the following oxidation method: ramp from room temperature to 260 °C followed by a 24 min. isothermal hold, ramp to 270 °C, 24 min. isothermal hold, ramp to 280 °C, 24 min.

isothermal hold, ramp to 290 °C, and 24 min. isothermal hold. The final temperature of 290 °C was selected to improve the extent of ring closure as this temperature was above the exotherm temperature for both NIPAM and NTAA-based precursors.

5.2.2.2.1 FTIR for Oxidation Trial 2

FTIR was performed on all three USM oxidized fibers at Deakin University to investigate the reacted nitrile %, and the results are listed in Table 5.11. Increasing the temperature parameters in trial two notably increased the reacted nitrile % of each USM precursor and suggested that ring closure was also increased. The improved reacted nitrile % was confirmed by our collaborators to be sufficient for these oxidized fibers to undergo carbonization.

Table 5.11 FTIR results of USM oxidized fibers under trial 2 processing parameters.

Oxidized Fiber	Reacted Nitriles (%)
2 mole % NIPAM FR	64.7
2 mole % NIPAM SB	65.9
2 mole % NTAA SB	64.5

Carbonization will be performed on the oxidized fibers as possible future work under the following protocol: 2 minute isothermal holds at 450, 650, 850, 1100, and 1400 °C. After carbonization, the fibers will be analyzed to further our understandings of the influence of precursor chemistries and processing parameters on ultimate black fiber morphologies.

5.3 Conclusions

Four precursors were spun into white and oxidized fibers with our collaborators at Deakin University, where processing parameters such as draw down ratio, gear pump speed, and oxidation temperature were varied in an effort to elucidate the effect of precursor chemistries and processing parameters on fiber morphologies. The coagulation bath conditions of 60 °C with a DMSO and H_2O (70: 30) concentration within white fiber spinning afforded the favorable circular fiber cross-sectional areas and diameters. RAFT-based white fibers could also withstand increased draw down ratios and possessed fewer defects as compared to the FR counterparts. Additionally, oxidation temperature was determined to significantly affect ring closure.

These results highlighted that precursor chemistries do indeed influence fiber processing conditions, properties, and morphologies. However, white fiber spinning parameters were not optimized as evident by the differences between the break stress values of white fibers prepared from 2 mole % NIPAM FR spun at Deakin University and previously at the University of Kentucky, where only the spinning parameters varied. It is reasonable to assume that each precursor would require different white fiber spinning, oxidation, and carbonization parameters to obtain optimum performance. Therefore, future work is needed to investigate the optimum fiber processing parameters of these precursors to further reduce the amount and size of fiber defects, increase fiber mechanical properties, and increase our understandings of the effect of precursor design and processing on the semi-crystalline morphologies of PAN-based carbon fiber.

CHAPTER VI –ATTEMPTS TO SYNTHESIZE HIGH MOLECULAR WEIGHT PAN

COPOLYMERS VIA CONTINUOUS REACTOR

6.1 Abstract

Efforts to synthesize free radical PAN precursors with high molecular weights ($\geq$ 100,000 g/mol) via a continuous reactor were performed in four trials where pump rate, temperature, screw speed, and solvent concentration were varied. In the first trial, pump rates of 10, 15, and 30 ml/min. filled the screws sufficiently to afford a consistent output of solution with barrel temperatures ranging from 60 to 110 °C. Aliquots collected directly from the continuous reactor outlet did not precipitate and signified no high molecular weight polymer was formed; however, ^{1}H NMR indicated a small amount of polymer was synthesized. In trial two, the increased barrel temperature range of 90 °C to 140 afforded four aliquots that precipitated and possessed molecular weights between 41,000 to 42,000 g/mol. In the third trial, residence speed was varied from 20 to 55 seconds. All aliquots collected from trial three precipitated and indicated polymer was prepared as well as conversion varied from about 55 to 80 %. Lastly, increased monomer concentration of acrylonitrile in DMSO (40:60 wt. %) afforded increased molecular weight of ~ 45,000 g/mol. These four brief trials highlighted that PAN-based precursors can indeed be prepared with a continuous reactor which can significantly aid in the processing of large quantities of PAN as this method can reduce batch-to-batch variation and the amount of DMSO solvent used to afford substantial cost savings. Future work to understand the relationships between continuous reactor variables and PAN chemistries such as molecular weight and dispersity is necessary to fully vet the unique potential of this method to direct PAN copolymer architectures.

123

6.2 Results and Discussion

Continuous chemical reactors that possess fully intermeshing twin screws are an excellent method for reactive processing of polymers. The self-wiping geometry of the fully intermeshing screws affords high mixing, dispersion, and shear control. Additionally, utilization of continuous chemical reactors has the following benefits as compared to conventional batch polymerization techniques: (1) reduced reaction times, (2) decreased solvent cost as the modular techniques can be designed to be solvent free, (3) reduced temperature gradients, and (4) increased efficiency due to reaction mixture de-volatilization which drives reaction progress forward.[117–119] In the Wiggins research group, the Prism continuous chemical reactor, as depicted in Figure 6.1, was used to investigate the viability of this method to prepare PAN-based precursors as well as the effect of which continuous reactor variables influence precursor molecular weight. The 16 mm twin screws possessed length to diameter ratio of 25 and the continuous reactor possessed five controllable heating zones. This screw design was selected due to its success in mixing and conveying other solution chemistries throughout the continuous reactor barrel. Furthermore, the bottom screw image in Figure 6.1 was collected after a trial run to highlight the lack of polymer build up and the relative ease of cleaning the screws.

Free radical polymerization of poly(AN-co-NTAA) (98:2) was attempted for all trials according to the aforementioned procedure in Chapter II with a molar ratio of [AN] : [NTAA] : [AIBN] = 148 : 3 : 0.031 was prepared, where the V-70 initiator was replaced with AIBN due to the lack of V-70 availability. Reaction solutions for trials one, two, and three possessed an acrylonitrile to DMSO ratio of 20:80, whereas trial four used a

monomer to solvent ratio of 40:60. The 20:80 monomer to solvent ratio was chosen as

this concentration was used to successfully prepare batch free radical polymerizations of

PAN copolymers in the previous chapters. DMSO was used in place of ethylene

carbonate to simulate conditions used in industry. A peristaltic pump was used to deliver

the reaction solution to the inlet of the reactor with flexible polyethylene tubing. All trials

were conducted in a walk-in fume hood to eliminate exposure to any gaseous products

released during polymerization. After a trial was performed, all individual elements

within the screws should be removed and allowed to soak in acetone overnight. This

simple practice reduced acidic moieties (radicals within the reaction solution) from

damaging the screws.

Figure 6.1 Images of (top) continuous reactor and (bottom) twin screw design used.

Trial One

The continuous reactor conditions listed in Table 6.1 were used for trial one, where seven aliquots were collected with a screw speed of 300 revolutions per minute (rpm) and variations in pump rate and heating zone temperatures within the barrel. The aforementioned screw speed was critical in order to effectively convey reaction solution to the reactor outlet as the pump rate varied. The barrel temperature ranges between 60 and 110 °C were selected in an effort to supply sufficient heat to decompose the AIBN initiator, as AIBN decomposes at ~ 65 °C.[120] All aliquots were collected and light yellow in color as noted in Figure 6.2. Each aliquot was precipitated, similarly to the aforementioned precipitation method in Chapter II, into scintillation vials containing DI H_2O and methanol (80:20 v/v) as illustrated in Figure 6.2, where no precipitation was collected for any aliquots. The lack of precipitate indicated that a minimal amount of PAN was prepared under these continuous reactor conditions. ^{1}H NMR was performed on aliquot 6 and was listed in Figure 6.3, where common PAN backbone peaks were observed between δ= 1.6 to 2.3 ppm and 3.0 to 3.2 ppm.[62,63] These[1]H NMR peaks confirmed the presence of PAN within aliquot 6; therefore, aliquot 6 continuous reactor conditions were used as a starting point for trial two.

Table 6.1 Continuous reactor conditions for trial one.

Aliquot number	Pump Rate (mL/min.)	Barrel Temperature Range (°C)
1	10	60-90
2	15	60-90
3	15	60-90
4	15	60-100
5	15	60-110
6	30	60-110
7	30	60-110
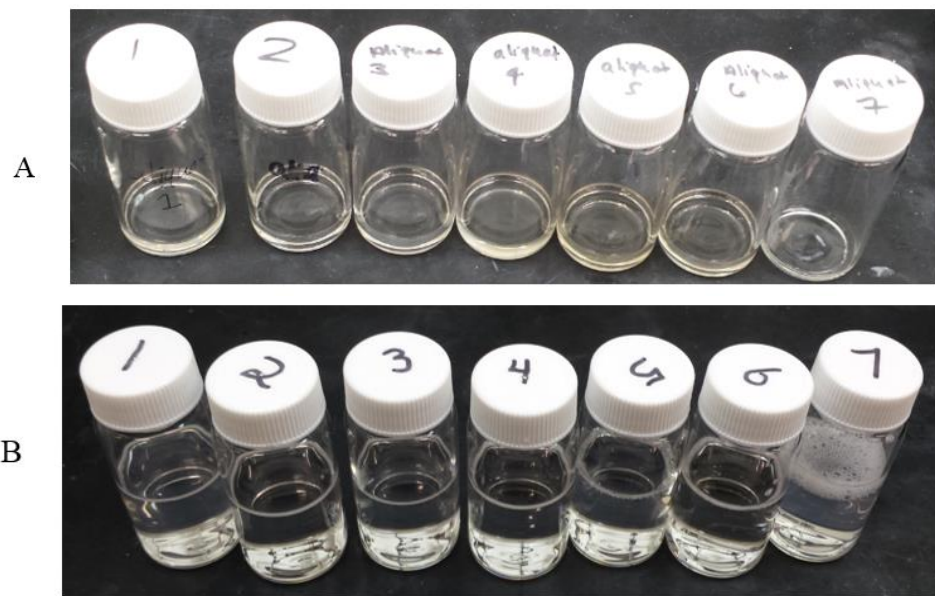
Figure 6.2 Trial one aliquots from A) the outlet of the reactor and B) after precipitation.
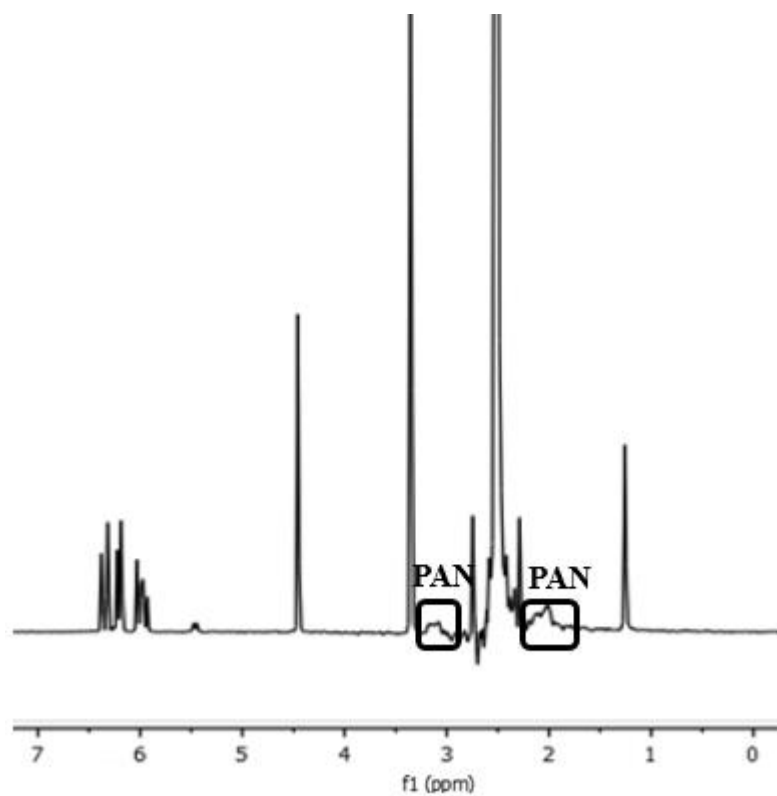
Figure 6.3 ^{1}H NMR of aliquot 6 for trial one.

6.2.2 Trial Two

The continuous reactor processing conditions used in trial two were listed in Table 6.2, where a constant screw speed of 300 rpm was used and six aliquots were collected. All aliquots were precipitated similarly as described in trial one. Once the barrel reached 130 °C, aliquots 3 to 6 precipitated and ^{1}H NMR confirmed polymer was successfully prepared via the continuous reactor as depicted in Figure 6.4 and 6.5, respectively. The significance of requiring a barrel temperature of 130 °C to afford polymer is not well understood as it is well above the necessary 65 °C to decompose AIBN.[120]

Table 6.2 Continuous reactor processing conditions for trial two.

Aliquot number	Pump Rate (mL/min.)	Barrel Temperature Range (°C)
1	5	60-110
2	5	70-120
3	5	80-130
4	5	90-140
5	7	90-140
6	10	90-140
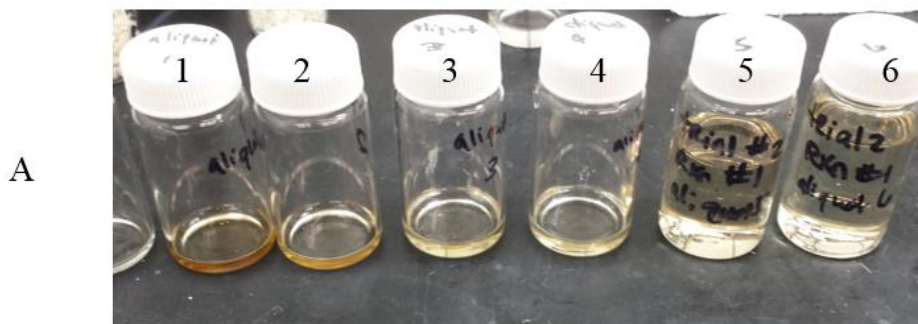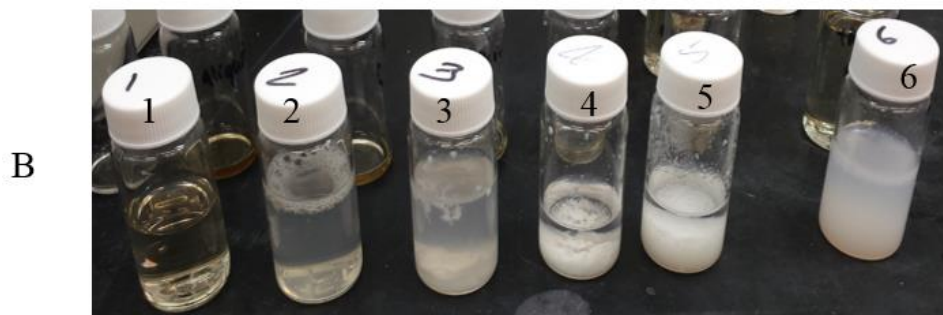
Figure 6.4 Trial two aliquots from A) the outlet of the reactor and B) after precipitation.
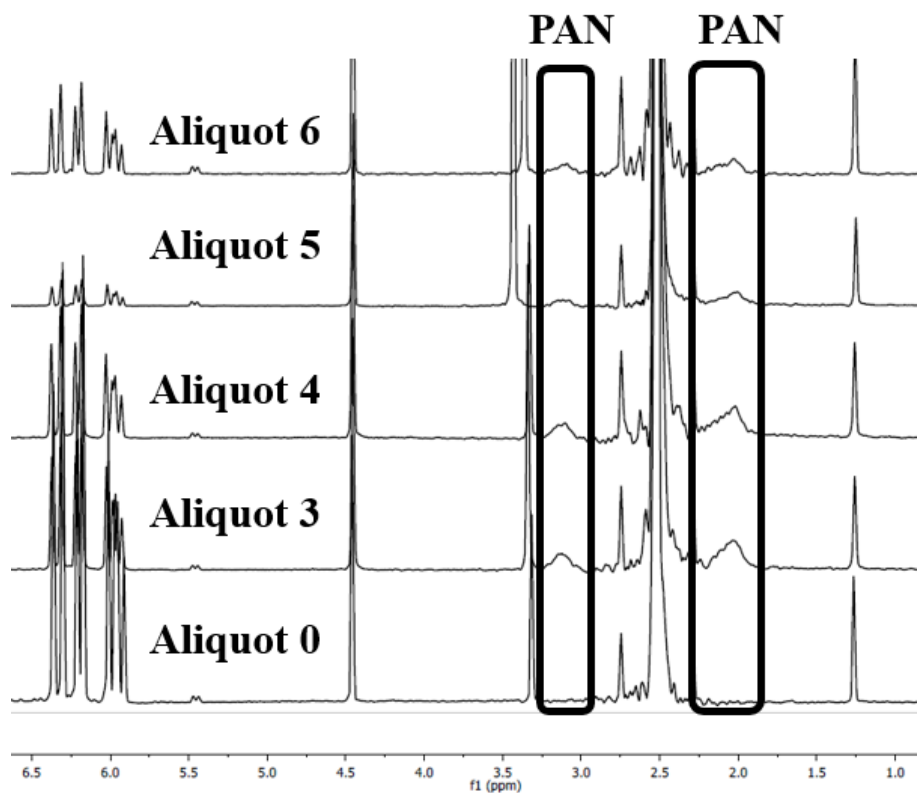
Figure 6.5 Stacked ^{1}H NMR spectra of various aliquots for trial two.

Larger samples were collected under the conditions used for aliquots 5 and 6 so that sufficient polymer would be precipitated for GPC analysis. ^{1}H NMR and GPC results of aliquots 5 and 6 were recorded in Table 6.3. Additionally during trial two, a gaseous product was released at the outlet of the reactor once the barrel reached temperatures above 130 °C as illustrated in Figure 6.6. This gaseous product could have resulted from the initiator AIBN, which released nitrogen upon decomposition or the acrylonitrile

monomer that boiled off as the barrel temperature exceeded its boiling point. If

acrylonitrile monomer was boiled off throughout the reaction, the conversion data may

not be accurate. However, trial two provided proof of concept that PAN with a molecular

weight of approximately 40,000 g/mol can be prepared via a continuous reactor. Future

work should include alleviating this gaseous by-product, as it is potentially a health and

safety concern. It is possible that the gaseous by-product could be avoided by using a

different initiator such as V-70 to reduce the barrel temperature required to initiate

polymerization.

Table 6.3 ^{1}H NMR and DMF GPC results from aliquots 5 and 6 for trial two.

Aliquot number	Conversion[a]	MW (g/mol)[b]	Đ[b]
5	80	42,080	1.610
6	78	41,360	1.528

[a]Conversion was determined by proton NMR according to a similar method described in Chapter II. [b]Molecular weight and dispersity

were analyzed via GPC according to the aforementioned procedure in Chapter II.
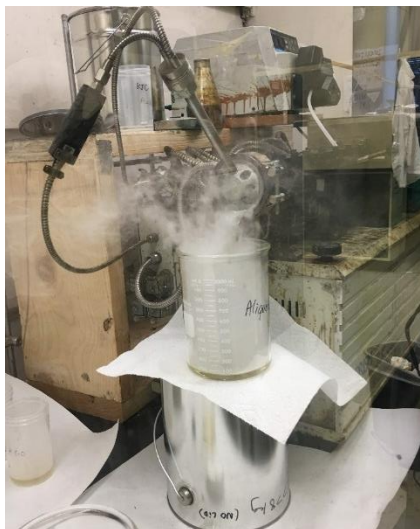
Figure 6.6 Evolution of gaseous product at the reactor outlet for trial two.

6.2.3 Trial Three

Temperature profile and pump rate conditions for trial three were the same as described in trial two for aliquot 5 as the reactor conditions for aliquot 5 yielded the highest molecular weight. The effect of residence time on conversion was investigated in trial three, where residence time varied from 20 to 55 seconds by adjusting screw speed. Here, residence time was measured as the time the reaction mixture took to travel from the reactor inlet to outlet. From Table 6.4, conversion decreased as residence time increased from 28 seconds. All aliquots precipitated as observed in Figure 6.7. Further research into the effect of molecular weight and dispersity as residence time varied is needed.

Table 6.4 Continuous reactor processing conditions for trial three.

Aliquot number	Screw Speed (rpm)	Conversion	Residence time (seconds)
1	300	79	28
2	300	78	Not collected
3	50	59	55
4	150	55	35
5	250	55	33
6	100	58	40
7	200	55	48

Figure 6.7 Trial three aliquots from A) the outlet of the reactor and B) after precipitation.

6.2.4 Trial Four

Temperature profile and pump rate conditions for trial four were the same as described in trial two for aliquot 5; however the [AN]:[DSMO] was increased from 80:20 to 40:60 to investigate if higher molecular weight could be prepared by reducing solvent content. Only one aliquot was collected during this brief trial. Interestingly, the polymer that was collected after precipitation and vacuum filtration, appeared whiter than previous trial aliquots, which were observed to be more yellow as illustrated in Figure 6.8. This whiter product could be the result of using a reduced solvent concentration which lead to less solvent removal and a more pure product.

Trial 2   Trial 2   Trial 4
Aliquot 5   Aliquot 6   Aliquot 1
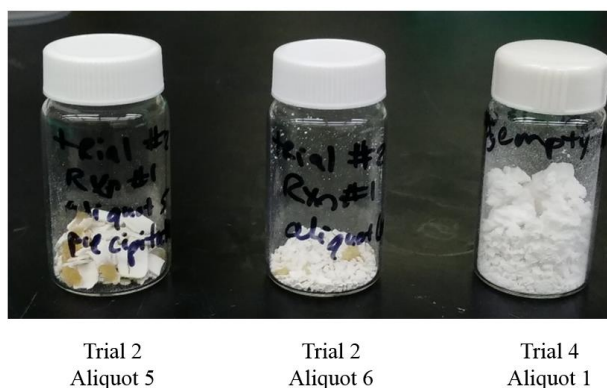
Figure 6.8 Appearance of polymer collected from trials two and four.

Additionally, GPC results in Table 6.5 indicated an increased molecular weight of ~ 45,000 g/mol as AN concentration increased. The increased MW may be due to an increased collision frequency as more AN monomer was available to react.

132

Table 6.5 DMF GPC results for trial four.

Aliquot	MW (g/mol)	Đ
1	44,930	1.652

6.3 Conclusions

These promising preliminary results suggested that, not only could PAN be prepared via a continuous reaction but also that molecular weight could be tuned by monomer to solvent concentration and processing conditions. Within Chapter VI, the monomer to initiator concentration was kept constant; however, it is reasonable to assume that by reducing the initiator concentration, this could lead to longer PAN chains with increased molecular weight. Additionally, by selecting an initiator with a lower decomposition temperature, such as V-70, it may also reduce the barrel temperature required to synthesize PAN and mitigate the evolution of a gaseous product likely due to the acrylonitrile monomer. Reducing the barrel temperature by utilizing V-70 may also afford a more favorable PAN architecture with less branching. PAN precursors prepared by free radical polymerizations are known to possess a branched architecture due to the increased frequency of chain transfer; however, decreased reaction temperatures have led to a PAN architecture with reduced branching.[93,121] Future work to fully understand how to control PAN precursor architecture via a continuous reactor by investigating the interdependencies of continuous reactor processing conditions and PAN chemistries may provide a unique opportunity to mitigate current PAN precursor processing drawbacks such as batch-to-batch variation and significant quantities of DMSO used.

CHAPTER VII CONCLUSIONS AND FUTURE WORKS

The mechanical properties, especially tensile strength, of PAN-based carbon fibers are restricted despite the large base of literature and commercial products available. These limitations stem from the lack of (1) communication between industry and academia as these materials are highly proprietary and processing conditions contain trade secrets in industry and (2) knowledge of how carbon fiber precursor design and processing conditions together affect ultimate black fiber morphologies and mechanical properties. Few research groups possess the ability to control the evolution of the ring-closed carbon fiber morphology via polyacrylonitrile chemistry, fiber spinning and processing.[9] Moreover, recent preliminary findings have highlighted that controlling key precursor design elements, such as high molecular weight and low dispersity via RAFT polymerization, indeed impacted black fiber performance; however, traditional comonomers (itaconic acid and methyl acrylate) were incorporated into the precursor by batch RAFT techniques and altered white fiber spinning conditions, such as draw rate were not investigated.[41] Herein, a unique academic collaboration allowed this research effort to direct precursor design with novel comonomers and multiple polymerization techniques for improved ring closing efficiencies and controlled fiber processing in an effort to further elucidate the complex interdependencies of precursor chemistries and fiber processing parameters on structural evolution of the PAN turbostratic morphologies.

In Chapters III and IV, the effect of precursor design, including comonomer selection, comonomer concentration, polymerization method, and copolymer architecture, on thermal ring closing was examined. In Chapter III, ten precursors were synthesized via free radical, batch RAFT, and semi-batch RAFT techniques with 2 mole

134

% of various acrylamide comonomers. RAFT copolymers afforded the desirable

characteristics of high molecular weights (> 100,000 g/mol) and low dispersity values (<

1.3) that are necessary for development of superior fibers.[40] Semi-batch RAFT copolymer

architectures afforded increased ring closure due to reduced dispersity as evident by the

increased extent of stabilization values, exotherm intensities, and heat release values with

reduced activation energy values as compared to free radical counterparts. The improved

ring efficiency of semi-batch RAFT copolymers determined in Chapter III spurred the

investigation of the influence of acrylamide comonomer concentration on copolymer

architecture and cyclization of semi-batch RAFT precursors in Chapter IV. Additionally,

DSC experiments from both Chapter III and IV highlighted that the incorporation NEAA,

NIPAM, and NTAA comonomers into the precursor copolymer expressed a single

exotherm peak. This exotherm behavior suggested that these acrylamide comonomers

participated in the free radical ring closing mechanism like neutral comonomers.

Reactivity ratios of acrylonitrile and NEAA, NIPAM, or NTAA were both ≤ 1, as

calculated by the non-linear least squares method, and suggested that favorable cross-

propagation of each monomer would afford an alternating copolymer architecture.

Comonomer concentration was determined to highly influence thermal ring closure. As

comonomer concentration increased, the average acrylonitrile sequence length, extent of

stabilization, cyclization length, heat release rate, and stabilization index all decreased.

This thermal behavior suggested that as comonomer concentration increased, the amount

of cyclization sites among the polymer backbone decreased to afford a reduced ring

closed graphitic structure, which led to a comonomer concentration of 2 mole % to be

selected for fiber processing to increase the final carbon fiber graphitic morphology.

From Chapters III and IV, the three USM precursors that were down-selected for white fiber spinning in Chapter V were 2 mole % NIPAM FR, 2 mole % NIPAM SB, and 2 mole % NTAA SB as these precursors demonstrated improved ring closure from thermal data, which suggested superior tensile strength as well as the ability to be synthesized at the necessary 7 to 10 gram scale required for white fiber spinning at Deakin University.

In Chapter V, the three USM precursors along with a commercially available control (Goodfellow FR) was spun into white fiber, where draw down ratio and gear pump speed were varied to gain insights into the effect of white fiber spinning conditions on white fiber morphology. Coagulation bath conditions of 60 °C and 70:30 (DMSO: H_2O) concentration afforded the desired circular white fiber shape, as deviations from circularity are known to reduce white and black fiber mechanical properties, and favorable white fiber diameters between 10 to 12 µm to dissipate heat buildup within the fiber core upon further oxidation and carbonization.[38–40] Interestingly, white fibers prepared from free radical precursors could not withstand increased fiber draw down ratios of 30 m/min. as compared to the semi-batch RAFT white fibers to signify that PAN polymer chains within RAFT-based white fibers could be further oriented. RAFT-based white fibers also possessed more consistent white fiber mechanical properties such as break stress due to the reduced fiber voids observed via SEM and TEM likely caused by the reduced precursor dispersity and processing conditions closer to ideal parameters. White fibers that were processed at a draw down ratio and gear pump speed of 20 and 0.33 m/min., respectively, were down-selected for further oxidation as these fibers possessed the fewest fiber defects and highest break stress values.

Oxidation parameters, especially temperature, significantly influenced the ring closure of the down-selected white fibers, where increased oxidation temperatures afforded improved ring closure as determined by FTIR. Additionally from SEM, fiber defects from the white fiber were translated into the oxidized fiber to highlight the importance of possessing defect-free white fiber as fiber defects propagate throughout fiber processing. Future work with our collaborators will be to carbonize these oxidized fiber to link precursor chemistry, white fiber spinning, oxidation and carbonization conditions to ultimate black fiber morphology and mechanical properties.

Spinning precursors into white fiber was significantly impeded by the amount of precursor that could be produced for Chapter V; therefore, attempts to synthesize several grams of high molecular weight PAN-based carbon fiber precursors was performed in Chapter VI via a continuous reactor technique. It would be advantageous to synthesize PAN precursors by this continuous method as it would reduce reaction times to seconds besides hours, reduce temperature gradients due to increased polymerization viscosity, and reduce the need for solvent which drives the cost of carbon fiber.[4,117–119] The four brief trials to produce high molecular weight PAN precursors yielded promising preliminary results that PAN can be prepared via a continuous reaction and that precursor molecular weight can be tuned by reducing solvent concentration and varying processing conditions. The highest molecular weight prepared continuous reactor was ~ 45,000 g/mol. Future work to further investigate the influence of PAN synthetic design such as initiator choice and concentration as well as processing conditions including screw design is needed to fully understand the capability of preparing high molecular weight carbon fiber precursors with a continuous reactor.

Carbon fiber research within the Wiggins research group, both previous and herein, has demonstrated our innate capabilities to control precursor design through multiple routes and our efforts to find the elusive link between precursor chemistry and fiber processing to direct fiber morphology and mechanical properties. These complex relationships are not obvious and are worth investigating further as over a decade's worth of research has just now allowed us to begin to probe the mechanical property differences between free radical and RAFT-based fibers and the compounding influence of precursor design, white fiber spinning and oxidation conditions on PAN morphologies. Broadening our understanding of processing PAN, via the continuous reactor and various white fiber spinning techniques (dry or wet), along with our current in-depth knowledge of PAN precursor design is the key to advancing the future of carbon fiber.

REFERENCES

(1)   Chung, D. D. L. *Carbon fiber composites*; 1994.

(2)   Chand, S. *J. Mater. Sci.* **2000**, *35* (6), 1303–1313.

(3)   Thompson, R. C.; Swan, S. H.; Moore, C. J.; Saal, F. S. *Philos. Transitions R. Soc. B* **2009**, *364*, 1973–1976.

(4)   Huang, X. *Materials (Basel).* **2009**, *2* (4), 2369–2403.

(5)   Das, T. K.; Ghosh, P.; Das, N. C. *Adv. Compos. Hybrid Mater.* **2019**, *2*, 214–233.

(6)   Chae, H. G.; Newcomb, B. A.; Gulgunje, P. V.; Liu, Y.; Gupta, K. K.; Kamath, M. G.; Lyons, K. M.; Ghoshal, S.; Pramanik, C.; Giannuzzi, L.; Şahin, K.; Chasiotis, I.; Kumar, S. *Carbon N. Y.* **2015**, *93*, 81–87.

(7)   Wanhill, R. J. H. *Aerospace Applications of Aluminum À Lithium Alloys*; Elsevier Inc., 2014.

(8)   Liu, J.; He, L.; Ma, S.; Liang, J.; Zhao, Y.; Fong, H. *Polymer (Guildf).* **2015**, *61*, 20–28.

(9)   Wangxi, Z.; Jie, L.; Gang, W. *Carbon N. Y.* **2003**, *41* (14), 2805–2812.

(10)   Ozcan, S.; Vautard, F.; Naskar, A. K. **2014**.

(11)   Edie, D. D. *Carbon N. Y.* **1998**, *36* (4), 345–362.

(12)   Frank, E.; Hermanutz, F.; Buchmeiser, M. R. *Macromol. Mater. Eng.* **2012**, *297* (6), 493–501.

(13)   Park, S.-J.; Gun-Young, H. *Carbon Fibers*; 2015; Vol. 210.

(14)   Johnson, D. J. *J. Phys. D. Appl. Phys.* **1987**, *20* (3), 286–291.

(15)   Bhanu, V. a.; Rangarajan, P.; Wiles, K.; Bortner, M.; Sankarpandian, M.; Godshall, D.; Glass, T. E.; Banthia, a. K.; Yang, J.; Wilkes, G.; Baird, D.;

McGrath, J. E. *Polymer (Guildf).* **2002**, *43* (18), 4841–4850.

(16) Jie, L.; Wangxi, Z. *J. Appl. Polym. Sci.* **2005**, *97* (5), 2047–2053.

(17) Hobson, R. J.; Windle, A. H. *Macromolecules* **1993**, *26* (25), 6903–6907.

(18) Oya, N.; Johnson, D. J.; Hamada, H. *Proc. Int. Conf. Compos. Mater.* **1999**, 1–10.

(19) Minus, M. L.; Kumar, S. *J. Met. Miner. Mater. Soc.* **2005**, *57* (2), 52–58.

(20) Moskowitz, J. D. *Dissertation* **2015**, *173* (December).

(21) Ruland, W.; Liu, X. D. *Macromolecules* **1993**, *2* (3), 3030–3036.

(22) Dalton, S.; Heatley, F.; Budd, P. M. *Polymer (Guildf).* **1999**, *40* (20), 5531–5543.

(23) Gupta, a.; Harriso, I. R. *Carbon N. Y.* **1996**, *34* (11), 1427–1445.

(24) Yu, M.; Wang, C.; Bai, Y.; Wang, Y.; Xu, Y. *Polym. Bull.* **2006**, *57* (5), 757–763.

(25) Ouyang, Q.; Cheng, L.; Wang, H.; Li, K. *Polym. Degrad. Stab.* **2008**, *93* (8), 1415–1421.

(26) Ju, A.; Luo, M.; Zhang, K.; Ge, M. *J. Therm. Anal. Calorim.* **2014**, *117* (1), 205–215.

(27) Badii, K.; Golkarnarenji, G.; Milani, A. S.; Naebe, M.; Khayyam, H. *React. Chem. Eng.* **2018**, *3*, 959–971.

(28) Nunna, S.; Naebe, M.; Hameed, N.; Creighton, C.; Naghashian, S.; Jennings, M. J.; Atkiss, S.; Setty, M.; Fox, B. L. *Polym. Degrad. Stab.* **2016**, *125*, 105–114.

(29) Ju, A.; Guang, S.; Xu, H. *Carbon N. Y.* **2013**, *54*, 323–335.

(30) Sayyar, S.; Moskowitz, J.; Fox, B.; Wiggins, J.; Wallace, G. *J. Appl. Polym. Sci.* **2019**, 1–10.

(31) Shlyakhtin, A. V.; Lemenovskii, D. a.; Nifant'Ev, I. E. *Mendeleev Commun.* **2013**, *23* (5), 277–278.

(32) Ju, A.; Xu, H.; Ge, M. *J. Therm. Anal. Calorim.* **2013**, *115* (2), 1037–1047.

(33) Ju, A. Q.; Li, M. J.; Luo, M.; Ge, M. Q. *Chinese Chem. Lett.* **2014**, *25*, 1275–1278.

(34) Devasia, R.; Reghunadhan Nair, C. P.; Sadhana, R.; Babu, N. S.; Ninan, K. N. *J. Appl. Polym. Sci.* **2006**, *100* (4), 3055–3062.

(35) Moskowitz, J. D.; Wiggins, J. S. *Polymer (Guildf).* **2016**, *84*, 311–318.

(36) Moskowitz, J. D.; Abel, B. a.; McCormick, C. L.; Wiggins, J. S. *J. Polym. Sci. Part A Polym. Chem.* **2016**, *54*, 553–562.

(37) Moskowitz, J. D.; Wiggins, J. S. *Polym. Degrad. Stab.* **2016**, *125*, 76–86.

(38) Morris, E. A. *Univ. Kentucky Master's Thesis* **2011**, *107*.

(39) Gupta, A. K.; Paliwal, D. K.; Bajaj, P. *J. Macromol. Sci. Part C Polym. Rev.* **1991**, *31* (1), 1–89.

(40) Morris, E. A.; Weisenberger, M. C. *Polymer Precursor Derived Carbon*; 2014.

(41) Cai, J. Y.; McDonnell, J.; Brackley, C.; O'Brien, L.; Church, J. S.; Millington, K.; Smith, S.; Phair-Sorensen, N. *Mater. Today Commun.* **2016**, *9*, 22–29.

(42) Niu, S.; Ding, M.; Chen, M.; Feng, T.; Zhang, L.; Wei, L.; Cheng, Z.; Zhu, X. *J. Polym. Sci. Part A Polym. Chem.* **2013**, *51* (24), 5263–5269.

(43) Tang, C.; Kowalewski, T.; Matyjaszewski, K. *Macromolecules* **2003**, *36* (23), 8587–8589.

(44) Wang, R.; Luo, Y.; Li, B.; Sun, X.; Zhu, S. *Macromol. Theory Simulations* **2006**, *15* (4), 356–368.

(45) Park, S.-J.; Heo, G. *Carbon Fibers*; 2015; Vol. 210.

(46) Rahaman, M. S. a; Ismail, a. F.; Mustafa, a. *Polym. Degrad. Stab.* **2007**, *92* (8), 1421–1432.

(47)   Michaelis, A.; Cherif, C.; Kirsten, M.; Meinl, J.; Sch, K. *J. Appl. Polym. Sci.* **2016**, *43698*, 1–9.

(48)   Frank, E.; Steudle, L. M.; Ingildeev, D.; Sporl, J. M.; Buchmeiser, M. R. *Angew. Chemie - Int. Ed.* **2014**, *53* (21), 5262–5298.

(49)   Zeng, X.; Hu, J.; Zhao, J.; Zhang, Y.; Pan, D. *J. Appl. Polym. Sci.* **2007**, *106*, 2267–2273.

(50)   Bajaj, P.; Sreekumar, T. V; Sen, K. *J. Appl. Polym. Sci.* **2002**, *86*, 773–787.

(51)   Chen, J.; Wang, C.; Ge, H.; Bai, Y. *J. Polym. Res.* **2007**, *14*, 223–228.

(52)   Takahaski, M; Nukushina, Y; Kosugi, S. *Text. Res. J.* **1964**, *34* (87).

(53)   Bell, J P; Dumbleton, J. H. *Text. Res. J.* **1971**, *41* (3), 196–203.

(54)   Xue, Y.; Liu, J.; Liang, J. *J. Appl. Polym. Sci.* **2013**, *127* (1), 237–245.

(55)   Arbab, S.; Zeinolebadi, A. *Polym. Degrad. Stab.* **2013**, *98* (12), 2537–2545.

(56)   Khayyam, H.; Naebe, M.; Zabihi, O.; Zamani, R.; Atkiss, S.; Fox, B. *IEEE Trans. Ind. Informatics* **2015**, *11* (4), 887–896.

(57)   Khayyam, H.; Jazar, R. N.; Nunna, S.; Golkarnarenji, G.; Badii, K.; Fakhrhoseini, S. M.; Kumar, S.; Naebe, M. *Prog. Mater. Sci.* **2019**, *100575*, 1–83.

(58)   Meinl, J.; Kirsten, M.; Cherif, C.; Michaelis, A. *Am. J. Anal. Chem.* **2016**, *7* (March), 282–293.

(59)   Wu, S.; Gao, A.; Wang, Y.; Xu, L. *J. Mater. Sci.* **2018**, *53* (11), 8627–8638.

(60)   Zhang, B.; Lu, C.; Liu, Y.; Zhou, P.; Yu, Z. *Polymer (Guildf).* **2019**, *179* (121618).

(61)   Katsuraya, K.; Hatanaka, K.; Matsuzaki, K.; Minagawa, M. *J. Polym. Sci.* **2001**, *42*, 6323–6326.

(62)   Rwei, S. P.; Way, T. F.; Chiang, W. Y.; Pan, S. Y. *Colloid Polym. Sci.* **2017**, *295*

(5), 803–815.

(63)   Burkanudeen, a.; Krishnan, G. S.; Murali, N. *J. Therm. Anal. Calorim.* **2013**, *112* (3), 1261–1268.

(64)   Venkatesh, M.; Ravi, P.; Tewari, S. P. *J. Phys. Chem. A* **2013**, *117* (40), 10162–10169.

(65)   Zhang, L.; Dai, Y.; Kai, Y.; Jin, R.-G. *Carbon Lett.* **2011**, *12* (4), 229–235.

(66)   Bajaj, P.; Sreekumar, T. .; Sen, K. *Polymer (Guildf).* **2001**, *42* (4), 1707–1718.

(67)   Anders, M.; Lo, J.; T, C.; Nutt, S. *SAMPE* **2016**, *52* (1), 44–55.

(68)   Nunna, S.; Maghe, M.; Fakhrhoseini, S. M. *Energies* **2018**, *11* (5), 1–10.

(69)   Fu, Z.; Gui, Y.; Cao, C.; Liu, B.; Zhou, C.; Zhang, H. *J. Mater. Sci.* **2014**, *49* (7), 2864–2874.

(70)   Beltz, L. a.; Gustafson, R. R. *Carbon N. Y.* **1996**, *34* (5), 561–566.

(71)   Fox, B. L.; Naebe, M.; Maghe, M.; Tobin, M.; Bambery, K.; Vongsvivut, J.; Hameed, N.; Mater, J. *J. Mater. Chem. A* **2017**, *5*, 7372–7382.

(72)   Fu, Z.; Liu, B.; Sun, L.; Zhang, H. *Polym. Degrad. Stab.* **2017**, *140*, 104–113.

(73)   Yu, M. J.; Bai, Y. J.; Wang, C. G.; Xu, Y.; Guo, P. Z. *Mater. Lett.* **2007**, *61* (11–12), 2292–2294.

(74)   Spörl, J. M.; Ota, A.; Beyer, R.; Lehr, T.; Müller, A.; Hermanutz, F.; Buchmeiser, M. R. *J. Polym. Sci. Part A Polym. Chem.* **2014**, *52* (9), 1322–1333.

(75)   Karacan, I.; Erdoğan, G. *Fibers Polym.* **2012**, *13* (7), 855–863.

(76)   Arbab, S.; Mirbaha, H.; Zeinolebadi, A.; Nourpanah, P. *J. Appl. Polym. Sci.* **2014**, *131* (11), 1–8.

(77)   Su, Y.; Park, J. G.; Koo, A.; Trayner, S.; Hao, A.; Downes, R.; Liang, R. *Microsc.*

Microanal. **2016**, *22*, 666–672.

(78)   Jolowsky, C.; Sweat, R.; Park, J. G.; Hao, A.; Liang, R. *Compos. Sci. Technol.*

        2018, *166* (March), 125–130.

(79)   Morris, E. A.; Weisenberger, M. C.; Abdallah, M. G.; Vautard, F.; Grappe, H.;

        Ozcan, S.; Paulauskas, F. L.; Eberle, C.; Jackson, D.; Mecham, S. J.; Naskar, A. K.

        Carbon N. Y. **2016**, *101*, 245–252.

(80)   Müller, A. H. E.; Matyjaszewski, K. *Controlled and living polymerizations*; 2009.

(81)   Bol'bit, N. M.; Dubova, E. a.; Duflot, V. R.; Chevychelov, V. a. *Polym. Sci. Ser. A*

        2011, *53* (4), 289–295.

(82)   Chen, J. C.; Harrison, I. R. *Carbon N. Y.* **2002**, *40* (1), 25–45.

(83)   Yu, M.; Wang, C.; Bai, Y.; Zhu, B. O.; Ji, M.; Xu, Y. *J. Polym. Sci. Part B-*

        polymer Phys. **2008**, *46* (7), 759–765.

(84)   Ge, Y.; Fu, Z.; Deng, Y.; Zhang, M.; Zhang, H. *J. Mater. Sci.* **2019**, *54* (19),

        12592–12604.

(85)   Lin, X.; Wang, C.; Yu, M.; Lin, Z. *Adv. Mater. Res.* **2013**, *781–784*, 2609–2613.

(86)   Collins, G. L.; Thomas, N. W.; Williams, G. E. *Carbon N. Y.* **1988**, *26* (5), 671–

        679.

(87)   Xiao, S.; Cao, W.; Wang, B.; Xu, L.; Chen, B. *J. Appl. Polym. Sci.* **2013**, *127* (4),

        3198–3203.

(88)   Xue, T. J.; McKinney, M. a.; Wilkie, C. a. *Polym. Degrad. Stab.* **1997**, *58* (1–2),

        193–202.

(89)   Gallaher, K.; Lukco, D.; Grasselli, J. *Can. J.Chem.* **1985**, *63*, 1960–1966.

(90)   Zeng, Z.; Shao, Z.; Xiao, R.; Lu, Y. *Chinese J. Polym. Sci.* **2017**, *35* (8), 1020–

1034.

(91)   Zhao, J.; Zhang, J.; Zhou, T.; Liu, X.; Yuan, Q.; Zhang, A. *RSC Adv.* **2016**, *6* (6), 4397–4409.

(92)   Ouyang, Q.; Cheng, L.; Wang, H. J.; Li, K. X. *J. Therm. Anal. Calorim.* **2008**, *94* (1), 85–88.

(93)   Peebles Jr., L. H. *J. Am. Chem. Soc.* **1958**, *80* (21), 5603–5607.

(94)   Vyazovkin, S.; Sbirrazzuoli, N. *Macromol. Rapid Commun.* **2006**, *27* (18), 1515–1532.

(95)   Arbab, S.; Zeinolebadi, A. *Polym. Degrad. Stab.* **2013**, *98* (12), 2537–2545.

(96)   Deng, W.; Lobovsky, A.; Iacono, S. T.; Wu, T.; Tomar, N.; Budy, S. M.; Long, T.; Hoffman, W. P.; Smith, D. W. *Polymer (Guildf).* **2011**, *52* (3), 622–628.

(97)   Moad, G.; Solomon, D. H. *The Chemistry of Radical Polymerization*; 2005.

(98)   Hou, C.; Ying, L.; Wang, C. *J. Mater. Sci.* **2005**, *40* (3), 609–612.

(99)   Brar, a. S.; Dutta, K. *Eur. Polym. J.* **1998**, *34* (11), 1585–1597.

(100) Patton, D. L.; Page, K. a.; Hoff, E. a.; Fasolka, M. J.; Beers, K. L. *Polym. Chem.* **2012**, *3* (5), 1174.

(101) Çatalgil-Giz, H.; Giz, a.; Alb, a. M.; Öncül Koç, a.; Reed, W. F. *Macromolecules* **2002**, *35* (17), 6557–6571.

(102) Gribanov, a. V.; Sazanov, Y. N. *Russ. J. Appl. Chem.* **2008**, *81* (6), 919–932.

(103) Hao, J.; Liu, Y.; Lu, C. *Polym. Degrad. Stab.* **2018**, *147* (September 2017), 89–96.

(104) Fkzer, E.; Miller, D. J. **1975**, *13* (Formula 4), 63–69.

(105) Rwei, S.; Way, T.; Hsu, Y. *Polym. Degrad. Stab.* **2013**, *98* (10), 2072–2080.

(106) Qiao, M.; Kong, H.; Ding, X.; Hu, Z.; Zhang, L.; Cao, Y.; Yu, M. *Polymers*

(Basel). **2019**, *11* (3), 1–11.

(107) Rahman, M. A.; Ismail, A. F.; Mustafa, A.; Ng, B. C.; Hasbullah, H.; Rahaman M. S. A.; Abdullab, M. S. 2004, pp 169–179.

(108) Law, S. J.; Mukhopadhyay, S. K. *J. Appl. Polym. Sci.* **1996**, *62*, 33–47.

(109) Tsai, J. S.; Lin, C. H. *J. Appl. Polym. Sci.* **1991**, *42* (11), 3045–3050.

(110) Wang, Y.; Wang, C.; Yu, M. *J. Appl. Polym. Sci.* **2007**, *104*, 3723–3729.

(111) Morris, E. A.; Weisenberger, M. C.; Bradley, S. B.; Abdallah, M. G.; Mecham, S. J.; Pisipati, P.; Mcgrath, J. E. *Polymer (Guildf).* **2014**, *55* (25), 6471–6482.

(112) Wang, C.; Dong, X.; Wang, Q. *J. Polym. Res.* **2009**, *16*, 719–724.

(113) Huson, M. G.; Church, J. S.; Hillbrick, L. K.; Woodhead, A. L.; Sridhar, M.; Meene, A. M. L. Van De. *Mater. Chem. Phys.* **2015**, *168*, 193–200.

(114) Loeber, T. H.; Laegel, B.; Wolff, S.; Schuff, S.; Balle, F.; Beck, T.; Fitschen, J. H.; Steidl, G.; Loeber, T. H.; Laegel, B.; Wolff, S. *J. Vac. Sci. Technol. B* **2017**, *35* (6).

(115) Paris, O.; Loidl, D.; Peterlik, H.; Lichtenegger, H.; Fratzl, P. *J. Appl. Crystallogr.* **2000**, *33*, 695–699.

(116) Tshai, K. Y.; Tan, H. J.; Khiew, P. S.; Hoque, M. E. *Polym. Res.* **2015**, *9* (2), 182–195.

(117) Giri, P.; Tambe, C.; Narayan, R.; Junction, M.; States, U. *Greener Products : From Laboratory Fundamentals to Commercial Scale*; 2018.

(118) Andersen, P. G.; Lechner, F. *Plast. Eng.* **2018**, *69* (4), 32–38.

(119) Lawal, A. D. E. N. M.; Kalyon, D. M. *Polym. Eng. Sci.* **1995**, *35* (17), 1325–1338.

(120) Zetterlund, P. B.; Gody, G. *Macromol. Theory Simulations* **2014**, *23*, 331–339.

146

(121) Lyoo, W. S.; Ghim, H. Do; Yoon, W. S.; Lee, J.; Lee, H. S.; Ji, B. C. *Eur. Polym. J.* **1999**, *35* (4), 647–653.